12-2004

IR Studies of the Interaction of Surfactants and Polyelectrolytes Adsorbed on TIO2 Particles

Haiyan Li

IR STUDIES OF THE INTERACTION OF SURFACTANTS AND POLYELECTROLYTES ADSORBED ON TIO_2 PARTICLES

By

Haiyan Li

B.S. Nankai University, P.R. China, 1997

A THESIS

Submitted in Partial Fullfillment of the

Requirements for the Degree of

Doctor of Philosophy

(in Chemistry)

The Graduate School

The University of Maine

December, 2004

Advisory Committee:

Carl Tripp, Professor of Chemistry, Advisor

Douglas Bousfield, Professor of Chemical and Biological Engineering

David Neivandt, Assistant Professor of Chemical and Biological Engineering

Alla Gamarnik, Assistant Professor of Chemistry

Bruce Jensen, Associate Professor of Chemistry

IR STUDIES OF THE INTERACTION OF SURFACTANTS AND POLYELECTROLYTES ADSORBED ON TIO_2 PARTICLES

By Haiyan Li

Thesis Advisor: Dr. Carl Tripp

An Abstract of the Thesis Presented
in Partial Fulfillment of the Requirements for the
Degree of Doctor of Philosophy
(in Chemistry)
December, 2004

Polymers/surfactants are used to control and modify the interfacial properties of particulate suspensions. The resulting properties are dependent on the amount of adsorbed surfactants/polymers on the surface as well as the nature of the aggregated structures. Often these interactions are complex and not well understood. In this thesis we have used Attenuated total reflection-Fourier transform infrared spectroscopy (ATR-FTIR) to identify surfactant, mixed surfactant, polyelectrolyte and mixed polyelectrolyte surfactant structures formed on charged TiO_2 particles. In addition, the change occurring to the structure of an adsorbed polymer layer on TiO_2 to flowing suspension of silica particles was studied. A particular focus has been on the headgroup bands of the surfactants and the functional groups of the polymer as this provides unique information on the nature of the aggregated structure.

For the measurement of cetyltrimethylammonium bromide (CTAB) onto TiO_2 at pH 10.3, it is found that there are abrupt changes in the intensity of the symmetric bending mode of the CTAB headgroup and these abrupt changes have been correlated to different aggregated structures along the adsorption isotherm. Furthermore, by measuring spectra as a function of time it is possible to obtain information on the dynamics of the

formation of aggregated CTAB structures on the surface. It is shown that aggregated hemimicellar, admicellar and micellar structures initially adsorb through intermediate structures that have a higher percentage of CTAB molecules bound directly to charged sites on the surface.

Mixed CTAB and SDS structures are produced when SDS is used to probe CTAB adsorbed hemimicelle, admicelle or micelle structures formed when CTAB was first added to a bare TiO_2 surface at three different solution concentrations. Each CTAB structure was studied as a function of contact time with a solution containing the deutero form of the anionic surfactant, sodium dodecyl sulfate (SDS). By measuring the changes in the headgroup bands for both SDS and CTAB along with the change in the adsorbed amount of each surfactant as a function of time, a clearer picture emerges of the mixed surfactant structures formed on the surface. Specifically, it was shown that the SDS intercalates into the CTAB structure leading to a variety of mixed surfactant structures that depend on the surfactant concentrations in solution.

The adsorption of sodium polyacrylate (NaPA) on charged TiO_2 particles and the subsequent interaction of the adsorbed polymer structure with cationic and anionic surfactants were also determined by ATR-FTIR. The nature of the polymer structure was deduced from the adsorbed amount in tandem with the information obtained from monitoring the change in the relative intensity of the COO^- and COOH infrared bands. It is shown that the initial NaPA approaching the bare surface adopts a flat conformation with high bound fraction. Once the bare sites on the surface are covered, the accommodation of additional polymer on the surface requires the existing adsorbed layer to adopt a conformation with a lower bound fraction. When the adsorbed NaPA is probed

with a solution containing the anionic surfactant, SDS, the SDS competes for surface sites and displaces some of the bound NaPA segments from the surface giving rise to an polymer layer adsorbed with an even lower bound fraction. In contrast, addition of a solution containing the cationic surfactant, CTAB results in the binding of the surfactant directly to the free COO^- sites on the adsorbed polymer backbone. Confirmation of a direct interaction of the CTAB headgroup with the free COO^- groups of the polymer is provided by intensity changes in the headgroup IR bands of the CTAB.

This vibrational approach was then used to study the adsorption of charged silica particles onto TiO_2 particles coated with anionic or cationic polyelectrolytes. It is shown that the deposition of positively charged silica particles on a sodium polyacrylate coated TiO_2 does not lead to any desorption of the polymer from the surface but rather to a change in the relative intensities of the bands due to COOH and COO^- groups. From this change in band intensity, it is calculated that only about 6% of the COO^- groups located in the loops and tails bind to the silica particle. This shows that the polymer bridges the two particles through an electrostatic interaction with the outer COO^- groups. Similarly, in the case of the TiO_2 particles coated with the cationic poly(diallyldimethylammonium) chloride, the deposition of negatively charged silica does not reduce the amount of polymer on the TiO_2 surface but rather leads to an increase in intensity of the symmetric bending mode of the $^+N(CH_3)_3$ group. This change in band intensity arises from the binding of these cationic sites of the polymer to the negative surface sites on the silica. The results show that once adsorbed on the TiO_2 particle, the PDADMAC or the NaPA does not migrate to the silica particles.

ACKNOWLEDGEMENTS

The author would like to express her sincere gratitude to the advisor of this project, Dr. Carl P. Tripp for providing her such a good opportunity to continue her education at University of Maine, and also for his constant support, encouragement, the time and energy he has spent with the author during the four years' graduate study. At the same time, a special thank is due to the thesis committee member, Dr. Douglas Bousfield for his guidance and financial support throughout the author's Ph.D program. The Author would also like to thank Dr. David Neivandt, Dr. Alla Gamarnik and Dr. Bruce Jensen for the time that was devoted to help lead direction in this project and for the time devoted to reading and commenting on this thesis.

The author wishes to express her appreciation to the following students in the same research group: Dr. Brian Ninness, Dr. Sofian Kanan, Shivashanker Bitla, Dr. Anil Waghe, Cuihong Jiang, Wei Gu, Dr. William Tze, Zhixiang Lu, Luke Doucette, Dr. Ben McCool and Parag Dhake. I also want to express my thanks to all faculty, staff and graduate students in Department of Chemistry and the Laboratory of Surface Science and Technology who have given me help during my study at University of Maine.

Finally I would like to express my sincere appreciation to Yihe Hu, who is not only my husband but also my best friend. Without his never-ending support, encouragement and love, I could not finish my thesis work. I also expand my gratitude to my parents for their nice support.

TABLE OF CONTENTS

ACKNOWLEDGEMENTS.....ii

LIST OF FIGURES.....vii

LIST OF SCHEMES.....xi

LIST OF TABLES.....xii

Chapter

1. INTRODUCTION.....1

1.1 Motivation.....1

1.2 Background.....5

1.2.1 Paper Coatings.....5

1.2.2 Adsorption of Surfactants and Polymers on Pigments.....6

1.2.2.1 Adsorption of Surfactants.....7

1.2.2.2 Co-adsorption of Multi-surfactants on Pigments.....10

1.2.2.3 Adsorption of Polymers on Pigments.....11

1.2.2.4 Adsorption of Single Polyelectrolytes on Pigments.....12

1.2.2.5 Co-adsorption of Ionic and Non-ionic Polyelectrolyte.....14

1.2.2.6 Co-adsorption of Polymers and Surfactants.....15

1.3 Attenuated Total Reflection.....16

1.4 Zeta Potential.....20

1.4.1 Definition of Zeta Potential.....20

1.4.2 Measurement of Zeta Potential from Electrophoretic Mobility.....22

2. EXPERIMENTAL.....23

2.1 Materials.....23

2.2 Modification of the IRE Surface.....24

2.3 ATR Experimental Setup.....26

2.4 Calibration of Adsorbed Amount of Surfactants and Polyelectrolyte on TiO_2.....27

2.5 FTIR and Zeta Potential Measurements.....33

3. SPECTROSCOPIC IDENTIFICATION AND DYNAMICS OF ADSORBED CETYLTRIMETHYLAMMONIUM BROMIDE (CTAB) STRUCTURES ON TIO_2 SURFACES.....34

3.1 Introduction.....34

3.2 Experimental Section.....36

3.3 Results and Discussion.....38

3.3.1 CTAB Adsorption Isotherm and CTAB Headgroup.....38

3.3.2 Dynamics of CTAB Adsorption.....47

3.4 Conclusion.....53

4. USE OF INFRARED BANDS OF THE SURFACTANT HEADGROUP TO IDENTIFY MIXED SURFACTANT STRUCTURES ADSORBED ON TITANIA.....55

4.1 Introduction.....55

4.2 Experimental Section.....57

4.3 Results and Discussion.....58

4.3.1 Interaction of d_{25}-SDS with CTAB Hemimicelles Adsorbed on TiO_2.....60

4.3.2 Interaction of d_{25}-SDS Solution with CTAB Admicelles adsorbed on TiO_2.....63

4.3.3 Interaction of d_{25}-SDS Solution with CTAB Micelles Adsorbed on TiO_2.....65

4.3.4 Headgroup Region of d_{25}-SDS.....68

4.3.5 CTAB Headgroup.....76

4.4 Conclusions.....79

5. INTERACTION OF SODIUM POLYACRYLATE ADSORBED ON TIO_2 WITH CATIONIC AND ANIONIC SURFACTANTS.....80

5.1 Introduction.....80

5.2 Experimental Section.....80

5.3 Results and Discussion.....82

5.3.1 IR spectrum of NaPA.....82

5.3.2 Adsorption of NaPA.....87

5.3.3 Dynamics of NaPA Adsorption.....91

5.3.4 Sequential Adsorption of NaPA then SDS.....93

5.3.5 Sequential Adsorption of NaPA then CTAB.....97

5.4 Conclusion.....101

6. AN INFRARED STUDY OF THE INTERACTION OF CHARGED SILICA PARTICLES WITH TIO_2 PARTICLES CONTAINING ADSORBED CATIONIC AND ANIONIC POLYELECTROLYTES.....103

6.1 Introduction.....103

6.2 Experimental Section.....106

6.3 Results and Discussion.....108

6.3.1 Adsorption of Bare and Aminosilanated Silica on Bare TiO_2.....108

6.3.2 Adsorption of Silica on NaPA Coated TiO_2.....110

6.3.3 Adsorption of Aminosilanated Silica with NaPA Coated TiO_2.....114

6.3.4 Adsorption of SiO_2 on PDADMAC Coated TiO_2.....117

6.4 Conclusion.....120

REFERENCES.....121

BIOGRAPHY OF THE AUTHOR.....131

LIST OF FIGURES

Figure 1.1 General shape of the adsorption isotherm of cationic surfactant onto silica gel.....9

Figure 1.2 Schematic of the IR radiation light reflection at ATR interface.....18

Figure 1.3 Electric double layer at the solid/liquid interface.....21

Figure 1.4 The relative magnitude of various electric double layer potentials at the solid/liquid interface.....21

Figure 2.1 Deposition of TiO_2 film on a ZnSe IRE 26

Figure 2.2 ATR experimental setup.....27

Figure 2.3 Symmetric and assymmetric CH_2 stretching modes of CH_2 of CTAB and SDS.....28

Figure 2.4 Symmetric and assymmetric CH_2 stretching modes of CD_2 of d_{25}-SDS.....29

Figure 2.5 Infrared bands of NaPA adsorbed on TiO_2.....29

Figure 2.6 Infrared peak of TiO_2 coated on ZnSe crystal.....30

Figure 3.1 Time dependent adsorption of CTAB on TiO_2 at pH 10.3 at CTAB concentrations of 6.7×10^{-7} M, 3.0×10^{-6} M, 1.0×10^{-4}M, 3.4×10^{-4} M and 1.0×10^{-2} M.....39

Figure 3.2 The adsorption isotherm of CTAB adsorbed on TiO_2 at pH 10.3.....40

Figure 3.3 Infrared spectra of CTAB adsorbed on TiO_2 41

Figure 3.4 Time dependent plots of the 1396/2850 ratios at CTAB concentration of a) 6.7×10^{-7} M, b) 3.0×10^{-6} M, c) 1.0×10^{-4}M, d) 3.4×10^{-4} M and e) 1.0×10^{-2} M.....50

Figure 3.5 The adsorption isotherm and 1396/2850 ratio (dashed curve) for the addition of CTAB at increasing concentrations sequentially to the same TiO_2 samples.....51

Figure 3.6 Time evolution of the intensity of the 1396/2850 ratio across Regions IV and V for the points shown in Figure 3.5.....52

Figure 3.7 Time evolution of the intensity of the 1396 cm^{-1} and 2850 cm^{-1} bands across the points shown in Figure 3.6.....53

Figure 4.1 Hemimicellar, admicellar and micellar structures formed on the TiO_2 surface at the indicated CTAB concentrations.....60

Figure 4.2 Time dependent change in the amount of CTAB and d_{25}-SDS adsorbed on TiO_2 at pH 10.3 using a 0.01 mM CTAB solution followed by addition of 0.05 mM d_{25}-SDS solution.....61

Figure 4.3 Time dependent change in the amount of CTAB and d_{25}-SDS adsorbed on TiO_2 at pH 10.3 using a 0.1 mM CTAB solution followed by addition of 0.5 mM d_{25}-SDS solution.....64

Figure 4.4 Time dependent change in the amount of CTAB and d_{25}-SDS adsorbed on TiO_2 at pH 10.3 using a 1.0 mM CTAB solution followed by addition of 5.0 mM d_{25}-SDS solution.....67

Figure 4.5 Change in the intensity of the S-O headgroup bands as a function of reaction time during the uptake of d_{25}-SDS into the preadsorbed CTAB layer as described in Figure 4.2.....69

Figure 4.6 Normalized values of the A and E ν_{as} S-O modes for the spectra shown in Figure 4.5.....73

Figure 4.7 Relative intensity of the ν_{as} S-O modes obtained at equilibrium for addition of d_{25}-SDS to the indicated CTAB structures.....76

Figure 4.8 IR bands of CTAB headgroup before and after d_{25}-SDS addition for adsorbed CTAB using CTAB solution concentrations of (a) 0.01 mM, (b) 0.1 mM and (c) 1mM.....78

Figure 5.1 Infrared spectrum of NaPA adsorbed from a 20 ppm solution onto TiO_2 at pH 3.5.....83

Figure 5.2 Infrared spectrum of 10,000 ppm NaPA in solution recorded at different pH.....86

Figure 5.3 pH dependence of %COOH and % COO^- for NaPA in solution.....86

Figure 5.4 Amount of NaPA adsorbed from a 20 ppm solution onto TiO_2 at different pH.....87

Figure 5.5 % COOH of NaPA in solution and adsorbed on TiO_2 89

Figure 5.6 Time evolution of the adsorbed amount and the bound %COO^- when NaPA is adsorbed from a 20 ppm solution onto TiO_2 at pH 3.5.....92

Figure 5.7 Representative structures consistent with bound %COO^- values during the adsorption of NaPA on TiO_2.....93

Figure 5.8 Adsorption dynamics for the sequential addition of NaPA followed by SDS onto TiO_2 at pH 3.5.....95

Figure 5.9 Representative structures consistent with bound %COO^- values and adsorbed amount of NaPA and SDS during the sequential addition of NaPA followed by SDS.....96

Figure 5.10 Adsorption dynamics for the sequential addition of NaPA followed by CTAB onto TiO_2 at pH 4.0.....98

Figure 5.11 Representative structures consistent with bound %COO^- values and adsorbed amount of NaPA and CTAB during the sequential addition of NaPA followed by CTAB.....100

Figure 5.12 Infrared spectrum of CTAB adsorbed onto NaPA coated TiO_2.....101

Figure 6.1 Infrared spectra recorded after contact of a 25 ppm suspension of (a) untreated silica with TiO_2 at pH 10.3 (b) untreated silica with TiO_2 at pH 3.5 (c) aminosilanated silica with TiO_2 at pH 3.5.....109

Figure 6.2 IR spectra of (a) NaPA adsorbed on TiO_2 from a 5 ppm NaPA solution at pH 3.5 followed by a 5 minute rinse with water at pH 3.5 and then (b) addition of a 25 ppm suspension of untreated silica at pH 3.5 for 120 minutes.....111

Figure 6.3 IR spectra of (a) NaPA adsorbed on TiO_2 from a 5 ppm NaPA solution at pH 3.5 followed by a 5 minute rinse with water at pH 3.5 and then (b) addition of a 25 ppm suspension of aminosilanated silica at pH 3.5 for 240 minutes.....115

Figure 6.4 IR spectrum of (a) PDADMAC adsorbed on TiO_2 from a 30 ppm PDADMAC solution at pH 10 followed by a 5 minute rinse with water at pH 10 and then (b) addition of a 25 ppm suspension of untreated silica at pH 10 for 240 minutes. (c) Absorbance spectrum of pure PDADMAC cast onto a ZnSe infrared window.....119

LIST OF SCHEMES

Scheme 1.1 The effects of polymer concentrations on particle interaction.....12

Scheme 2.1 Structures of CTAB, SDS, NaPA and PDADMAC.....24

Scheme 3.1 Transition dipole moments of headgroup bands of CTAB and SDS.....42

Scheme 3.2 Representative structures consistent with 1396/2850 ratios for Regions I to III.....44

Scheme 3.3 Representative structures consistent with 1396/2850 ratios for Regions IV and V.....46

Scheme 4.1 Uptake of SDS by CTAB hemimicelles.....62

Scheme 4.2 Uptake of SDS by CTAB admicelles.....65

Scheme 4.3 Uptake of SDS by CTAB micelles.....68

Scheme 4.4 Transition dipole moment vectors for S-O stretching modes of SDS.....70

Scheme 5.1 (I) bidentate chelating and (II) bidentate bridging structures on metal oxide surfaces.....84

Scheme 5.2 Competing Equilibrium Processes for NaPA Adsorption on TiO_2 surfaces.....88

Scheme 6.1 Structures of polyacrylate sodium (NaPA) and Poly(diallyldimethylammonium) chloride (PDADMAC).....107

Scheme 6.2 Interaction of Silica with NaPA coated TiO_2.....117

LIST OF TABLES

Table 1.1 Typical IRE materials for the ATR applications.....20

Table 2.1 Extinction coefficients of the surfactant, polymer and pigment.....31

Table 5.1 Assignment for IR bands of NaPA in solution (10,000 ppm) and after adsorption from 20 ppm NaPA solution onto the TiO_2 particles at pH 3.5.....83

Table 5.2 Computed bound $\%COO^-$ for NaPA in solution and adsorbed on TiO_2 from a 20 ppm solution at different pH conditions.....90

Table 6.1 Computed values for NaPA adsorbed on TiO_2 before and after addition of 25 ppm suspension of aminosilanated silica.....116

CHAPTER 1. INTRODUCTION

1.1 Motivation

Polymers/surfactants are used to control and modify the surface properties of particulate suspensions and find widespread use in areas such as detergency, pharmaceutical production, cosmetics, mineral separation and paper coatings.[1] The interaction of the polymers and surfactants on surfaces are complex leading to a variety of aggregated structures that depend on factors such as the nature of the surfactant and polymers, the properties of the surface, pH, ionic strength, solution concentration of the adsorbates as well as kinetic factors such as the order and time of addition of surfactant/polymer.[2-7]

While adsorbed mixtures of polymers and surfactants on surfaces are used to modify the rheological behavior and dispersion stability of colloidal systems,[8-13] the complex molecular interactions leading to these macroscopic properties are not well understood. Clearly, knowledge of the amounts of polymer and surfactant adsorbed is important, but this information alone is insufficient in predicting the properties of colloidal systems. In most cases, the structure of the adsorbed layer is a contributing factor to the colloidal properties. For example, it was recently shown that it was the structure of adsorbed cetyltrimethylammonium bromide (CTAB) on TiO_2, and not the adsorbed amount, that dictated the level of adsorption of an anionic surfactant with the adsorbed CTAB layer.[14] In addition, the dynamics of the adsorption process is equally important as the colloidal properties strongly depend on factors such as sample history and order and time of addition of surfactant/polymers.[15] Given this level of complexity, it is important to develop methods and techniques that can simultaneously measure the

dynamic and equilibrium adsorbed amount of each surfactant and polymer in tandem with identification of surface architectures. As a result, there is voluminous literature dedicated to developing techniques for studying surfactant/polymer adsorption on single well-defined surfaces.[13, 14, 16-23]

Several techniques such as scanning angle reflectometry(SAR),[24, 25] sum frequency spectroscopy(SFS),[26], surface plasmon resonance (SPR),[27] calorimetry,[28] UV spectroscopy,[29-32] surface tension,[6] fluorescence,[33] atomic force microscopy(AFM)[5, 7, 34, 35] as well as turbidity measurements[15] have been used to study the co-adsorption of aqueous polyelectrolyte-surfactant mixtures at the solid/liquid interfaces. These methods however do not provide simultaneous measurements of the amount of each adsorbate and/or the identification of aggregated structures formed during the adsorption process. In an attempt to overcome these limitations, Brian Ninness in his thesis work[36] developed a method involving TiO_2 particles bound to a ZnSe internal reflection element (IRE) and the use of Attenuated Total Reflection Infrared Spectroscopy (ATR-IR). This method was used by Brian Ninness to study to adsorption of mixed surfactants on charged TiO_2.[14] The approach is not limited to TiO_2, as I have extended this initial approach developed by Brian Ninness to a SiO_2 interface by converting the TiO_2 surface to SiO_2 using atomic layer deposition.[37] Alternatively, adsorption onto other high surface area particles can be studied spectroscopically by using a polymer binder to anchor the particles onto the ZnSe crystal.[38]

While it was possible to monitor the dynamic change in the adsorbed amount of different surfactants, Brian Ninness's thesis work showed that extracting information on the adsorbed structures was more difficult and was inferred from the observed shifts in

the bands due to the alkyl chains. This turns out to have limited use as it was only the compact micellar structures formed with mixtures of cationic and anionic surfactants that lead to appreciable shifts in the modes due to alkyl chains.[14]

A typical approach to obtaining structural information in ATR-IR measurements is to record spectra using polarized light. For example, the intensity ratio of the CH_2 stretching mode for a surfactant on a surface of an oxidized silicon IRE recorded using parallel or perpendicular polarized light, provided a means for determining the average orientation of a surfactant molecule on a surface.[39-41] However, these polarization measurements require a flat surface and therefore are not applicable for surfactants adsorbed on TiO_2 powders deposited on an IRE. Given the insensitivity of the position of the CH_2 bands to pure surfactant structures and the ineffectiveness of polarization studies, it appeared that an ATR-IR method using powders would not provide information on the nature of aggregated surfactant structures.

However, there is an additional advantage when the ATR technique is applied to the adsorption onto particles bound to the IRE. An attraction of this ATR-IR approach is that the high surface area associated with the particles enables detection of the weak, yet information-rich headgroup IR bands of surfactants. The high surface area also provides good signal-to-noise in detection of the strong CH_2 stretching modes during time-dependent measurements of the adsorbed amount.[23] It is the application of these two aspects that form the backbone of this thesis work. Specifically, in this thesis I have identified the relationship between changes in position and intensity of the headgroup IR bands of surfactants and bands due to functional groups on polymers with the nature of the structures formed dynamically on TiO_2.

In chapter 3, the adsorption of CTAB on TiO_2 at pH 10.3 is reinvestigated with a particular focus on measuring the nature of the aggregated structures by monitoring the changes occurring in the bands due to the surfactant headgroup. In chapter 4, this approach is extended to study the interaction of the anionic sodium dodecyl sulfate (SDS) with the adsorbed CTAB structures. In this case, the nature of the mixed surfactant structure is deduced from changes in IR bands due to both surfactant headgroups. In chapter 5, the interaction of SDS and CTAB with sodium polyacrylate (NaPA) is examined. As with chapters 3 and 4, the important structural information is derived from the changes in headgroup bands of the surfactants and the bands due to functional groups along the polymer chains. From this information it was possible to identify the nature of the mixed surfactant/polymer aggregated structures on the surface.

The overarching goal of this project was to use this ATR approach to measure the migration of polymer and surfactants between different pigment surfaces. There are relatively few studies of surfactant/polymer adsorption in mixed particulate systems. This is not because of a lack of interest. Most industrial processes involving particulate suspensions are not single component systems. For example, in the paper coating industry, it is common to prepare a final coating formulation by mixing different pre-stabilized pigment and binder suspensions. The behavior of the resulting formulation is often unpredictable. Clearly, the interfacial interactions are more complex in a mixed particulate system as additional processes such as migration of polyelectrolytes/surfactants between the different pigments are possible.

The findings reported in chapters 3-5 provided the framework for the work in chapter 6 involving different pigment surfaces. It was found that the ATR technique used

to measure surfactant and polymer adsorption on TiO_2 could easily be extended to flowing suspensions of particulates. Specifically, bare or aminosilanated silica particles were passed through the ATR flow cell containing bare or polymer coated TiO_2 particles. By monitoring the changes to the bands due to the functional groups of the polymer and those assigned to bulk modes of the silica, it was possible to monitor deposition of the silica on the surface as well as changes to the amount and structure of the polymer coated on the TiO_2.

1.2 Background

The work described in this thesis is directed in the area of paper coating formulations. In this case, adsorbed polymers and surfactants on pigments are used to create stable dispersions of pigments and binders for coatings used in the paper industry. In this section I provide background on the nature of the paper coatings, a brief survey of literature on the adsorption of surfactants and polymers on pigments and provide a background on ATR techniques and zeta potential measurements used in this work.

1.2.1 Paper Coatings

Pigments are generally applied to paper surfaces to improve 1) smoothness and receptivity for printing 2) to change the color of the raw stock and 3) to improve opacity. A traditional coating consists mainly of 80-90% of mineral pigments. The most common pigments used in the paper coating industry are silica, kaolin, $CaCO_3$ and TiO_2. The remaining constituents are chemical binders and other functional chemical additives. The chemical binders are used to "glue" the pigments to the paper surface and may be natural products such as starch and protein or synthetic polymers like poly(styrene butadiene) and poly(vinyl alcohol).

Calcium carbonate ($CaCO_3$) and kaolin are the most popular pigments used for the coatings. The two main types of $CaCO_3$ used in paper coatings are ground calcium carbonate (GCC) and precipitated calcium carbonate (PCC). GCC is ground from natural deposits such as chalk, marble and limestone. PCC is formed through a chemical process in which the $CaCO_3$ is first heated to form CaO, then reacted with water to form $Ca(OH)_2$ which is then reacted with CO_2 to convert back to $CaCO_3$. The advantage of the chemical method is that the size and morphology of the PCC can be controlled by the processing steps.

Kaolin is a natural mined pigment with a formula of $Al_2O_3 \bullet 2SiO_2 \bullet 2H_2O$. The kaolin has a structure of 1:1 layered aluminosilicate consisting a tetrahedral silica surface and an octahedral alumina surface. The special layered structure of the kaolin is good for making lightweight, coated grades (LWC). The sheet-like structure of the kaolin produces coatings with favorable gloss properties. Other common pigments include silica and titania. The coatings made with the fine grades of amorphous silica have a marked resistance to calendar darkening. In addition, small percentages of silica in coating mixtures show a notable improvement in sheet smoothness. Titanium dioxide pigments are used in the paper coatings primarily to improve the opacity and brightening of the paper surface. Titanium dioxide has a high refractive index and therefore, it is a better opacifying and brightening particle than other pigments.

1.2.2. Adsorption of Surfactants and Polymers on Pigments

The combination of high surface area pigment particles, polyelectrolytes, and surfactants can lead to complex colloidal properties when mixed together to form a coating formulation. These species will interact both physically and chemically, and

knowledge of the associative behavior and adsorption properties of these species will aid in the proper formulation of these complex colloidal systems. For example, cationic polyelectrolytes have been used in the paper industries for many years to improve retention of fine material from the fibers or from added mineral fillers in the produced paper or to improve the strength properties of the paper. The dispersion of the pigments particles is influenced by the amount of polymer/surfactant adsorbed as well as the conformation of the aggregated structure on the surface.

The collective work of surfactant and polymer adsorption on particles is enormous. The brief survey of studies involving surfactants and polymers on surfaces provided below is a very small portion of the total work in this area. The intent of this brief survey is to provide an overview of the types of measurements and techniques used to extract information of the nature of the interaction of these complex systems with surfaces.

1.2.2.1 Adsorption of Surfactants

Surfactants adsorb onto pigments by one or a combination of 1) electrostatic interaction between the charged surface sites and the ionic headgroup of the surfactant 2) hydrophobic interaction between the surfactant hydrophobic tails and 3) by forming covalent bands between the surface and the surfactant. Knowledge of the structure and dynamics of adsorbed surfactants on charged metal oxide surfaces across the entire adsorption isotherm has importance to many industrial processes.[1, 42] Adsorption isotherms typically are characterized by two plateau regions giving rise to a "double S" shape shown in Figure 1.1.[43] The boundaries between the plateau regions are defined by abrupt changes in the adsorption curve and these have been attributed to changes in the

nature of the surfactant aggregation on the surface. It is generally accepted that hemimicelles form on the surface in which the adsorbed surfactant molecules begin to associate through the hydrophobic effect into surface aggregates. The solution concentration point at which this occurs in Figure 1.1 is indicated as the hemimicellar concentration (h.m.c.). This concept of a hemimicellar structure in which the molecules tend to adsorb in clusters was proposed almost 50 years ago[44] and explains the rapid rise in the S-shaped isotherm.[20, 45] Above the critical micelle concentration (c.m.c.), there is a second plateau region in the adsorption isotherm and recent AFM data on various surfaces[46] has shown that the surfactant exists as globular micelles rather than a patchy bilayer.

The adsorbed surfactant structure has been the subject of numerous theoretical[19, 47-49] and experimental[17, 18, 39, 40, 46, 50-57] studies. A common model system in both theoretical and experimental studies involves the adsorption of cetyltrimethylammonium bromide (CTAB) at the metal oxide-aqueous surfactant solution interface. The structure of the adsorbed CTAB has been probed by a variety of experimental techniques including depletion methods,[17, 50, 51] AFM,[18, 52-55, 57, 58] Fourier transform infrared attenuated total reflection (ATR) spectroscopy[39, 40, 56] and optical reflectometry.[57]

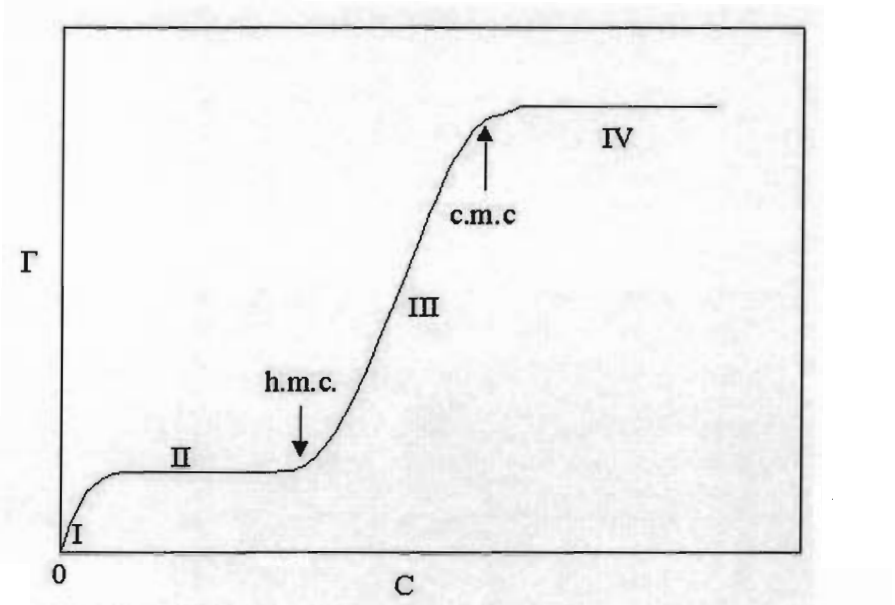

Figure 1.1 General shape of the adsorption isotherm of cationic surfactant onto silica gel

Fleming. *et. al.* investigated the formation of CTAB aggregated structures on silica surfaces using AFM.[58] The AFM data provided the first direct evidence of lateral organization of adsorbed surfactant at an order of magnitude below the c.m.c.. Neivandt *et. al.* used polarized Infrared attenuated total reflection (IR-ATR) to determine the average orientation of the methylene tail of the CTAB adsorbed at the silica/solution interface under equilibrium and nonequilibrium conditions.[39] They found that during initial adsorption at low surface excess, the surfactant adsorbs in a near random orientation. As the adsorbed amount increases with longer contact time, a corresponding rapid rise in the orientation of the surfactant is observed. The surfactant adopts a more tightly vertical arrangement from the surface in order to facilitate further CTAB adsorption and an even higher packing density.

Atkin, *et. al.*[57] used AFM and optical reflectometry to measure the kinetics of adsorption and the structures formed at the SiO_2/aqueous interface for solutions

containing cetylpyridinium bromide (CPB). The optical reflectometry is used to measure the surface excess concentration and AFM is used to identify the equilibrium structures of the surfactant adsorbed on the silica as a function of pH and concentration of the CPB with or without the presence of electrolyte. It was found that admicelles were formed on the surface in the absence of electrolyte. These admicelles cover about 45% of the surface area and were cylindrical in shape with a thickness of ~2 nm and a diameter of ~ 8.4 nm. In the presence of electrolyte, no admicelles were found and the surfactant adopted a structure elongated in the plane of the surface.

1.2.2.2 Co-adsorption of Multi-surfactants on Pigments

Most industrial processes using pigment suspension involve more than one surfactant. The extension of studies to mixed surfactant systems is more complex than single surfactant systems as it may involve synergistic processes between surfactants and the surface. From an experimental perspective, it is desirable to measure the individual amount of each surfactant on the surface as well as the nature of the mixed surfactant structure.

Portet-Koltalo, *et. al.*[59] used high-performance liquid chromatography (HPLC) to measure the concentration changes in the solution before and after the adsorption of the anionic surfactant sodium dodecyl sulfate (SDS) and the nonionic nonylethylene glycol n-dodecyl ether ($C_{12}E_9$) from a mixed aqueous solution onto negatively charged silica particles. At low solution concentrations, it was found that the adsorption of the $C_{12}E_9$ on the silica induces the adsorption of the SDS by forming mixed surfactant structures. While at higher concentrations (about 100 times higher than the cmc of the mixed-surfactant), there was desorption of the mixed surfactants from the silica surface and this

was attributed to two processes: 1) a strong interaction between the SDS and $C_{12}E_9$ in the aqueous solution leading to a re-adjustment of the equilibria and extraction of material from the surface and 2) the formation of mixed micelles by the SDS and $C_{12}E_9$ in the solution which led to highly negatively charged mixed micelles that are repelled from the negatively charged silica surface. Thibaut, *et. al.* found a similar behavior in a study of the adsorption of mixtures of SDS and pentaethylene glycol monodecyl ether ($C_{10}E_5$) on silica by applying surface tension measurement, micorcalorimetry measurement and thermometric measurement.[60]

1.2.2.3 Adsorption of Polymers on Pigments

Polymers are widely used to modify the interfacial properties of pigments because they provide both charge and steric stabilization. The steric stabilization arises from the extension of the polymer chains away from the pigment surfaces. Thus, when polymers are added to the particles in solution, the dispersion stability of the particles will depend on the adsorbed amount as well as the conformation of the polymer. As with surfactants, there are numerous theoretical and experimental studies on polymers on surfaces.[9, 12, 61-70]

At very low polymer concentrations, adsorption of the polymer onto the surface often leads to bridged flocculation. In essence, the surface is not completely covered by the polymer leading to bare sites in which the polymer adsorbed on one particle can bind to free sites on a second particle. Once the surface becomes saturated with an adsorbed polymer layer when using higher solution concentrations, the polymer typically adopts a conformation extending further from the surface to accommodate more polymer. In a good solvent, this leads to steric stabilization as shown in scheme 1.1.

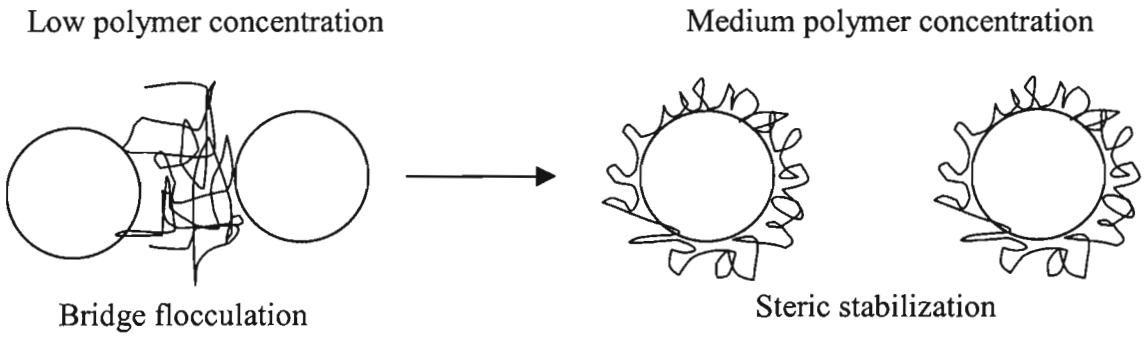

Scheme 1.1 The effects of polymer concentrations on particle interaction

1.2.2.4 Adsorption of Single Polyelectrolytes on Pigments

The sodium salt of polyacrylic acid, sodium polyacrylate (NaPA), is the primary pigment dispersant used in paper coating industry. Vermohlen, *et. al.*[68] used Diffuse Reflectance Fourier Transform Infrared (DRIFT) spectroscopy to measure the adsorption of polyacrylic acid on aluminum oxide. The adsorbed amount of the polymer on the alumina surface was measured by colorimetric titration. From the band position and intensity of the COOH and COO^- modes in the DRIFT spectra, it is found that the polyacrylic acid (PAA) polymer coordinates directly with the surface of hydrous metal oxides. Strauss, *et. al.*[12] measured the effect of PAA adsorption on the stability and rheology of TiO_2 suspensions by using zeta potential measurement and rheological measurement. The zeta potential measurement showed that the adsorbed amount of the PAA on TiO_2 was pH dependent. After the adsorption of PAA onto the TiO_2 surface, the point of zero charge (PZC) shifted to lower pH values. This shift was due to the presence of a negatively charged PAA on the particle surface. The pKa of PAA is 4.8 which is lower than the TiO_2 PZC which occurs at pH 6.5. They also found that the addition of the

PAA to the aqueous TiO_2 suspension lead to a higher content of fine grains and a lower viscosity in highly concentrated TiO_2 suspensions. It was reported that the improvement of the properties of the solid suspensions depended on the adsorbed amount of polyacrylic acid and solution pH.

Jarnstrom, *et. al.*[70] added sodium polyacrylate (NaPA) to ground calcium carbonate suspensions and measured the viscosity, zeta potential and the adsorbed amount by UV spectrometry. They related the zeta potential to surface charge and found that the NaPA acts as a dispersant by forming an electrostatic repulsive barrier. They found that polyacrylates with high levels of bound Ca^{2+} ions were poor dispersants. The average amount of bound calcium ions per monomer of the NaPA depended strongly on the pH value and NaPA concentration and did not vary with the specific surface area of the particles. The amount of NaPA required to achieve the minimum in viscosity was interpreted as the amount required to decrease the degree of Ca^{2+} ion binding to the polymer to below a certain level.

Chen, *et. al.*[9] measured the amount of NaPA adsorbed on calcium carbonate by depletion methods and correlated the results to the viscosity of the suspension. In the depletion method the amount of polymer remaining in the solution phase is measured. The amount adsorbed is the amount of polymer initially added minus the amount remaining in solution. They found the adsorbed amount of NaPA on $CaCO_3$ was significantly affected by the pH condition of the slurry, and the saturation adsorbed amount decreased as pH value increased. Thus, the viscosity of the $CaCO_3$ suspension was determined both by the pH condition of the slurry and the adsorbed amount of NaPA

on the $CaCO_3$. The higher the pH conditions of the slurry, the lower the viscosity of the nano-sized $CaCO_3$ suspension.

1.2.2.5 Co-adsorption of Ionic and Non-ionic Polyelectrolyte

Esumi, *et. al.*[71] investigated the adsorption of poly(ethyleneglycol) (PEG) and poly(amidoamine) (PAMAM) dendrimer with pendent carboxyl groups on alumina and silica particles at pH 5 by depletion methods, zeta potential measurements, sedimentation measurements and electron spin resonance (ESR) measurements. The sedimentation measurement was correlated to the stability of the dispersion. By using a spin-labeled PEG, the ESR spectrum was used to follow conformational changes of the adsorbed PEG on the silica. It was found that the PAMAM adsorbed on both the alumina and silica particles while the PEG preferred to adsorb only on the silica particles. For co-adsorption from PEG-PAMAM mixtures with a constant concentration of PEG, it was found that the PEG competes with the PAMAM for sites on the silica and alumina particles at all concentration conditions.

Ishiduki, *et. al.*[72] studied the effect of pH on the adsorption of PAA and PVP on α-alumina from their binary mixtures by measuring the adsorbed amount of polymers, the dispersion stability, and ESR spectra. The adsorption of PAA from PAA solutions showed that there was a strong affinity of the PAA for surface sites and that the adsorbed amount of PAA decreases gradually with an increase of solution pH from 5.2 to 10.2. In contrast, the adsorption of PVP from PVP solutions showed a weak interaction with surface sites and a low adsorbed amount over the entire pH region studied. However, it was shown that the adsorbed amount of PVP on an alumina surface containing

preadsorbed PAA showed a considerable increase and this was attributed to hydrogen bonding of PVP with PAA adsorbed on alumina.

1.2.2.6 Co-adsorption of Polymers and Surfactants

Water-soluble polymers and surfactants are sometimes used together in the paper coating process. Surfactants are usually used to control the flocculation and wetting properties and the polymers are used to dictate rheological properties. Liu, *et. al.* used AFM to examine the competitive adsorption of the surfactants CTAB and hexadecyltrimethylammonium chloride (CTAC) with the polyelectrolytes poly(diallyldimethylammonium chloride) (PDADMAC), polyvinylbenzyltrimethylammonium chloride (PVBTAC), and poly-L-lysine hydrobromide (PLL).[73] Both the polyelectrolytes and the surfactants are positively charged. This means that the polyelectroytes and the surfactants compete for the negatively charged sites on the silica surface. The AFM data showed that the CTAC micelles adsorbed on the silica surface hindered the adsorption of PDADMAC. When the PDADMAC adsorbed in the absence of the CTAC, it formed a featureless, neutral layer. This was not observed in the AFM image containing pre-adsorbed CTAC micelles. This is because the adsorption of CTAC generates a surface having the same charge as the polymer. When a PDADMAC coated surface was exposed to a CTAC solution above the critical micelle concentration, the CTAC adsorbed on the polymer modified silica surface had a similar structure as when adsorbed on a bare silica surface under the same conditions.

Fan. *et. al.* studied the sequential adsorption of polymer (polyacrylic acid-PAA)/surfactant (sodium dodecyl sulfate-SDS) mixtures on the alumina particles using a

turbidimeter and fluorescence spectroscopy.[74] They found that the sequence of addition of the polymer and surfactant is of critical important in determining the flocculation / deflocculation properties of the system. It was found that the addition of PAA solutions to a surface precoated with SDS, led to different PAA conformation on the surface and suspension stability as a function of the amount of SDS on the surface. When the PAA was added first, both the conformation and suspension stability of the PAA was not changed when exposed to solutions containing SDS. The non-effect of the adsorbed SDS was explained as a masking of the SDS species by the larger polymer chains.

Thibaut, *et. al.*[28] has studied the adsorption of binary mixtures of poly(vinylpyrrolidone) (PVP) and sodium dodecyl sulfate (SDS) onto silica by measuring the amount of the PVP and the heat of the adsorption using total concentration depletion method and microcalorimetry. The amount of PVP adsorbed from solutions containing PVP/SDS mixtures decreased as the SDS concentration increased. It was suggested that this is due to the formation of negatively charged PVP/SDS complexes in solution that do not absorb on the negatively charged silica. From microcalorimetric measurements it was concluded that at SDS concentration above the c.m.c, a "comblike" structure with less segments adsorbed to the surface and large segments dangling in the solution were formed at the silica/aqueous interface.

1.3 Attenuated Total Reflection

The work in this thesis centers on the use of Attenuated total Reflection (ATR). The need to use ATR stems from the strong absorption of infrared radiation by water. For example, simple transmission measurements would require pathlengths less than 25 μm to obtain transparency in the infrared region. This clearly is not practical for dynamic

measurement of the adsorption of polymer surfactants on pigment surfaces. The common approach to circumvent the limitation arising from the opacity due to water is to perform experiments using ATR.

ATR operates on the principles of internal reflection. The internal reflection originates from the fact that radiation propagating in an optically dense medium of refractive index n_1 undergoes total internal reflection at an interface of an adjacent medium of lower optical density n_2. A total internal reflection occurs when the angle of incidence exceeds a critical angle θc determined by:

$$\sin\theta_c = \frac{n_2}{n_1} \qquad (1.1)$$

In equation 1.1, the critical angle θc was determined by the refractive index where n_1 is from the denser region and n_2 is from the less dense region ($n_2<n_1$). R, the reflectivity is defined as the ratio of the reflected intensity to that of the incident intensity shown in equation 1.2.

$$R = \frac{I_{out}}{I_{in}} \qquad (1.2)$$

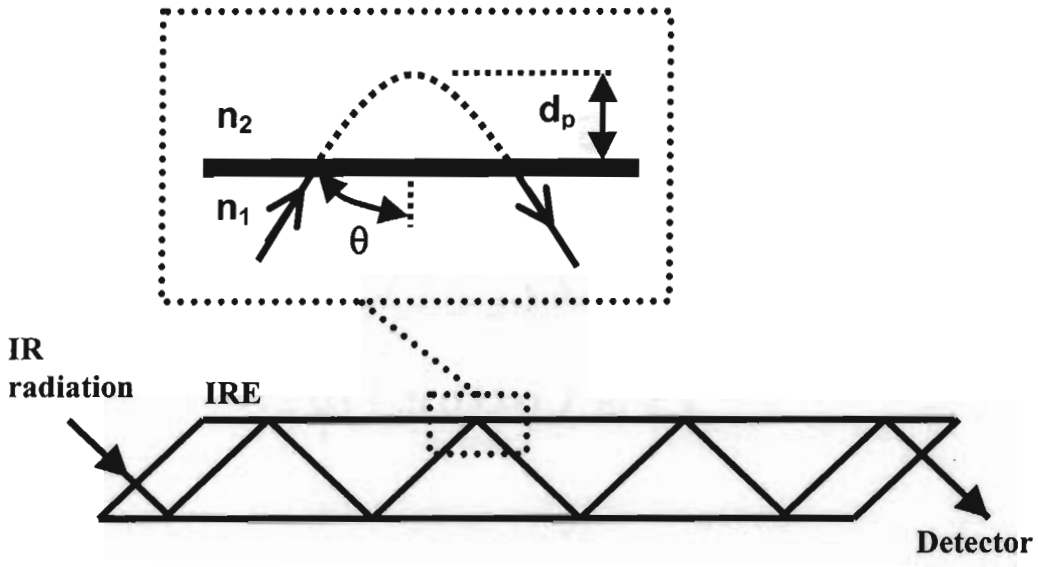

Figure 1.2 Schematic of the IR radiation light reflection at ATR interface.

d_p is the penetration depth

Figure 1.2 shows the schematic of the beam passage through a trapezoidal internal reflection element (IRE). At each reflection, an evanescent electric field (E) is generated in the less dense medium whose intensity decays exponentially with distance (z) into the rare medium as described by Equation 1.3.

$$E = E_0 e^{-zd_p} \tag{1.3}$$

where E_0 is intensity of the incident radiation and d_p, depth of penetration represents the distance at which the evanescent wave drops to 1/e times the intensity at the surface.

The depth of the penetration is calculated by the following equation.

$$d_p = \frac{\lambda}{2\pi n_1(\sin^2\theta - n_{21}^2]^{1/2}} \quad (1.4)$$

Where λ is the wavelength of the light, n_1 is the refractive index of the ATR crystal, n_2 is the refractive index of the less dense medium and $n_{21}=n_2/n_1$.

Table 1.1 shows the typical internal reflection elements used in ATR applications. For this study the ZnSe is used as the material because it is insoluble in water, relatively inert over a wide pH range, and has a wide transparency range in the infrared region. For a 45° beveled ZnSe crystals used in this work the effective penetration depth in water is calculated as 0.50 μm at 3000 cm^{-1} and 1.51 μm at 1000 cm^{-1}. This penetration depth is large enough to pass through a 500 nm TiO_2 coatings used in this studies.

When an absorbing species is present in the medium with lower reflective index, the intensity of the internal reflected light is attenuated due to absorption by the species. An infrared spectrum is produced and this can be used to measure the adsorbed amount of each component as well as the orientation of the molecule on the surface.

Table 1.1 Typical IRE materials for the ATR applications

Material	Refractive Index ($1000cm^{-1}$)	ATR Spectral Range (cm^{-1})	Water Solubility (g/100g H_2O)
Zinc Selenide (ZnSe)	2.4	20,000-650	Insoluble
Diamond	2.4	4200-200	Insoluble
Germanium	4.0	5500-870	Insoluble
Zinc Sulfide (ZnS)	2.2	17,000-950	Insoluble
Cadmium Telluride (CdTe)	2.65	10,000-450	Insoluble
Sapphire (Al_2O_3)	1.74	25,000-1800	Insoluble
KRS-5 ($TiI_2/TiBr_2$)	2.4	20,000-350	0.05
Cubic Zirconia (ZrO_2)	2.2	25,000-1800	Insoluble

1.4 Zeta Potential

1.4.1 Definition of Zeta Potential

Zeta potential measurements are used in this thesis to determine the isoelectric point of surfactant/polymer coated particles. When the particles are dispersed in the aqueous solution, their surfaces carry an electrical charge. The surface charge arises from several mechanisms. Among these are the dissociation of the ionic group on the particle surfaces and the adsorption of different ions from the solution. The net charge at the particle surface will affect the charge distribution in the nearby region and thus produce an electrical double layer at the solid/liquid interface shown in Figure 1.3. The stern plane is drawn through the ions that are strongly adsorbed to the surface, and the shear plane is

the liquid layer adjacent to the particle surface and will move with the same velocity as the particles.

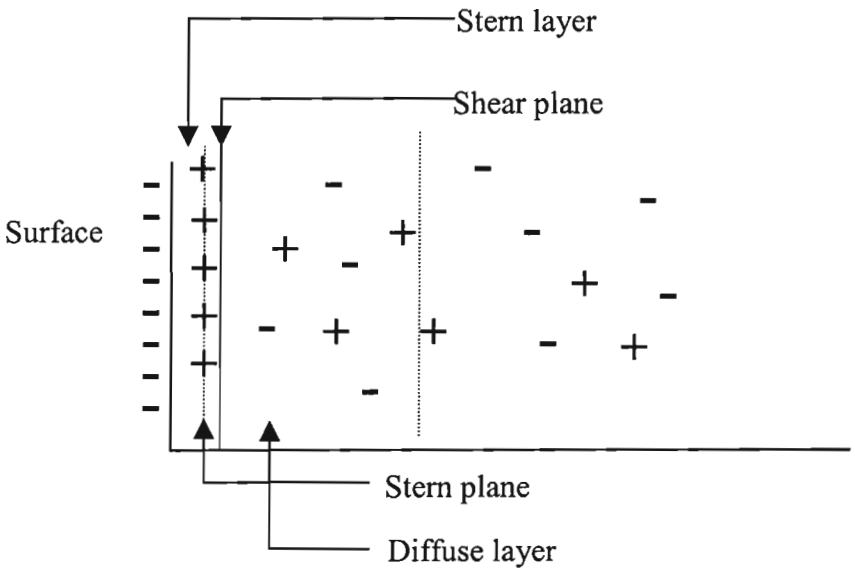

Figure 1.3 Electric double layer at the solid/liquid interface

According to the model in Figure 1.3, the shear plane occurred within the double layer and the zeta potential, ξ, is defined as the potential at the shear surface shown in Figure 1.4. The zeta potential is different from the Ψ_0 and Ψ_δ which are the potentials on the actual particle surface and stern surface.

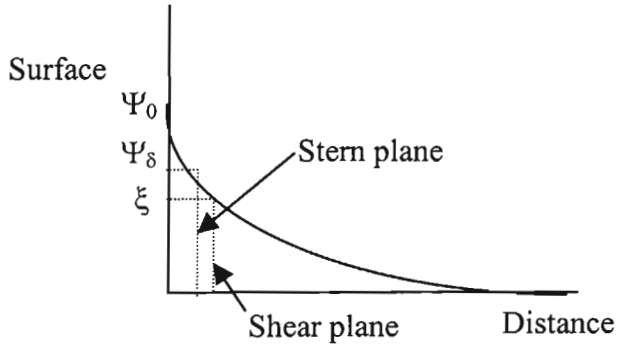

Figure 1.4 The relative magnitude of various electric double layer potentials at the solid/liquid interface

1.4.2 Measurement of Zeta Potential from Electrophoretic Mobility

Zeta potential is electrical potential exists at the shear plane of the particle and it is derived from measuring the mobility distribution of a dispersion of charged particles. Mobility is defined as the velocity of a particle per electric field and is measured by applying an electric field to the dispersion of the particles and measuring their average velocity. Zeta potential is related to the electrophoretic mobility by the Henry equation shown in Equation 1.9.

$$u = \frac{2\varepsilon\zeta}{3\eta} f(\kappa a) \qquad (1.9)$$

Where u = electrophoretic mobility

ζ = zeta potential

ε = dielectric constant

η = viscosity

$f(\kappa a)$ = Henry's function

Henry's function depends on the shape of the particle undergoing the motion and the ionic environment. κ^{-1} is a measure of the thickness of the double layer which is called the Debye length. Depending on the concentration of the ions in the diluent, either the Smoluchowski (for higher ionic strength, $\kappa a=1.5$) or Huckel (for lower ionic strength, $\kappa a=1$) approximation can be used to get the zeta potential from the measured mobility. The exact values for the Henry function can be used when the particle size is know because the Debye length can be calculated while the concentration of the ionic species are known.

CHAPTER 2. EXPERIMENTAL

This chapter describes the equipment, materials and experimental procedures that are common for performing the work described in chapters 3 to 6. Experimental procedures, materials or equipment unique to a specific chapter are described in the experimental section of that chapter.

2.1 Materials

Fumed TiO_2 (P25) and silica powder (Aerosil 380) were obtained from Dugussa. The TiO_2 has a BET N_2 surface area of 50 m^2/g and the corresponding value for silica is 380 m^2/g, the electrophoretic measurements showed TiO_2 and silica had an isoelectric point (IEP) of pH 6.5 and 2-3, respectively. The cationic surfactant cetyltrimethylammonium bromide (CTAB) was obtained from Aldrich and was purified by double recrystallization from an acetone/ethanol mixture. The anionic sodium dodecyl sulphate (SDS) was obtained from Aldrich and double recrystallized with acetone.[14] Deuterated sodium dodecyl sulphate (d_{25}-SDS, 98.5% deuterated) was obtained from CDN Isotopes and used as received. Sodium polyacrylate (NaPA) and poly(diallyldimethylammonium) chloride (PDADMAC) were purchased from Aldrich and used as received. The average molecular weight for the NaPA is 30,000 and average molecular weight for the PDADMAC is 150,000. The structures of the two surfactants and polymers are shown in scheme 2.1. 3- aminopropyldimethylethoxysilane (APDMES) is used to modify the silica surface and was obtained from United Chemical Technologies, Inc. The solvents, toluene and methanol were purchased from Aldrich.

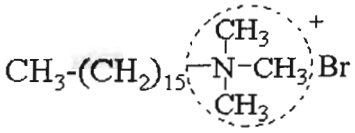

CTAB

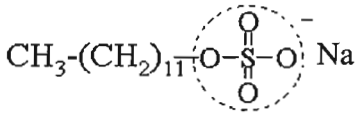

SDS

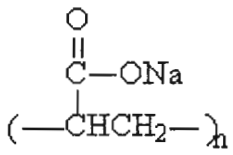

NaPA

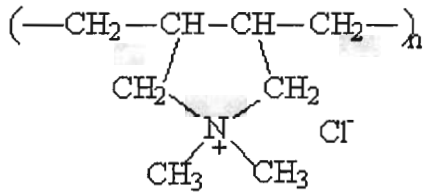

PDADMAC

Scheme 2.1 Structures of CTAB, SDS, NaPA and PDADMAC

2.2 Modification of the IRE Surface

In the ATR studies, ZnSe internal reflection elements (IRE) were used. ZnSe was selected because it has good transmission over a wide infrared region (20,000 – 650 cm^{-1}) and is inert in water over a wide pH range (2-12). Our interest is not in studying adsorption onto the ZnSe surface, but rather the adsorption on pigments used in the paper coating industry. As a consequence, there is a need to modify the surface of the ZnSe in a way to mimic the surface properties of the desired pigment or to devise methods for directly attaching pigments to the ZnSe IRE. In the latter case, the pigment should not be removed to flowing aqueous solutions containing surfactants and polyelectrolytes.

Brian Ninness in his thesis work[36] investigated several methods for attaching pigments to this surface. Pigments such as silica, kaolin and $CaCO_3$ could be deposited by solvent evaporation of a known concentration of a pigment dispersion on top of the ZnSe IRE. However, the resulting films were not stable and easily removed by simply flowing water through the ATR cell. On the other hand, Ninness found that the use of

polyethylene binder to glue the particles to the ZnSe IRE[38] provided a general method for anchoring particles to the surface. The method involved formation of a high solid content dispersion of the pigment and polyethylene in toluene. A known volume of the dispersion was applied to the surface of the ZnSe crystal and the solvent was allowed to evaporate. Stable films were produced but it was found that the large molecules such as surfactants and polymers could not access the surface of pigments.

However, it was found that stable films of TiO_2 formed on the ZnSe by simple deposition from a suspension in methanol followed by evaporation of the solvent. The films produced were stable to flowing water and solutions containing surfactants and polymers over a pH range of 2-12. As a result, the work described in this thesis uses the simplified method of preparing TiO_2 coated ZnSe IRE developed by Brian Ninness.

The following procedure was used to prepare the TiO_2 coated IRE. A suspension containing 30 mg of TiO_2 in 25 ml of methanol was prepared and placed in an ultrasonic bath for 30 min. A total of 200 μl of the titanium dioxide suspension was deposited evenly using a pipette onto the ZnSe surface. A 45° ZnSe internal reflection element (IRE) from Harrick with the dimensions of 50 x 10 x 2 mm was used in this work. Methanol was chosen as the deposition solvent because it can wet the ZnSe surface completely. After the methanol evaporated, a thin and uniform TiO_2 film of about 500 nm thickness is formed on the IRE. This leads to a random array of particles deposited on the surface as diagramed in Figure 2.1. The film thickness is near or less than the 0.5-1.51 μm penetration depth of the evanescent wave.

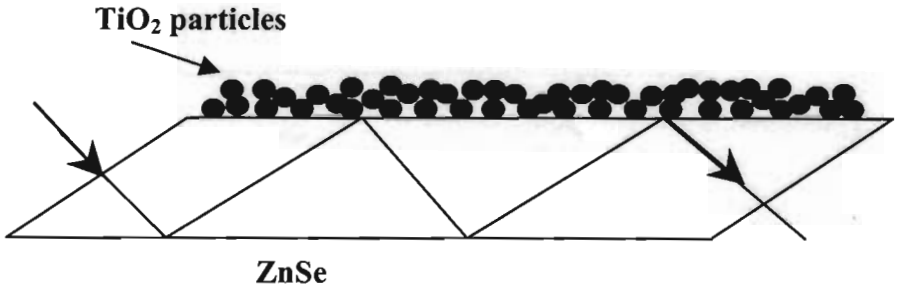

Figure 2.1 Deposition of TiO_2 film on a ZnSe IRE

2.3 ATR Experimental Setup

ATR experiments were conducted using a flow-through ATR cell from Harrick. A picture of the flow cell is shown in Figure 2.2. The coated ZnSe IRE with TiO_2 particles was mounted in the flow-through cell and flushed continually with water adjusted to the desired pH until reproducible spectra (i.e., no change in the water peaks) were obtained at 15 minute intervals until the water spectrum was stable without any bubbles. The pH was adjusted using dilute solutions of HCl or NaOH. All experiments were conducted at ambient temperature and a peristaltic pump operation at a rate of 5.8 ml/min was used to flow water and the polymer/surfactant solutions in the flow-through cell. A solution containing surfactant, polyelectrolyte or pigment particles will then be introduced into the cell and spectra were recorded at specified intervals.

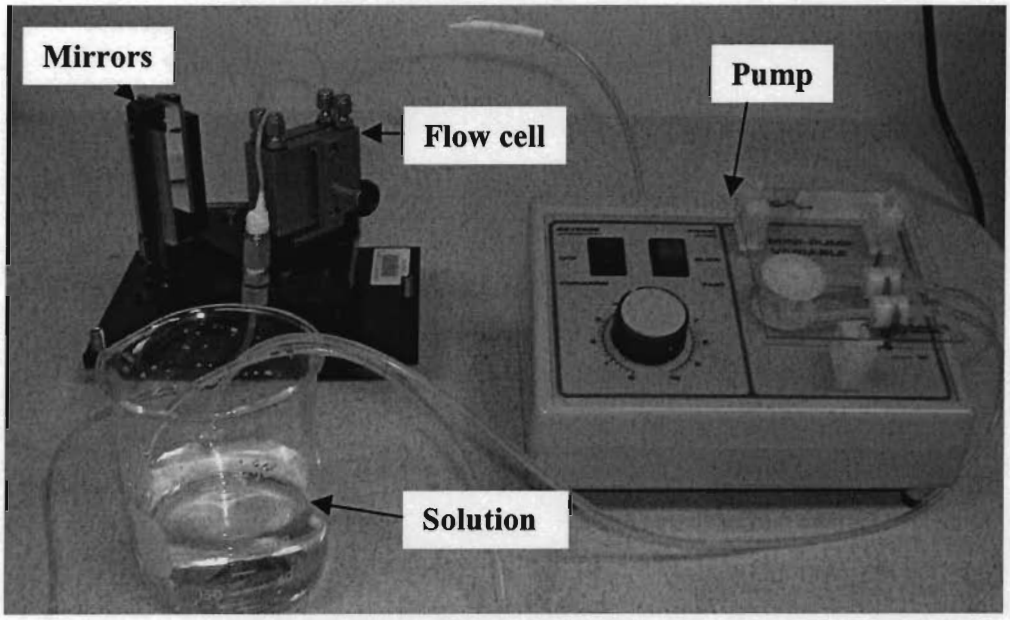

Figure 2.2 ATR Experimental Setup

2.4 Calibration of Adsorbed Amount of Surfactants and Polyelectrolyte on TiO_2

The qualitative information of the nature of the adsorbed structure was determined from the relative band position and intensities. The details for interpreting the qualitative information are described in detail in each chapter. To quantify the amounts of each adsorbent from the IR spectra required calibration of the intensity or integrated intensity of a specific IR band for each compound. This calibration was performed in order to quantify the amount of adsorbed surfactant (molecules/nm^2) and polyelectrolyte (mg/m^2) as well as to measure sample-to-sample variations in the amount of TiO_2 deposited on the ZnSe crystal.

Both the CTAB and SDS have strong CH_2 stretching mode ν_{as} at 2922 cm^{-1} and ν_s at 2850 cm^{-1}. The adsorbed amount of SDS or CTAB was calculated using the strong ν_s mode at 2850 cm^{-1}. A typical ATR spectrum obtained for CTAB adsorbed onto TiO_2 is shown in Figure 2.3. A valley-valley baseline from 2880 to 2830 cm^{-1} was used to calculate the integrated intensity of the 2850 cm^{-1} band. In chapter 4, SDS and CTAB were both adsorbed on the TiO_2 surface. Both SDS and CTAB have overlapping bands at 2922 and 2850 cm^{-1}. In this case, experiments using d_{25}-SDS were used to quantify the adsorbed amount of each surfactant, The d_{25}-SDS has strong CD_2 modes as shown in Figure 2.4 and the integrated intensity was calculated by a valley-valley baseline from 2130 to 2050 cm^{-1}.

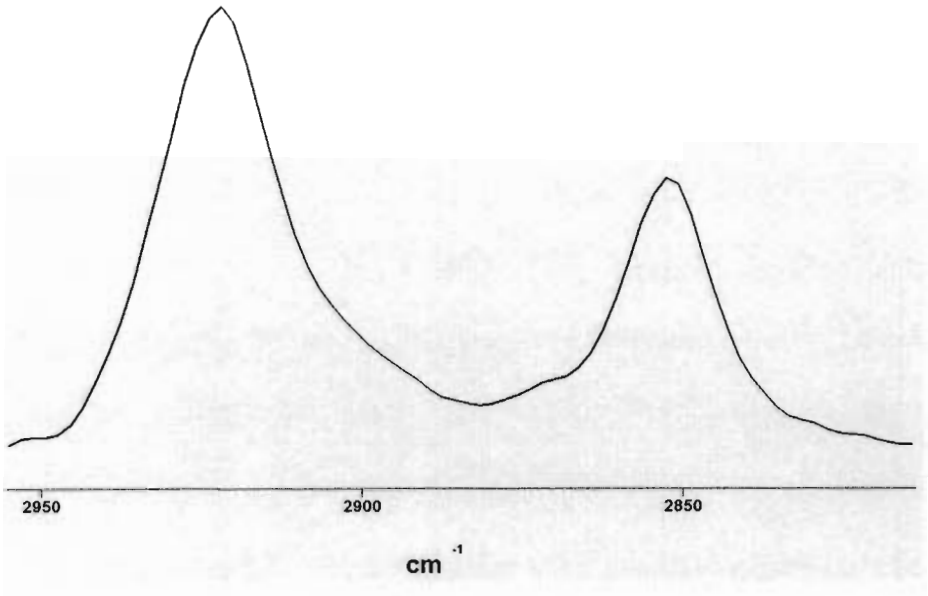

Figure 2.3 Symmetric and assymmetric CH_2 stretching modes of CTAB adsorbed on TiO_2

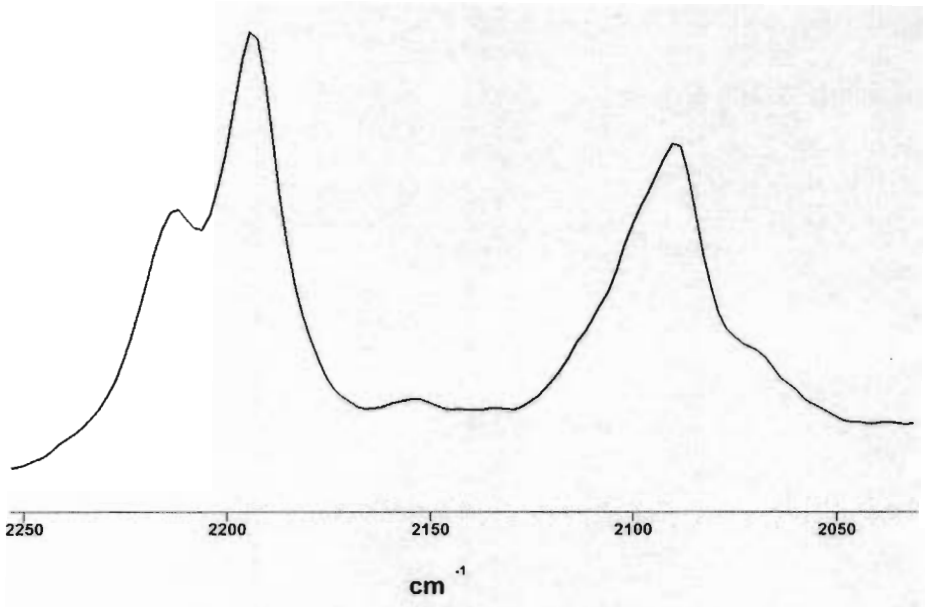

Figure 2.4 Symmetric and assymmetric CD_2 stretching modes of d_{25}-SDS adsorbed on TiO_2

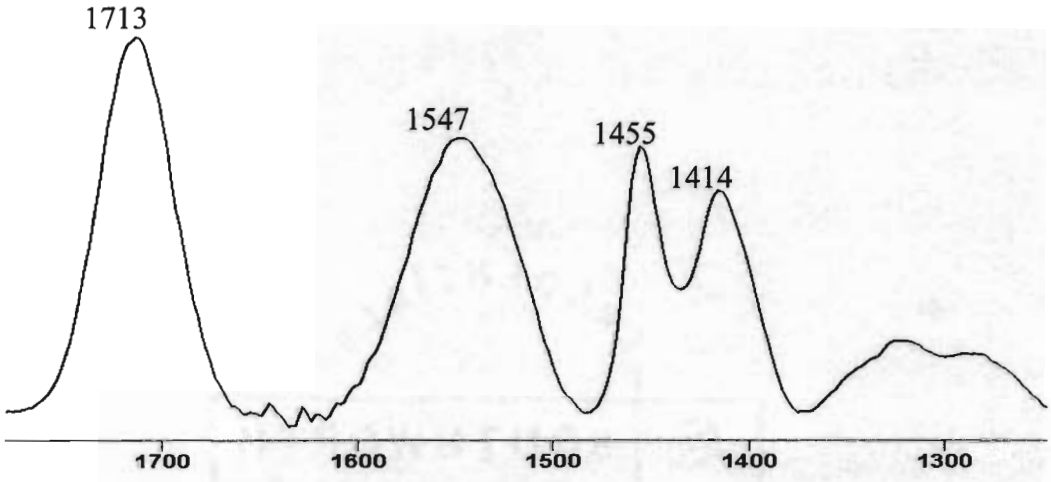

Figure 2.5 Infrared bands of NaPA adsorbed on TiO_2

Figure 2.5 shows a typical spectrum obtained for adsorbed NaPA on TiO_2. The amount of NaPA was determined from the integrated intensity of the CH_2 mode at 1455 cm^{-1}. The 1455 cm^{-1} band overlapped with the COO^- symmetric stretching mode at

1414 cm^{-1} (see Figure 2.5). To determine the integrated intensity of the 1455 cm^{-1} band, the region between 1480 and 1370 cm^{-1} was fitted to two peaks using the curve fitting program provided by Grams/32 version 4.04 from Galactic Software using a 75% Lorentzian fraction.

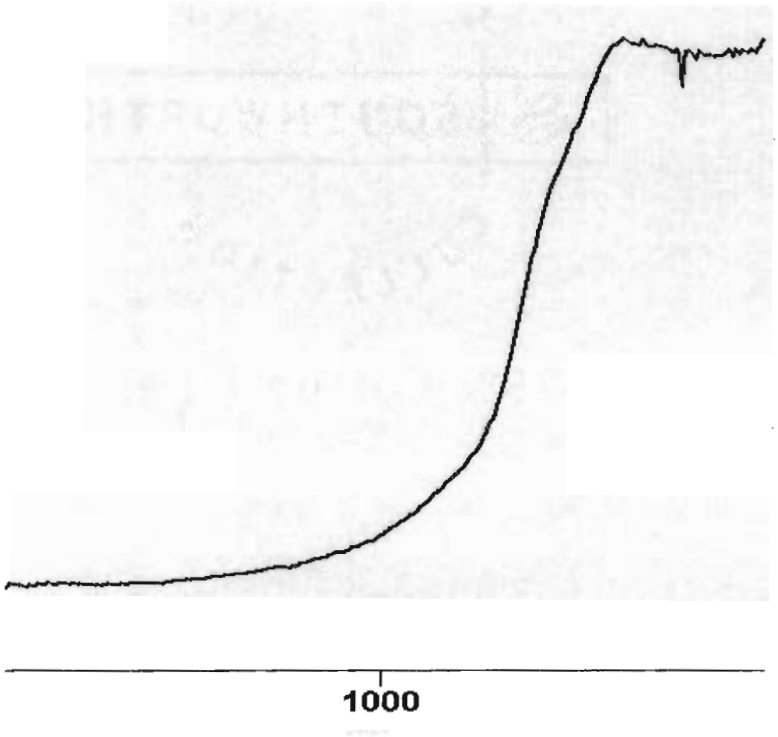

Figure 2.6 Infrared peak of TiO_2 coated on ZnSe crystal

The amount of TiO_2 deposited on the ZnSe IRE varied by ± 10% from experiment to experiment. The amount of TiO_2 deposited on the crystal was measured using the height of the Ti-O bulk mode at 635 cm^{-1} shown in the transmission spectrum in Figure 2.6. To record this spectrum, the ZnSe IRE containing the deposited TiO_2 was dried and a spectrum was recorded in transmission through the ZnSe IRE. This was done at the end of each experiment.

The following general procedure was used to calibrate the intensity of various bands. The molar adsorption of the each of the adsorbing species along with the TiO_2 was determined by dispersing known quantities in a 13 mm diameter KBr pellet and recording the transmission spectra. The extinction coefficient for each of the above bands was calculated from Beer's-Law plots using transmission spectra of KBr pellets containing different amounts of each compound. Calculation of the integrated intensity of the 2850 and 1455 cm^{-1} bands for the KBr pellets were performed using the same procedures (i.e. valley-valley baseline for the band at 2850 cm^{-1} and curve fitting for the 1455 cm^{-1} band). The band position for the NaPA band at 1455 cm^{-1} in solution appeared at 1461 cm^{-1} in the dried sample. Therefore, the limits for the curve fitting were changed to 1490 cm^{-1} and 1360 cm^{-1} for the dried samples. The calculated values of the extinction coefficients are given in Table 2.1.

Table 2.1 Extinction coefficients of the surfactant, polymer and pigment

	CTAB	SDS	d_{25}-SDS	NaPA	TiO_2
Extinction coefficients (mm^2/mg)	1331	1558	761	105	135

The above procedure provided a calibration for transmission spectra. The next step was to relate the intensity (or integrated intensity) of a band to the corresponding band recorded in the ATR experiment with flowing water through the cell. To calibrate the ATR spectrum, a spectrum of the TiO_2 coated ZnSe crystal containing adsorbed surfactant or polyelectrolyte with distilled water passing through the flow-through cell was recorded. A spectrum recorded with flowing water instead of a solution containing

the adsorbate in order to eliminate the possibility of casting of the surfactant or polymer from solution when the ZnSe was removed from the cell. Once the spectrum was recorded, the ZnSe crystal was immediately removed from the flow cell, dried and a transmission spectrum was recorded. The conversion factor between the ATR spectrum and transmission spectrum was computed from comparing the integrated intensities obtained in the two spectra. The amount of polymer, surfactant and TiO_2 (mg/cm^2, where cm^2 refers to the IR beam area) was calculated using the extinction coefficients obtained from the KBr spectra and shown in Table 2.1. To obtain a value of adsorbed amount per cm^2 area of TiO_2, the value for mg/cm^2 beam area for TiO_2 was multiplied by the surface area of the TiO_2 (50 mg/m^2) to obtain a value for the surface area of the TiO_2 per cm^2 of the IR beam.

In the above calculation, the assumption is that the surfactant or polymer in solution does not contribute to the spectrum. For experiments conducted using polymer solutions, the spectral contributions from the surfactant in solution were not detected. This was confirmed in several control experiments. For example, NaPA does not adsorb on TiO_2 at solution pH above 7. When a 25 ppm solution of NaPA (the same concentration used in experiments at pH < 7) is flowed across a TiO_2 surface at solution pH 10, no bands due to NaPA are detected in the spectrum.

In chapters 3 and 4, experiments were conducted at different CTAB and d_{25}-SDS solution concentrations. At solution concentrations above 0.1 mM, bands due to CTAB and d_{25}-SDS in solution did contribute to the overall spectrum. In this case, this spectral contribution from the CTAB or d_{25}-SDS in solution was determined by recording spectra through the ATR setup containing a bare TiO_2 coated ZnSe crystal at a pH where CTAB

or d_{25}-SDS does not adsorb on TiO_2. For CTAB this was pH 3 and for d_{25}-SDS the solution pH was 10.3. These spectra recorded for CTAB and d_{25}-SDS at different solution concentrations was then used to subtract out the spectral contribution from the surfactant in solution from the overall spectrum recorded during an adsorption experiment. It is noted that this correction was small, accounting for less than 10% of the total band intensity at the highest d_{25}-SDS and CTAB concentrations.

2.5 FTIR and Zeta Potential Measurements

All the ATR experiments were carried out on a Bomem Dual Beam modified FTIR spectrometer with a liquid-nitrogen-cooled detector.[39,40] Typically, 100 scans were coadded at a resolution of 4 cm^{-1}. The transmission of the TiO_2 coated on ZnSe IRE and all the calibration experiments for surfactants and polymers were measured by a Bomem 102 Infrared spectrometer. The zeta potential values of the particle suspension were measured by Zetasizer 3000 HS_A from Malvern Instruments. The suspension was prepared by mixed less than 5 mg pigments with 500 ml di-water and sonicated for 30 min before use.

CHAPETER 3. SPECTROSCOPIC IDENTIFICATION AND DYNAMICS OF ADSORBED CETYLTRIMETHYLAMMONIUM BROMIDE (CTAB) STRUCTURES ON TiO_2 SURFACES

3.1 Introduction

Knowledge of the structure and dynamics of adsorbed surfactants on charged metal oxide surfaces across the entire adsorption isotherm has importance to many industrial processes.[1, 42] Adsorption isotherms typically are characterized by two plateau regions giving rise to a "double S" shape.[43] The boundaries between the plateau regions are defined by abrupt changes in the adsorption curve and these have been attributed to changes in the nature of the surfactant aggregation on the surface. It is generally accepted that hemimicelles form on the surface in which the adsorbed surfactant molecules begin to associate through the hydrophobic effect into surface aggregates. This concept of a hemimicellar structure in which the molecules tend to adsorb in clusters was proposed almost 50 years ago[44] and explains the rapid rise in the S-shaped isotherm.[20, 45] Above the critical micelle concentration (c.m.c.), there is a second plateau region in the adsorption isotherm and recent AFM data on various surfaces[46] has shown that the surfactant exists as globular micelles rather than a patchy bilayer.

The adsorbed surfactant structure has been the subject of numerous theoretical[19, 47-49] and experimental[17, 18, 39, 40, 46, 50-57] studies because the structure is important in dictating interfacial and colloidal properties.[58] A common model system in both theoretical and experimental studies involve the adsorption of cetyltrimethylammonium

bromide (CTAB) at the metal oxide-aqueous surfactant solution interface. The structure of the adsorbed CTAB has been probed by a variety of experimental techniques including depletion methods,[17, 50, 51] AFM,[18, 52-55] Fourier transform infrared attenuated total reflection (ATR) spectroscopy[39, 40, 56] and optical reflectometry.[57]

In this work I have used ATR spectroscopy to study the dynamics of the adsorption of CTAB on an oxidized silicon wafer[39, 40] and on TiO_2 powders supported on a ZnSe crystal.[14] Amphiphilic molecules such as CTAB have long hydrocarbon tails giving rise to two intense methylene modes near 2922 and 2850 cm^{-1}. By monitoring the change in intensity of the methylene modes, it was possible to obtain information on the equilibrium and dynamic adsorbed amount of CTAB on both substrates. However, the two ATR methods require different approaches to extract structural information.

Information of the orientation of the surfactant tails can be obtained by employing IR polarization techniques with the oxidized silicon wafers[39] but these measurements are not possible with the TiO_2 powder coated ATR crystal because the powder surface is randomly orientated with respect to the flat ZnSe crystal. In this case, Ninness *et. al.*[14] demonstrated that the frequency location and width of the methylene stretching modes are sensitive to the ratio of gauche/trans conformers ratio of the chains and thus provide structural information of the packing density of the surfactants. Typically, a highly ordered structure leads to an all-trans conformation resulting in a shift to lower frequency and a decrease in width (measured by the full width at half height, FWHH) of the CTAB methylene stretching modes. The identification of the CTAB structure on the TiO_2 surface was determined by measuring the uptake of the anionic surfactant sodium dodecylsulfate (SDS) and the resultant shift in frequency in the methylene asymmetric

stretching band near 2922 cm^{-1}. By using the SDS as a probe molecule, it was shown that the structure of the CTAB hemimicelle was critical in dictating the subsequent interaction with oppositely charged surfactants and polyelectrolytes.[14]

The ATR work with CTAB adsorption on TiO_2 powders was conducted only at a single surfactant concentration in the range where hemimicellar structures are expected to form on the TiO_2 surface. The work described here is an extension of the previous ATR work with TiO_2 powders to encompass a wider range of concentration regions of the CTAB adsorption isotherm. An additional advantage of using the high surface area TiO_2 powders compared to the oxidized silicon wafer is that it provides the necessary sensitivity and spectral range for detection of the weak bands due to the CTAB surfactant headgroups. By now extending these studies to a range of CTAB concentrations, it is found that the relative intensity of bands due to CTAB headgroup provides a unique glimpse of the structure of the surfactant layer on the surface and shows the potential of this method for elucidation of the various structures occurring at various points along the surfactant adsorption isotherm.

3.2 Experimental Section

Fumed titanium dioxide (P25) powder was obtained from Degussa, (BET N_2 surface area of 50 m^2/g) and electrophoretic measurements showed it had an isoelectric point (IEP) of pH 6.5. All CTAB adsorption experiments were conducted at a pH of 10.3 and at this pH, the TiO_2 surface is negatively charged. The cationic surfactant cetyltrimethylammonium bromide (CTAB) was obtained from Aldrich and was purified by double recrystallization from an acetone/ethanol mixture.[75] The surface tension vs. log

concentration plot (not shown here) for CTAB showed no indication of surface-active impurities.

All aspects of the experimental setup, the protocols for addition of the CTAB, recording of spectra and the use of calibration curves are described in chapter 2. One additional procedure is described here and was added in order to compensate for the spectral contributions for the bulk solution at the highest surfactant concentrations. The earlier work[58] was conducted at a single CTAB concentration of 0.01 mM and at this dilute concentration, the spectral contributions from CTAB in solution were negligible in comparison to the spectral features due to adsorbed species. However, at higher concentrations (>1 mM) there is a spectral contribution from the bulk solution that must be considered. In these experiments, the integrated intensity of the methylene mode at 2850 cm^{-1} is used to measure the amount of CTAB on the surface. The contribution to the overall integrated intensity of the 2850 cm^{-1} band from CTAB in the solution phase was determined using the following procedure. Spectra were recorded as a function of CTAB concentration using the same TiO_2 coated ZnSe at a pH of 2.5. At this pH there is no CTAB adsorption on the positively charged TiO_2 and all spectral features are due to the CTAB in the bulk. These bulk values are then used to calculate the contributions to the spectra from adsorbed and solution CTAB in the experiments conducted at a pH of 10.3. The amount of CTAB adsorbed at pH of 10.3 for a given CTAB concentration is determined from the overall integrated intensity of the methylene mode at 2850 cm^{-1} minus the value obtained for bulk contribution. Typically this was a small correction as at the highest solution concentrations (10 mM), the contribution from the bulk was approximately 10% of the total integrated intensity.

3.3 Results and Discussion

3.3.1 CTAB Adsorption Isotherm and CTAB Headgroup

Figure 3.1 shows the time dependant adsorption of CTAB on TiO_2 at pH of 10.3 recorded for several concentrations. The curves in Figure 3.1 are generated from a plot of the integrated intensity of the methylene mode at 2850 cm^{-1} and are converted to CTAB molecules/nm^2 surface area using a procedure described elsewhere.[14] Although all curves show different initial rates of adsorption, the amount of adsorbed CTAB plateaus to a constant value and these values are then used to generate the adsorption isotherm shown in Figure 3.2. The curve in Figure 3.2 is the typical two-step adsorption isotherm for an ionic surfactant onto an opposite charged surface.[43] Five regions were identified and labeled I through V that are associated with abrupt changes in the adsorption isotherm or in the 1396/2850 cm^{-1} band ratio. The use of an abrupt change in the 1396/2850 cm^{-1} band ratio to determine structural changes is described in more detail later in this section.

For all points on the adsorption isotherm the frequency position and FWHH of the methylene stretching modes (2922 and 2850 cm^{-1}) remain unchanged and this is characteristic of loosely packed surfactant tails for all structures across the entire adsorption isotherm (spectra not shown). This is not surprising, as solution studies have shown that the methylene stretching modes for both micelle and free CTAB in solution appear at the same frequency (2922 cm^{-1}) and have similar FWHH.[76,77]

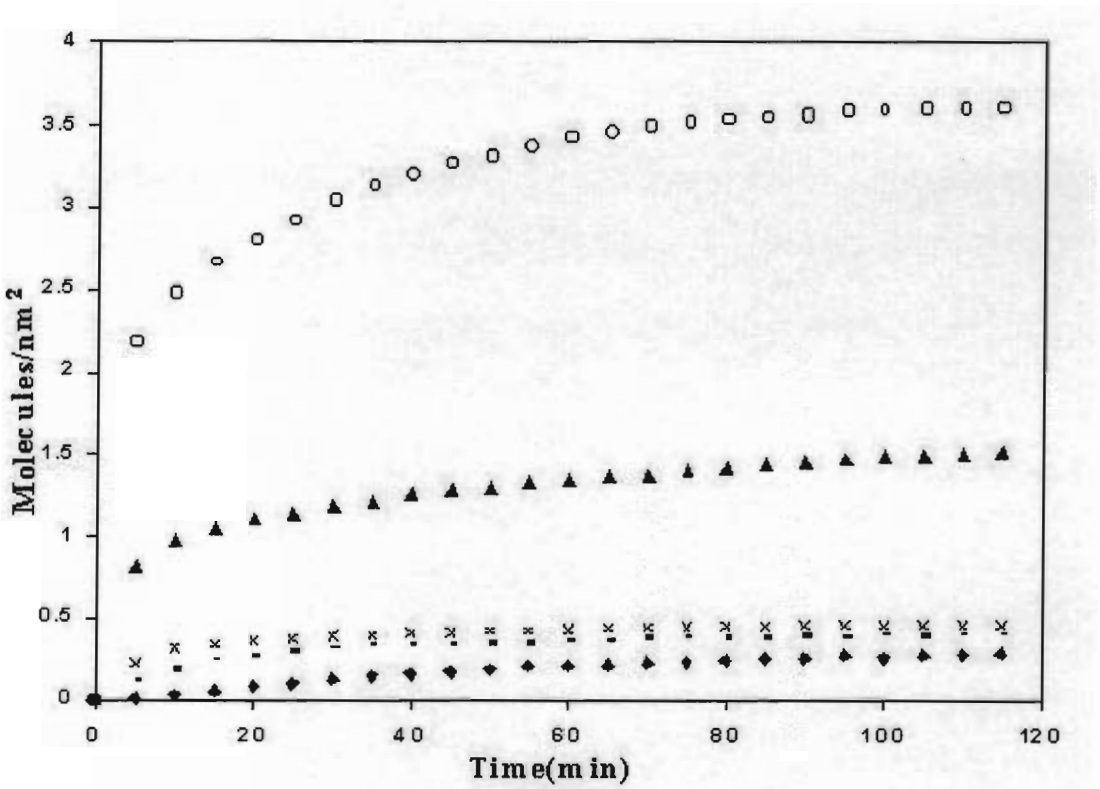

Figure 3.1 Time dependent adsorption of CTAB on TiO_2 at pH 10.3 at CTAB concentrations of 6.7×10^{-7} M (♦), 3.0×10^{-6} M (- - -), 1.0×10^{-4}M (x), 3.4×10^{-4} M (▲) and 1.0×10^{-2} M (o)

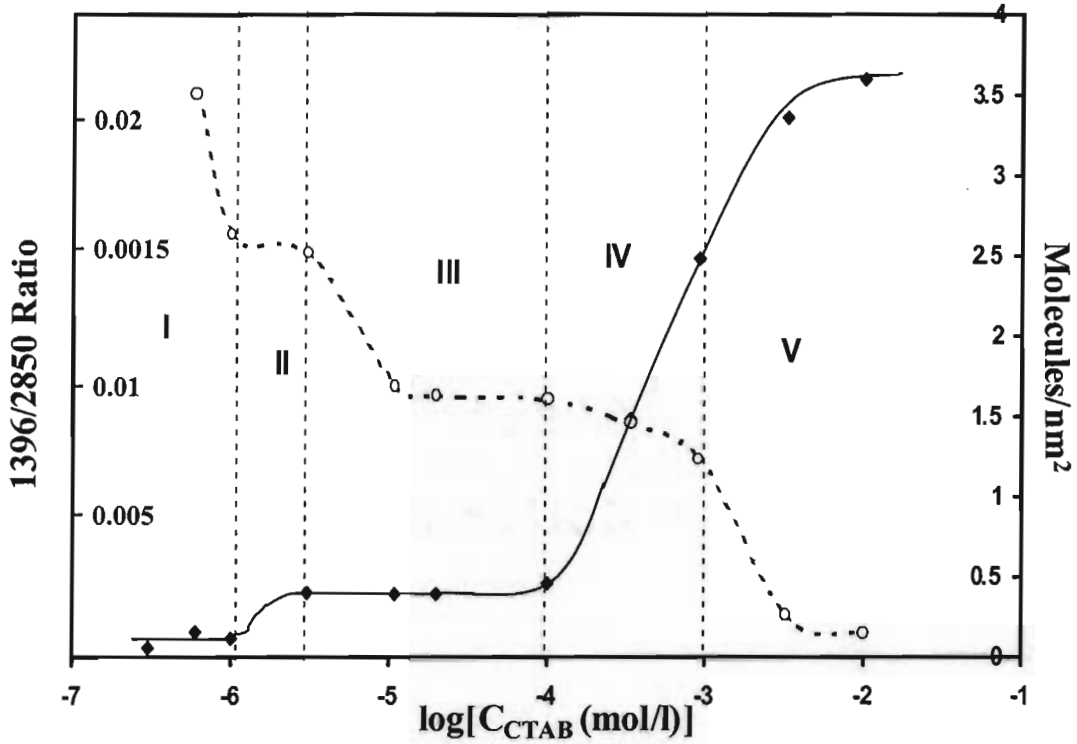

Figure 3.2 The adsorption isotherm of CTAB adsorbed on TiO_2 at pH 10.3. The dashed curve (o) is the 1396/2850 cm^{-1} ratio recorded at each point of the isotherm.

Typical IR spectra of the headgroup region of adsorbed CTAB on TiO_2 in Regions I, III, and V of the adsorption isotherm are shown in Figure 3.3. While there is little change in the position and FWHH of bands due to methylene tail, the headgroup region has detectable changes in relative intensities of various bands. The spectra in Figure 3.3 contain bands assigned to the headgroup interspersed with bands at 1468 cm^{-1} (δ CH_2), 1420 cm^{-1} (δ αCH_2) and 1380 cm^{-1} (δ CH_3-R) due to various bending modes of the surfactant tail.[77] The two bands at 1490 and 1480 cm^{-1} are the asymmetric CH_3-N^+ deformation modes (δ_{as} CH_3-N^+) of the CTAB headgroup and these bands are sensitive to the packing density.[76,77] The appearance of two bands at 1490 and 1480 cm^{-1} in all three spectra shows that a fully hydrated, disordered headgroup region occurs at all points

across the adsorption isotherm. This is consistent with the disordered state of the surfactant tails as determined by the common frequency and FWHH of the CH_2 methylene stretching modes.

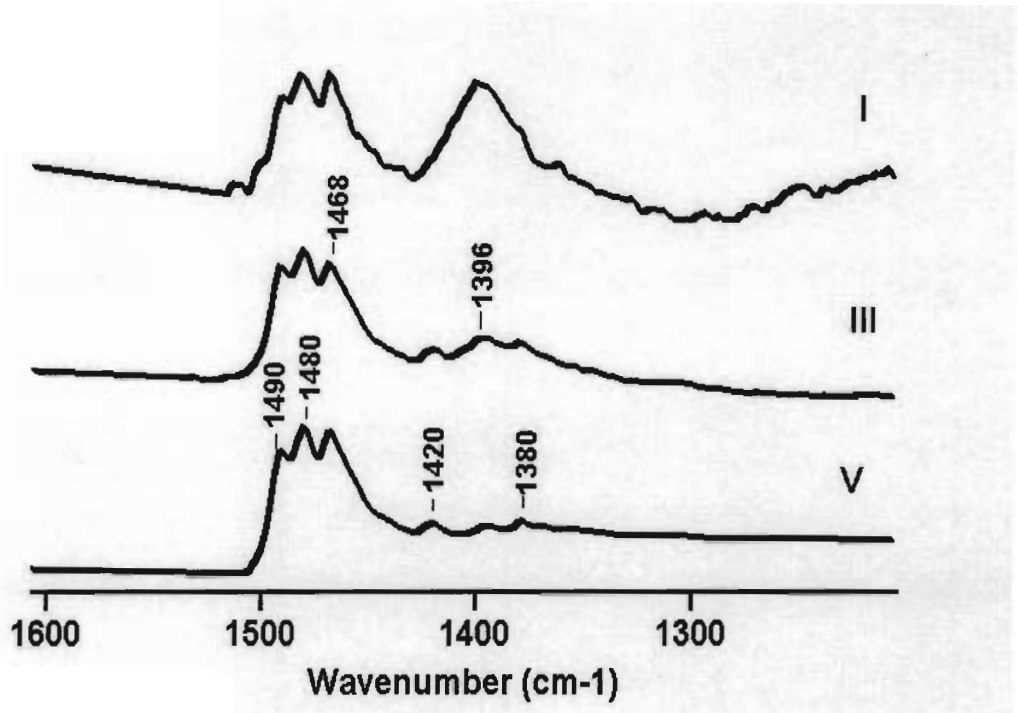

Figure 3.3 Infrared spectra of CTAB adsorbed on TiO_2. The labels I, III, and V refer to the regions defined in Figure 3.2 and represent CTAB solution concentrations of 6.7×10^{-7} M, 1.0×10^{-4} M, and 1.0×10^{-2} M, respectively.

By far, the most prominent difference in the CTAB headgroup region of the spectra is the change in the relative intensity of the symmetric deformation mode (δ_s CH_3-N^+) at 1396 cm^{-1}. To explain this change in intensity, An analogy was drawn with the trends observed for the sulfate headgroup bands of SDS in solution.[76, 77] The transition moment vectors associated with the symmetric and asymmetric S-O stretching modes of the sulfate headgroup are normal to each other. (see Scheme 3.1) The asymmetric stretching mode is nearly parallel to the micellar surface of SDS in the direction of

neighboring surfactants and consequently, changes in intensity in this band are sensitive to surfactant packing density. On the other hand, the transition moment vector for the symmetric S-O stretching mode is normal to the surface and its intensity is dependent on the presence of oppositely charged ions normal to the micelle surface.[78] It is found that the trend for the δ_s CH_3-N^+ mode at 1396 cm^{-1} mimics that of the S-O symmetric stretching mode of SDS. That is, the transition moment vector for the δ_s CH_3-N^+ band at 1396 cm^{-1} of CTAB is normal to the micelle surface. Furthermore, in separate solution studies, it was found that the spectra of micellar solutions of CTAB show an increase in intensity of 1396 cm^{-1} band with increasing NaCl concentration.

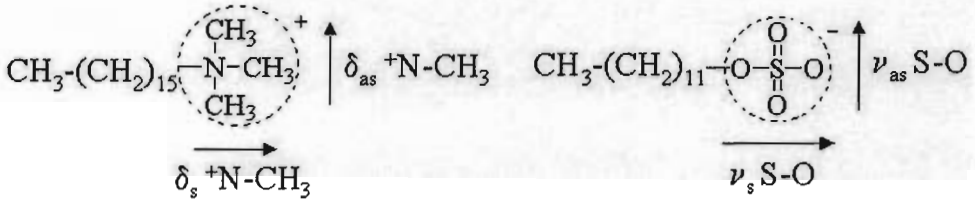

Scheme 3.1 Transition dipole moments of headgroup bands of CTAB and SDS

Given that the three curves shown in Figure 3.3 are recorded under the same pH and ionic strength, the only source of counter charge giving rise to an increase in intensity of the 1396 cm^{-1} band are those on the TiO_2 surface. Thus the intensity of the 1396 cm^{-1} bands provides an indication of the number of CTAB molecules bound to the surface through electrostatic interactions with negative charge sites on the surface. The value computed for the intensity of the 1396 cm^{-1} band (i.e., number of CTAB molecules adsorbed via electrostatic interactions with surface sites) ratiod to the methylene band at 2850 cm^{-1} (i.e., total number of CTAB molecules adsorbed on the surface) reflects the

percentage of CTAB molecules in the aggregated structure that interact directly with charged sites on the surface.

$$\frac{1396}{2850} \propto \frac{\textit{Number of bound CTAB to charged sites on the surface}}{\textit{Total number of adsorbed CTAB}}$$

These values have been calculated and are plotted as the dotted curve superimposed on the adsorption isotherm of Figure 3.2. Using the absolute values of 1396/2850 ratio to provide a direct measurement of the absolute number of surfactant molecules bound electrostatically to the surface is an oversimplification because there are several factors contributing to the intensity of the 1396 cm^{-1} band (e.g., strength of the electrostatic interaction, type of charged sites on the surface, orientation of the surfactant on the surface). Therefore, of particular interest are the points along the adsorption isotherm where an abrupt change in the slope of the 1396/2850 ratio occurs as this indicates a change in the organized surfactant structure on the surface.

At very low concentration (Region I), the generally accepted picture is that unassociated molecules are adsorbed via attractive electrostatic interactions between the cationic CTAB and the anionic TiO_2 surface (see scheme 3.2). Since each adsorbed CTAB molecule interacts with the charged sites on the surface through an electrostatic interaction, the highest 1396/2850 ratio is expected and is observed. However, there is a decrease in the 1396/2850 ratio with increasing concentration across Region I. A lower 1396/2850 ratio is expected when a fraction of the surfactant molecules is not directly involved with electrostatic interactions with the surface. This then would imply that the onset of aggregated structures occurs in this very low concentration region and before reaching the start of Region II.

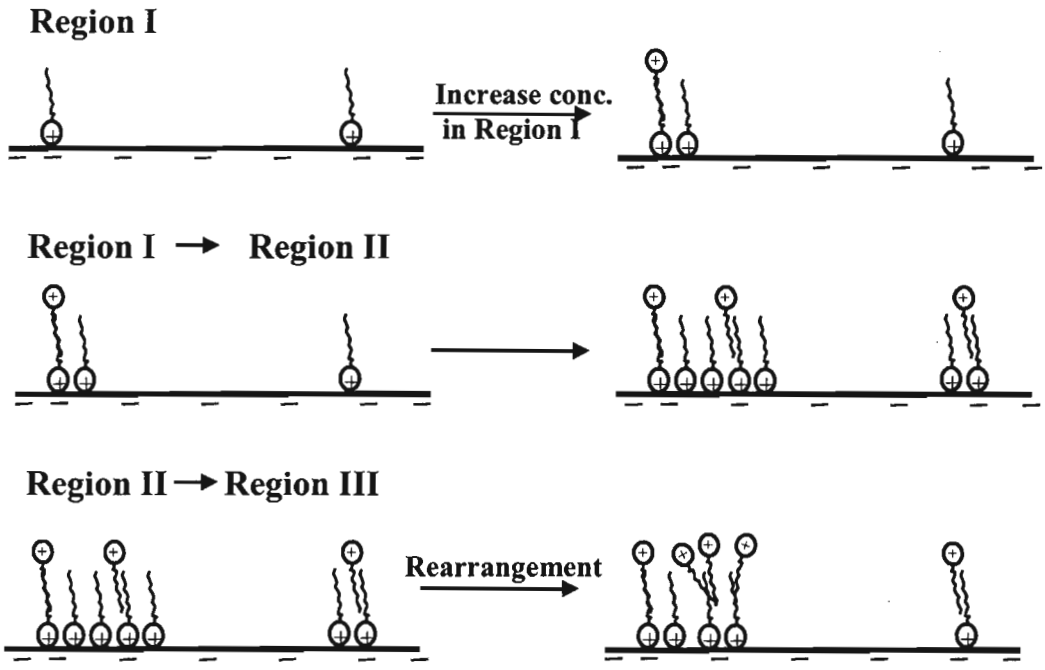

Scheme 3.2 Representative structures consistent with 1396/2850 ratios for Regions I to III.

The first rise in the adsorption isotherm (Region II) characterized by an increase in the adsorbed amount of CTAB has been attributed to the onset of formation of hemimicelles.[57] It is found that the increase in CTAB is accompanied by no change in the 1396/2850 ratio. This means that both the 1396 and 2850 cm^{-1} bands increase at the same rate suggesting that this rise is due to an increase in density of similar aggregated structures and not from a transition from isolated adsorbed CTAB to aggregated structures (scheme 3.2).

A second abrupt decrease in the 1396/2850 ratio occurs at the Region II/III border. At this point, the adsorbed amount of CTAB reaches a plateau, which means that the decrease in 1396/2850 ratio is due to a decrease in intensity of the 1396 cm^{-1} band. This implies that there is a rearrangement in structure in which there is a transfer of some

adsorbed CTAB interacting with charge surface sites to the second patchy layer. One possible explanation is that the increase in aggregated structures across Region II occurs in close proximity to each other that then coalesces into a hemimicellar structure on the surface (see scheme 3.2). Region III is relatively uninteresting as both the amount of adsorbed CTAB and the 1396/2850 ratio remain almost constant showing that there is no change in structure or amount of surfactant on the surface.

Despite the large change in adsorbed amount occurring across Region IV, the IR data shows that this is accompanied by only a small decrease in the 1396/2850 band ratio. There has been much debate on the structural origin leading to the largest increase in adsorbed surfactant that occurs across Region IV of the adsorption isotherm. One suggestion for this rapid rise has been a transition from a hemimicellar structure to an admicelle described as a transition to a contiguous patchy bilayer containing a significant number of surfactants with head groups pointing away from the surface into the solution (see Scheme 3.3).[77] A transition from hemimicelle to admicelle may account for the small change in the 1396/2850 ratio but it is not the major source for the 5-fold increase in adsorbed CTAB. One could argue that the 1396/2850 cm^{-1} ratio is no longer sensitive to structural changes at the higher surface concentrations but this is not the case as there is another abrupt change in the 1396/2850 ratio in traversing between Regions IV and V. Given that both the intensity of the 1396 and 2850 cm^{-1} increase at about the same rate across Region IV, it is most likely that the rise in adsorbed surfactant is primarily due to an increase in the density of similar structures (either hemimicellar or admicelle) on the surface.

Region III → Region IV

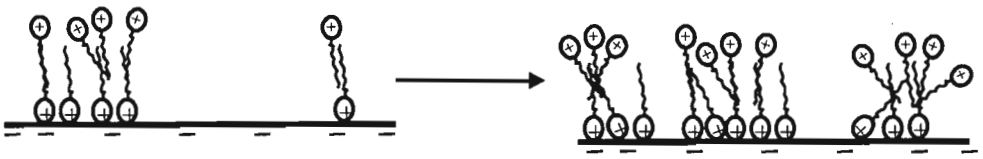

Region IV → Region V

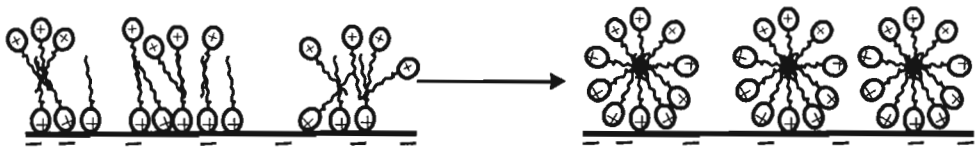

Scheme 3.3 Representative structures consistent with 1396/2850 ratios for Regions IV and V.

The transition from Region IV to V occurs at a concentration of CTAB near the c.m.c. (9.0×10^{-4} M) and is defined by an abrupt decrease in the 1396/2850 cm^{-1} intensity ratio. The location for the Region IV/V border occurs well before the transition to a plateau value for the amount of surfactant on the surface. Although the amount of adsorbed surfactant increases to a plateau value in Region V, the abrupt decrease in the 1396/2850 ratio is primarily due to a decrease in intensity of the 1396 cm^{-1} band which, in turn, translates to a drop in the number of CTAB surfactant molecules electrostatically adsorbed with surface charged sites. In fact, the absolute intensity of the 1396 cm^{-1} band in Region V is about 50% lower that the same value for the first point (Region I) of the 1396/2850 curve shown in Figure 3.2. This decrease in intensity occurs even though there is 24 times more CTAB adsorbed in the plateau of Region V compared to the first point of Region I.

One proposed structure for explaining the plateau above the CMC is that micelles act as a reservoir for surfactant adsorption.[43] The adsorption isotherm would be predicted to plateau in Region V because the surface is largely congested with hemimicelles/admicelles and steric interactions between these surface structures inhibit further surfactant adsorption on the surface. However, the data suggests an alternative explanation. The dramatic decrease in the 1396/2850 ratio is consistent with the adsorption occurring through micellar structures in Region V. From simple geometric arguments, the number of CTAB molecules in contact with the surface is lower in a micelle structure than with a hemimicellar structure (see scheme 3.3). This assignment is consistent with a recent AFM study reporting that formation of globular surface micelles of CTAB on rutile crystal surfaces above the c.m.c..[46]

3.3.2 Dynamics of CTAB Adsorption

One consequence of measuring the time dependence of CTAB adsorption is that it is possible to obtain information on the dynamics of the surfactant structural formation on the surface. An estimate of the time for an aggregated structure to form on the surface is given by the time for the initial decay in the time dependence plot of the 1396/2850 ratio in Figure 3.4 to a plateau value. From Figure 3.4, the time for the formation of the organized surfactant structures occur within 5 minutes of the initial contact (initial contact is defined as the time for the first appearance of surfactant bands in the infrared spectrum) in Regions II- IV and about 15-40 minutes in Region V. In Region I, the 1396/2850 ratio is not plotted below the 25 minute contact time because the 1396 cm^{-1} band was too weak in intensity. This initial drop in the 1396/2850 ratio for Regions II- V suggests that aggregated structures appear in all regions and that the adsorption occurs in

a stepwise process. For example, in Regions III and IV the CTAB initially adsorbs on charged surface sites (higher 1396/2850 ratio) followed by aggregation within 5 minutes to hemimicellar/admicelle structures. The longer decay time for Region V could be explained by a transition from an initial "pancake" type micellar structure to a more spherical micelle with an increase in packing density. An alternative explanation is that micelle adsorption does not occur directly but rather through a stepwise process involving intermediate hemimicellar/admicelle type structures.

To test this possibility, in a separate experiment, a CTAB solution above the CMC concentration was added to a TiO_2 surface already containing a hemimicellar CTAB structure. Specifically, a more general experiment was performed where CTAB solution was added in increasing concentrations from 0.001 mM to 10 mM in incremental steps. At each concentration the CTAB was allowed to reach the equilibrium adsorbed amount before increasing the solution concentration. The equilibrium adsorbed amount and the 1396/2850 ratio for this experiment is plotted in Figure 3.5. There is a good agreement in the values obtained for the equilibrium adsorbed amounts of CTAB and the 1396/2850 ratio shown in Figure 3.5 with the same curves shown in Figure 3.2. Furthermore, the rate of change in the time dependent plots of the 1396/2850 ratio followed the same trends at concentrations below the c.m.c. (see Figure 3.6). At concentrations near and above the c.m.c. of CTAB, the 1396/2850 ratio continues to decrease over much longer periods than observed when the same CTAB concentrated solutions are exposed to a bare TiO_2 surface as shown in Figure 3.4. For example, at point C in Figure 3.6, the 1396/2850 initially shows a sharp drop in value and then continues in a linear decrease over the total 2 hr incubation period. To help illustrate the

origin of this slower decrease in 1390/2850 ratio, the individual changes in intensity for both the 2850 and 1396 cm^{-1} bands are plotted in Figure 3.7. At point C in Figure 3.7, both the 2850 and 1396 cm^{-1} bands show an initial sharp increase but as shown in Figure 3.6, this translates to a sharp decrease in the 1396/2850 ratio. This can be explained by adsorption of micelles onto bare areas of the TiO_2. Once these bare areas are filled, the adsorbed amount increases more slowly and this is accompanied by a linear decrease in the 1396 cm^{-1} band. This shows that there is a slow exchange or transition of the existing adsorbed hemimicellar/admicelle structure to a micelle structure on the surface. This is clearly the case at point D where addition of 3 $x10^{-3}$ M CTAB results in almost no increase in adsorbed amount of CTAB while at the same time, there is a dramatic decrease in intensity of the 1396 cm^{-1} band. Given that the 1396 cm^{-1} band decreases in intensity when exposed to concentrations above the c.m.c. and all the other common trends in both the dynamic and equilibrium behavior with CTAB addition to either a bare or CTAB covered TiO_2 surface, it is concluded that CTAB adsorption could proceed through a series of intermediate structures on the surface and not necessarily by a direct adsorption of micelles.

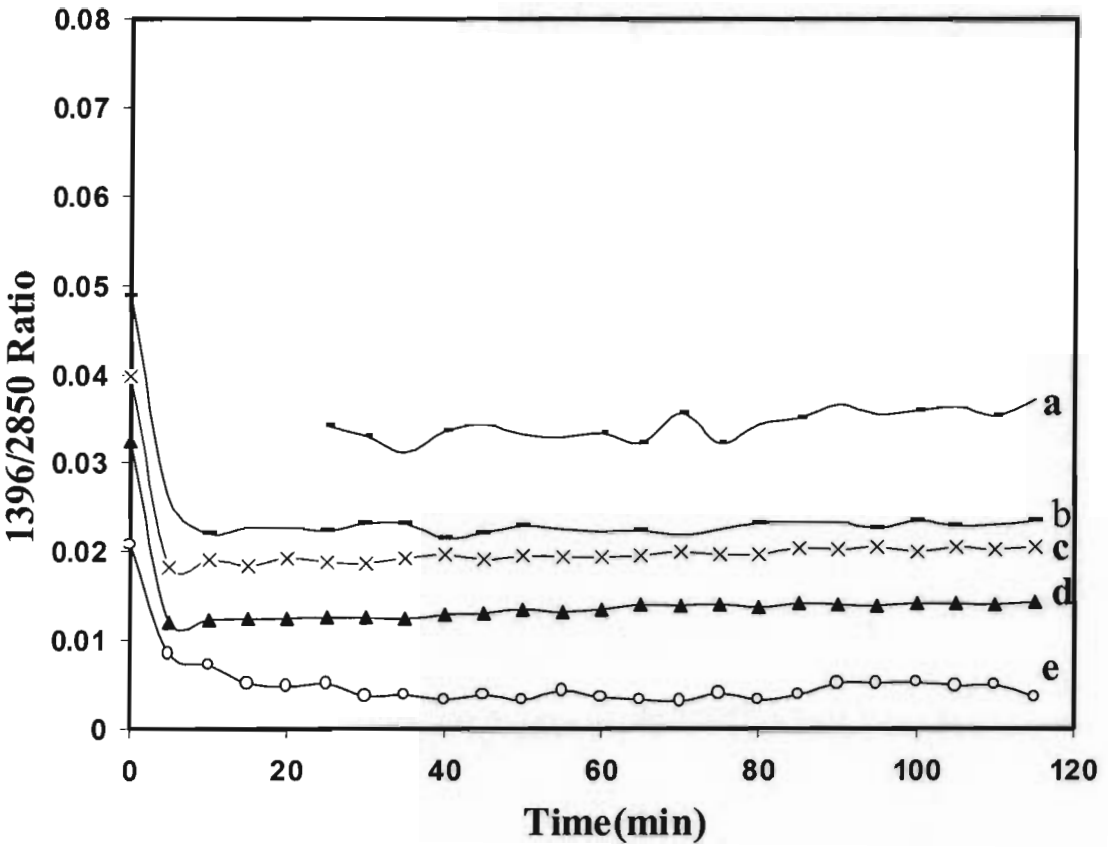

Figure 3.4 Time dependent plots of the 1396/2850 ratio at CTAB concentrations of a) 6.7×10^{-7} M, b) 3.0×10^{-6} M, c) 1.0×10^{-4}M, d) 3.4×10^{-4} M and e) 1.0×10^{-2} M. The curves for the 1390/2850 ratio have been offset for clarity.

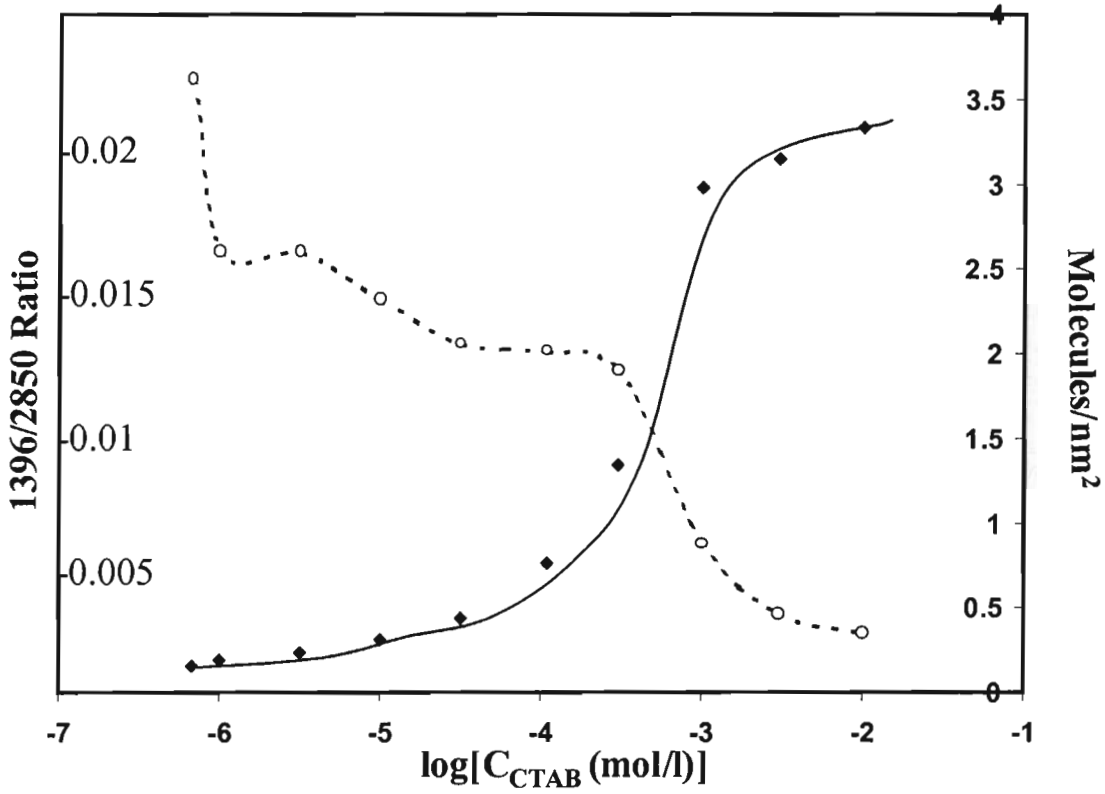

Figure 3.5 The adsorption isotherm and 1396/2850 ratio (dashed curve) for the addition of CTAB at increasing concentrations sequentially to the same TiO_2 sample.

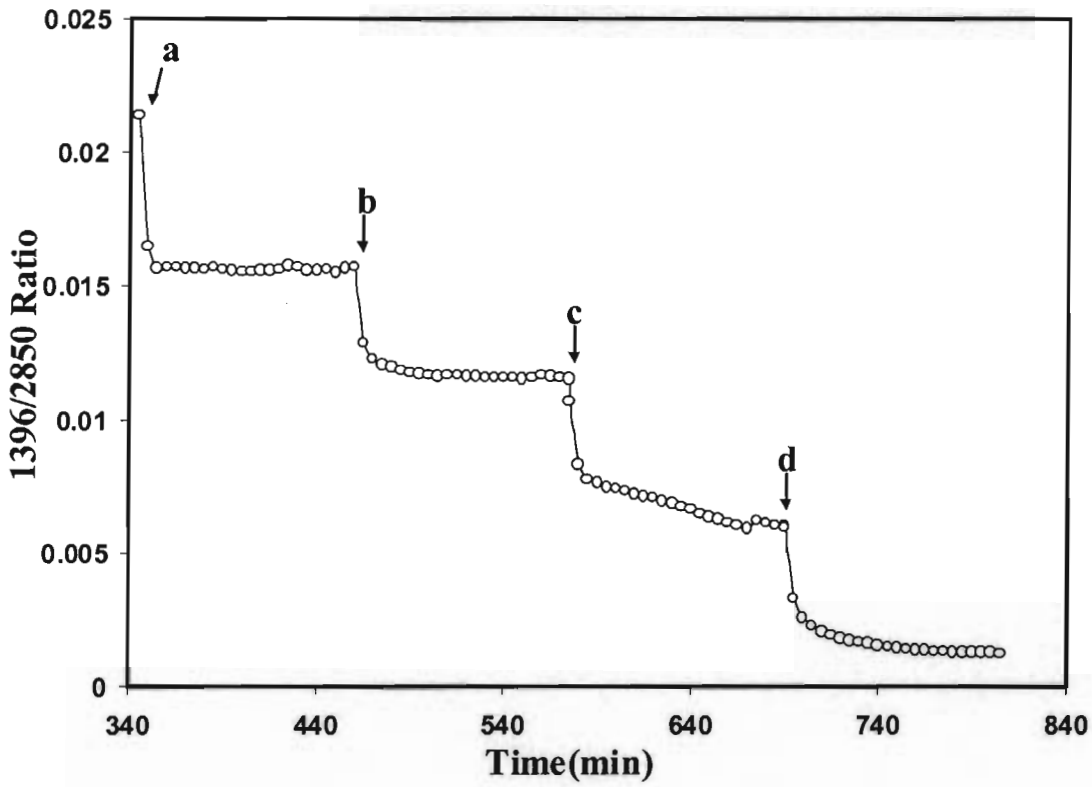

Figure 3.6 Time evolution of the intensity of the 1396/2850 ratio across Regions IV and V for the points shown in Figure 3.5. The arrows indicate the time when CTAB concentration was increased from a) 1.0×10^{-4} M, b) 3.0×10^{-4} M, c) 1.0×10^{-3} M and d) 3.0×10^{-3} M.

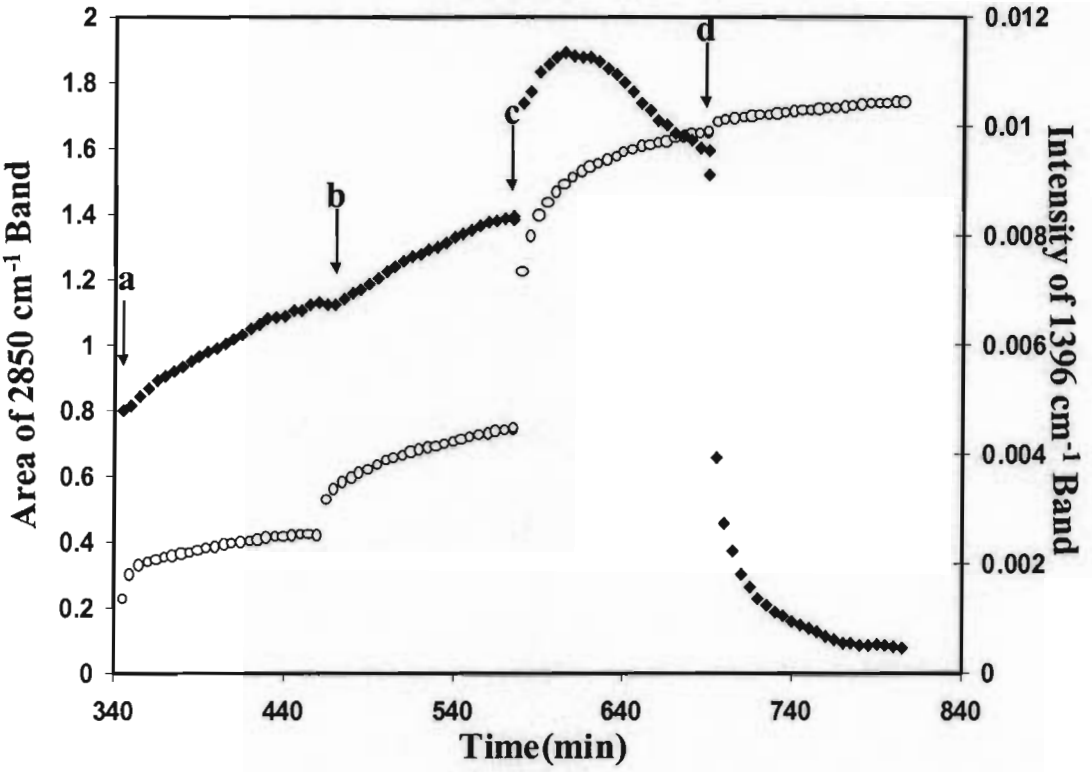

Figure 3.7 Time evolution of the intensity of the 1396 cm^{-1} (◆) and 2850 cm^{-1} (o) bands across the points shown in Figure 3.6. The arrows indicate the time when CTAB concentration was increased from a) 1.0 x 10^{-4} M, b) 3.0 x 10^{-4} M, c) 1.0 x 10^{-3} M and d) 3.0 x 10^{-3} M.

3.4 Conclusion

It is found that the relative intensity of the symmetric bending mode (δ_s CH_3-N^+) of CTAB increases when the adsorbed surfactant molecule interacts through electrostatic interaction with negative charged sites on a TiO_2 surface. From this information, an estimate is obtained of the percentage CTAB within an adsorbed structure in direct contact with charged sites on the surface. Across the adsorption isotherm, there are

abrupt changes in the percentage of CTAB bound to charge sites and this is correlated with a change in aggregated structure on the surface.

Even at very low concentrations (10^{-7} to 10^{-6} M), small aggregated CTAB structures adsorbs through electrostatic interaction with negative sites on the surface, which gives way to hemimicellar and possibly, admicelle structures at higher CTAB concentrations. Above the critical micelle concentration (c.m.c.) micellar structures adsorb on the surface.

By measuring the dynamics of aggregation of the surfactant, it is concluded that the equilibrium aggregated structure could form stepwise through intermediate structures. Hemimicelles form through initial adsorption of small aggregated structures that coalesce into sites on the surface followed by aggregation. Above the c.m.c., micelles are present on the surface but could form through initial free surfactant adsorption on charged sites followed by hemimicellar/admicelles, which in turn are transformed into micellar structures on the surface.

CHAPTER 4. USE OF INFRARED BANDS OF THE SURFACTANT HEADGROUP TO IDENTIFY MIXED SURFACTANT STRUCTURES ADSORBED ON TITANIA

4.1 Introduction

Mixtures of polymers and surfactants are used extensively to modify the colloidal behavior of particulate suspensions.[1, 11, 13, 78, 79] However, the relationship between the complex surfactant/polymer interactions on surfaces and their interfacial properties is an area that is not well understood. This area of research would clearly benefit from the development of new methods and techniques that can be used to identify the molecular structures and dynamics of surfactant/polyelectrolyte mixtures on surfaces.

In chapter 3, an infrared (IR) spectroscopic approach was established to detect CTAB adsorbed on TiO_2 particulates from aqueous solutions.[14] An attraction of this IR-ATR approach is that the high surface area associated with the particles enables detection of the weak, yet information-rich headgroup IR bands of surfactants. The high surface area also provides good signal-to-noise in detection of the strong CH_2 stretching modes during time-dependent measurements of the adsorbed amount.[23]

One advantage of the IR-ATR approach is that the amount of each adsorbate can be monitored separately when the particles are exposed to mixtures of surfactants. In one ATR study in our research group, CTAB was added to negatively charged TiO_2 particles at a solution concentration where hemimicelles form on the surface.[14] The CTAB structure on the surface was then probed by adding a solution containing SDS. It was shown that the nature of the aggregated CTAB structure and not the adsorbed amount,

that dictated the quantity of SDS incorporated into the CTAB layer. In this study, structural data was inferred from the frequency shift in the CH_2 stretching modes. The CH_2 stretching bands near 2922 cm^{-1} and 2850 cm^{-1} are generally the strongest bands in the spectra. The frequencies and widths of these bands are sensitive to the gauche/trans conformer ratio of the methylene chains, exhibiting a shift to lower frequencies characteristic of highly packed, all trans conformations.[14, 76, 80, 81] However, the shifts in position of the CH_2 stretching modes are not very sensitive to different structures in pure surfactant systems. For example, the frequency position for solutions containing free CTAB or CTAB micelles appear at the same frequency.[80, 81] This is because the packing density in the CTAB micelle is not sufficient to produce a frequency change in the CH_2 stretching modes. It was only in more highly packed mixed cationic/anionic surfactant structures that a shift in frequency was detected.[14, 80]

However, Chapter 3 showed that the weak headgroup bands located in the 1450 - 1300 cm^{-1} region provided the key information on the nature of the aggregated CTAB structure.[23] This rich information content on the nature of the self-assembled architecture gleaned from analysis of the CTAB headgroup region, has led to this study of the interaction of the CTAB layer with SDS. Our earlier work of SDS uptake into the adsorbed CTAB layer used the intensity of CH_2 stretching modes to measure adsorbed amount and the shift in the CH_2 stretching modes to determine packing density.[14] Structural information deduced from changes in the CTAB headgroups bands were not reported. The interaction of deuterated SDS adsorbed on TiO_2 with adsorbed CTAB hemimicelles was reinvestigated with a focus on the structure interpretation of changes

occurring in the headgroup region. Furthermore, I have extended this work to deuterated SDS uptake by CTAB admicelles and micelles adsorbed on TiO_2.

An important aspect of the work entails a detailed analysis of changes that occur in the SDS headgroup bands when mixed SDS/CTAB structures form on the surface. As with the CTAB headgroup bands, it is shown that changes in the SDS headgroup bands provide information on the nature of the aggregated structure. By examining the changes occurring to infrared bands due to the CTAB and SDS headgroups, along with the adsorbed amounts determined from the intensity of the CH_2 and CD_2 stretching bands, a clearer picture emerges on the type of mixed architectures that occur on a charged metal oxide surface.

4.2 Experimental Section

Fumed titania powder (P25) was obtained from Degussa and used as received. The P_{25} powder has a BET N_2 surface area of 50 m^2/g and a measured isoelectric point (IEP) of 6.5. Cetyltrimethylammonium bromide (CTAB) and sodium dodecyl sulphate (SDS) were obtained from Aldrich. CTAB was recrystallized twice with an acetone/ethanol mixture and SDS was double recrystallized with acetone.[14, 23] Deuterated sodium dodecyl sulphate (d_{25}-SDS, 98.5% deuterated) was obtained from CDN Isotopes and used as received. The integrated intensity of the CH_2 stretching mode at 2850 cm^{-1} is used to compute the adsorbed amount of surfactant. Since this band is common to both SDS and CTAB, experiments were conducted using d_{25}-SDS in order to separately determine the adsorbed amount of SDS from the amount of adsorbed CTAB. The calibration procedure for converting the integrated intensity of the CD_2 and CH_2 stretching modes to an adsorbed amount of CTAB or SDS is described in chapter 2.

All solutions were made with deionized water (18 MΩ) obtained from a Milli-Q purification system. Solutions of NaOH and HCl were used to adjust the pH of the water and surfactant solutions. Unless stated, all experiments were carried out at pH 10.3 and at this pH, the titania surface is negatively charged.

In a typical experiment, water adjusted to pH 10.3 was flowed at a rate of 5.8 ml/min through the ATR setup for at least 30 minutes. A reference spectrum was then recorded with the water flowing through the ATR cell. Next, a fresh CTAB solution at a specified concentration was adjusted to pH 10.3 and then flowed into the ATR cell. Spectra were then recorded as a function of time for 2 hrs. The cell was then flushed with water for 1 min followed by addition of a fresh solution of d_{25}-SDS at the specified concentration and pH 10.3.

Experiments were conducted at three different CTAB and d_{25}-SDS solution concentrations. At the lowest concentrations (0.01 mM CTAB and 0.05 mM d_{25}-SDS) the spectral contributions from either d_{25}-SDS or CTAB in solution were not detected. However at the higher solution concentrations (0.1 mM and 1mM CTAB, the bands due to CTAB and d_{25}-SDS in solution did contribute to the overall spectrum. This spectral contribution from the CTAB or d_{25}-SDS in solution was determined by recording spectra through the ATR setup containing a bare TiO_2 coated ZnSe crystal at a pH where CTAB or d_{25}-SDS does not adsorb on TiO_2 and are described in chapter 2.

4.3 Results and Discussion

The amount of CTAB adsorbed on TiO_2 at pH 10.3 plotted as a function of log[CTAB] follows a double "S" curve having two sharp increases in adsorbed amount separated by plateau regions.[23] These two abrupt rises in the adsorbed amount are

associated with the onset of formation of different aggregated structures. The three CTAB solution concentrations used in this study (0.01 mM, 0.1mM and 1.0 mM) were chosen because they lie in three different regions of the adsorption isotherm and thus result in the formation of different aggregated structures on the surface. The three structures formed on the surface in the order of increasing CTAB solution concentration have been attributed to hemimicelle, admicelle and micelle structures (see Figure 4.1) on the surface, respectively.[23, 82, 83] A hemimicelle is described as a patchy bilayer in which the second layer is incomplete. The admicelle can be described as a more complete or less defective bilayer structure. At the highest CTAB concentration (1mM), micelles adsorb on the surface.

The time dependent change in the amount of CTAB adsorbed on TiO_2 at the three solution concentrations, and the subsequent change in adsorbed amount of CTAB with the uptake of d_{25}-SDS are shown in Figures 4.2-4.4. In all three cases, the addition of d_{25}-SDS leads to an abrupt decrease in the amount of CTAB adsorbed on the TiO_2. It is noted that this decrease in the amount of CTAB on the surface is due to the uptake of d_{25}-SDS by the CTAB layer. This abrupt change in CTAB does not occur when pure water is flowed through the cell. Flowing water through the cell instead of the d_{25}-SDS solution leads to a slow and gradual decrease in the amount of CTAB adsorbed on TiO_2. It is also noted that the uptake of d_{25}-SDS is due to interaction with the CTAB structure on the surface and not due to adsorption of the d_{25}-SDS directly on the TiO_2. In a separate experiment, there was no adsorption of d_{25}-SDS when exposed to a bare TiO_2 surface at a solution pH of 10.3.

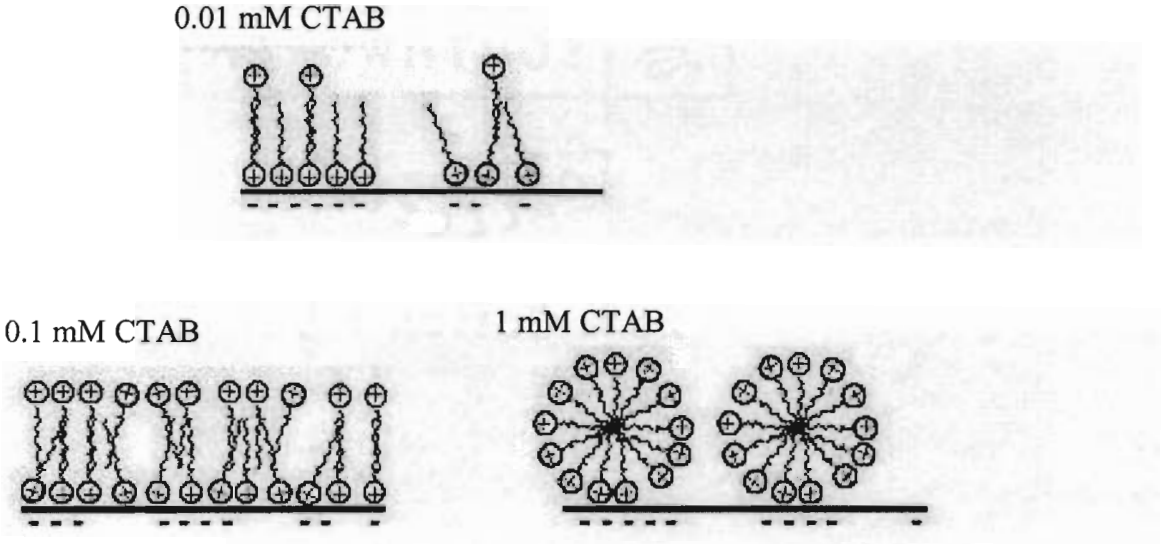

Figure 4.1 Hemimicellar, admicellar and micellar structures formed on the TiO_2 surface at the indicated CTAB solution concentration.

4.3.1 Interaction of d_{25}-SDS with CTAB Hemimicelles Adsorbed on TiO_2

The changes in adsorbed amount of the two surfactants with the addition of 0.05 mM d_{25}-SDS solution to the hemimicelle CTAB adsorbed on TiO_2 is shown in Figure 4.2. Addition of the d_{25}-SDS solution to the pre-adsorbed CTAB layer results in the total uptake of about 0.29 molecules/nm^2 d_{25}-SDS and the removal of about 12% of the original amount of adsorbed CTAB. The final CTAB concentration is 0.53 CTAB molecules/nm^2 and thus a mixed surfactant structure is formed that is enriched in CTAB. The final CTAB/SDS number ratio is 1.8. Furthermore, the uptake of SDS is accompanied by a decrease in frequency in the CH_2 mode from 2922 cm^{-1} to 2918 cm^{-1}. Actually, the addition of non-deuterated SDS leads to a shift of about 4 cm^{-1} to 2918 cm^{-1} while addition of d_{25}-SDS leads to a shift of 2 cm^{-1} to 2920 cm^{-1} and the corresponding CD_2 mode shifts from 2195 cm^{-1} to 2194 cm^{-1}. Experiments using non-deuterated SDS

were performed in order to measure the total shift in CH_2 stretching modes for comparison of the overall packing densities of the three different SDS/CTAB mixed surfactant structures.

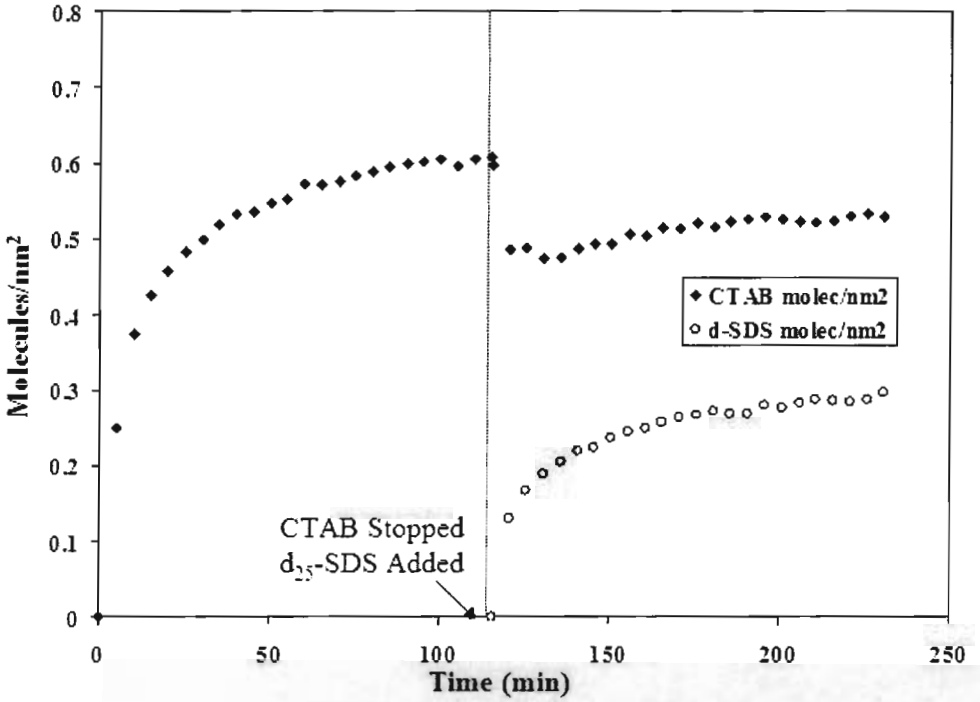

Figure 4.2 Time dependent change in the amount of CTAB and d_{25}-SDS adsorbed on TiO_2 at pH 10.3 using a 0.01 mM CTAB solution followed by addition of 0.05 mM d_{25}-SDS solution.

Incorporation of SDS has been attributed to favorable headgroup-headgroup and tail-tail interactions with the patchy second layer of the hemimicellar structure. The qualitative picture proposed by Ninness *et. al.*[14] is that a rapid adsorption of SDS produces highly ordered structures with the bilayer portion of CTAB hemimicelle (scheme 4.1). The uptake of d_{25}-SDS in the second patchy CTAB layer would explain a low number of CTAB molecules expelled from the surface. In essence, the second patchy layer contains sufficient gaps to accommodate the d_{25}-SDS. The favorable

headgroup-headgroup and tail-tail interactions that occur with incorporation of the d_{25}-SDS into the second patchy layer would produce a more tightly packed mixed surfactant structure, as evidenced by the 4 cm^{-1} shift to lower frequency in the CH_2 antisymmetric stretching mode. Because the uptake of the d_{25}-SDS occurs primarily in the second layer, the overall mixed surfactant structure would be enriched in CTAB. This is consistent with the measured 1.8 CTAB/SDS number ratio. It is noted that Scheme 4.1 also shows some CTAB migration from the first layer to the second layer. This was not deduced from either the adsorbed amount data or frequency shift of the CH_2 modes but from changes in the headgroup bands. The information derived from the headgroup region will be discussed in a later section.

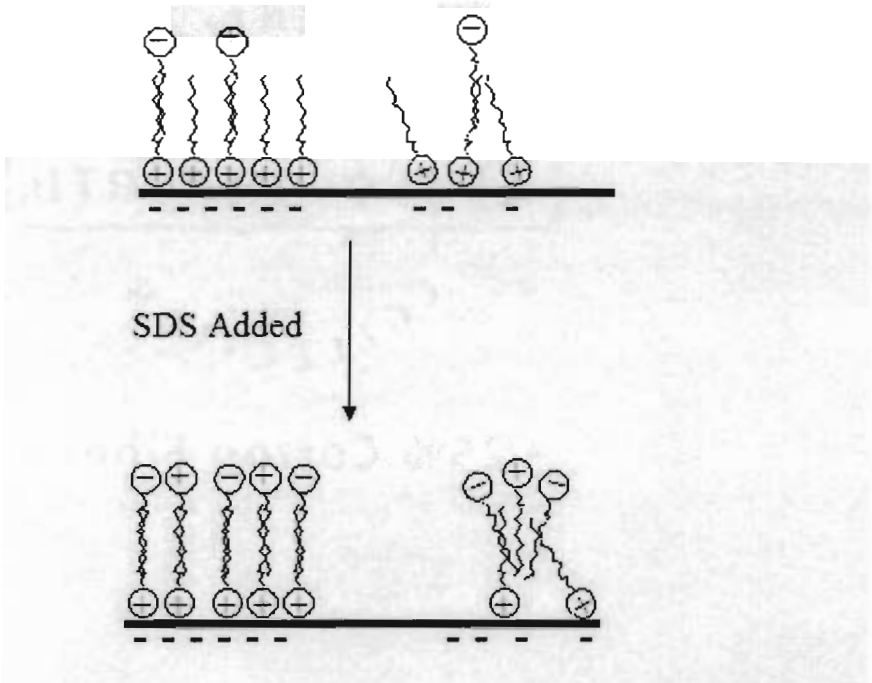

Scheme 4.1 Uptake of SDS by CTAB hemimicelles

4.3.2 Interaction of d_{25}-SDS Solution with CTAB Admicelles Adsorbed on TiO_2

The change in the amount of CTAB adsorbed on TiO_2 in contact with a 0.1 mM CTAB solution is added to TiO_2 at pH 10.3 is plotted in Figure 4.3. The plateau in the CTAB adsorption curve in Figure 4.3 is about 1.31 CTAB molecules/nm^2 and this about 2.2 times higher than the value obtained for the adsorbed amount from a 0.01mM CTAB solution. The higher amount of CTAB adsorbed corresponds to a more contiguous CTAB structure that is also less patchy in the second layer (admicelles).[23] Addition of 0.5 mM d_{25}-SDS to this CTAB layer results in the expulsion of about 28.5% of the CTAB from the surface and an uptake of about 0.71 d_{25}-SDS molecules/nm^2. In terms of CTAB/SDS number ratio, the final equilibrium value obtained for the mixed surfactant structure on the surface is 1.3 CTAB/SDS. This is lower than the 1.8 CTAB/SDS ratio measured for the uptake of d_{25}-SDS by the adsorbed CTAB hemimicelles. In a separate experiment using non-dueterated SDS, a 5 cm^{-1} shift to lower frequency in the CH_2 antisymmetric stretching mode was observed. It was recalled that the corresponding shift of 4 cm^{-1} was measured for the mixed surfactant structure produced by d_{25}-SDS incorporation into the CTAB hemimicelles. This indicates a higher packed mixed surfactant structure is produced with the uptake of SDS into the CTAB admicelles. A more highly packed structure produced by the interaction of d_{25}-SDS with CTAB admicelles is consistent with the higher amount of both CTAB and d_{25}-SDS adsorbed on the TiO_2 as well as the more favorable headgroup-headgroup electrostatic interactions as the CTAB/SDS number ratio lowers and approaches a value of 1.

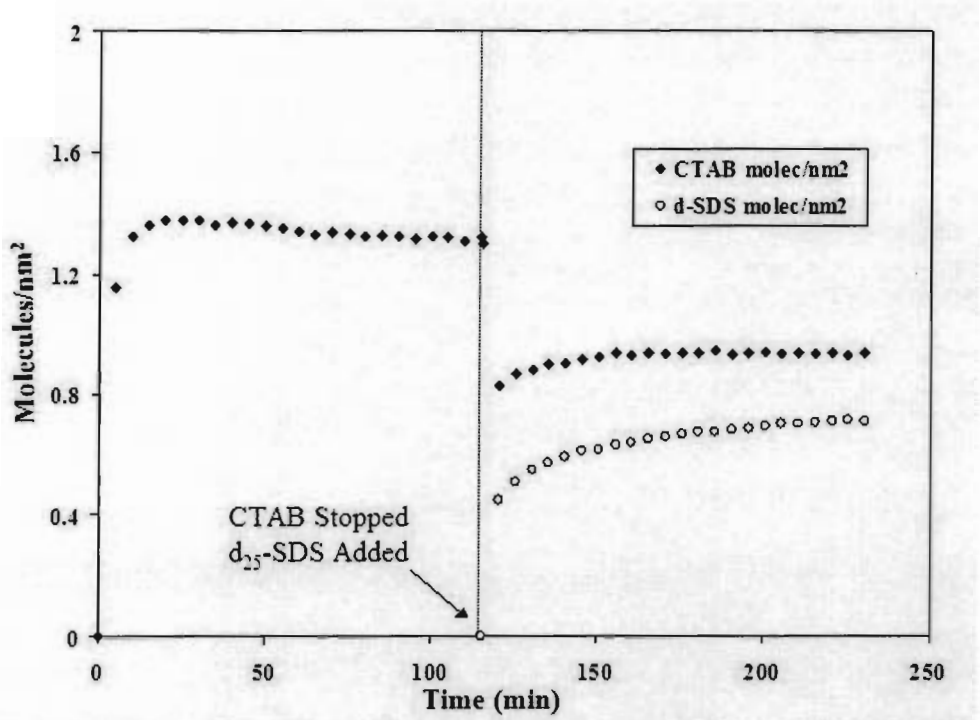

Figure 4.3 Time dependent change in the amount of CTAB and d_{25}-sds adsorbed on TiO_2 at pH 10.3 using a 0.1mM CTAB solution followed by addition of 0.5 mM d_{25}-SDS solution

The uptake of d_{25}-SDS in a CTAB structure having a more complete second layer (less gaps than a hemimicelle) occurs by ejecting CTAB molecules from the admicelle in order to create space for the incoming d_{25}-SDS molecules.(see Scheme 4.2) Given that 28.5% of CTAB is expelled, it is highly unlikely that all the CTAB removed would come solely from the second layer as this would lead to too few CTAB molecules in this second layer to sustain the large uptake of d_{25}-SDS. Also, given a 1.3 CTAB/SDS number ratio, it is more likely that both upper and lower layers of the admicelle structures contain significant levels of CTAB and d_{25}-SDS. As a result, some CTAB in the first layer is removed or transfers to the second layer.

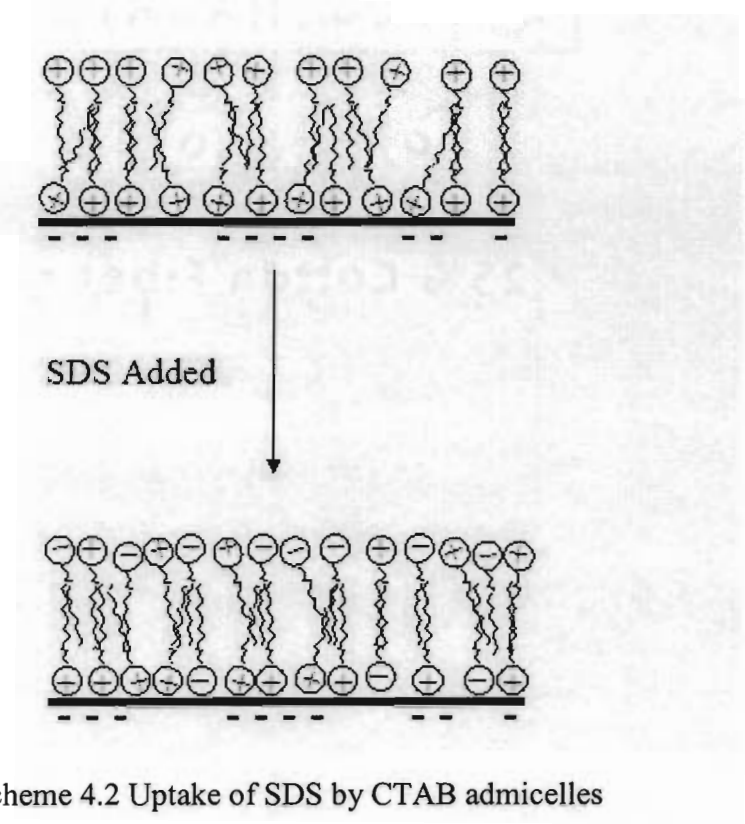

Scheme 4.2 Uptake of SDS by CTAB admicelles

A possible explanation for the uptake of d_{25}-SDS in the first layer of the admicelle is that sections of the admicelle form over regions of the surface that have low or no charged sites. These regions would more easily accommodate mixed surfactant structures. In the case of hemimicelles, the structures are more clustered over charged surface sites and these regions would be less likely to expel CTAB or accommodate d_{25}-SDS in the first layer.

4.3.3 Interaction of d_{25}-SDS Solution with CTAB Micelles Adsorbed on TiO_2

The CTAB solution concentration used in generating the curve shown in Figure 4.4 was 1 mM and this concentration is above the critical micelle concentration (c.m.c. 9.0×10^{-4} M).[77, 83] This CTAB solution concentration in contact with the TiO_2 surface leads to an adsorption of about 2.53 CTAB molecules/nm^2. At solution concentrations

above the c.m.c., the high adsorbed amount has been attributed to micelles on the surface.[76] When a 5 mM d_{25} -SDS solution is introduced to this CTAB layer, 63% of the amount of CTAB on the surface was removed and this was accompanied by the uptake of 0.8 d_{25}-SDS molecules/nm^2. A white precipitate formed in the effluent due to CTAB-SDS salts confirming the expulsion of CTAB from the surface. Because there is a significant percentage of CTAB displaced from the surface, the remaining amount of CTAB and total d_{25}-SDS on the surface is only slightly higher than shown in Figure 4.3. As a result, the number ratio of CTAB/SDS is only slightly lower at 1.2 CTAB/SDS compared to the 1.3 CTAB/SDS obtained for adsorption of d_{25}-SDS with CTAB admicelles. When non-deuterated SDS was added, the CH_2 asymmetric band is now shifted lower by 6 cm^{-1} and this larger shift indicate that mixed surfactant structure are more tightly packed than the mixed surfactant structures produced using lower CTAB and d_{25}-SDS solution concentrations. The picture that emerges is that a mixed micelle structure is formed on the surface (see scheme 4.3). This is not surprising as the critical aggregation concentration for mixed CTAB and SDS micelles are two orders in magnitude lower than the c.m.c. for the pure surfactant systems.[76] Since a small percentage of the molecules in a CTAB micelle directly interact with charged sites on the surface, it is anticipated that a high level of expulsion of CTAB would occur to accommodate large incorporation of d_{25}-SDS in the mixed micelle structure. It is only in the region near the charged sites on the surface that the enrichment in CTAB is anticipated and this conclusion is supported by spectral data obtained in the headgroup region.

So far, the identification of the mixed surfactant structures was based solely upon changes in the amount of CTAB and d_{25}-SDS adsorbed on TiO_2 and the degree of

packing determined from the shift in the CH_2 stretching modes. The attention is turned to the analysis of the headgroup regions of both d_{25}-SDS and CTAB which should, at least, support the conclusions drawn from the changes in the adsorbed amount. In the next section I describe the changes occurring in the d_{25}-SDS headgroup region and this will then be followed by a similar analysis of the CTAB headgroup region.

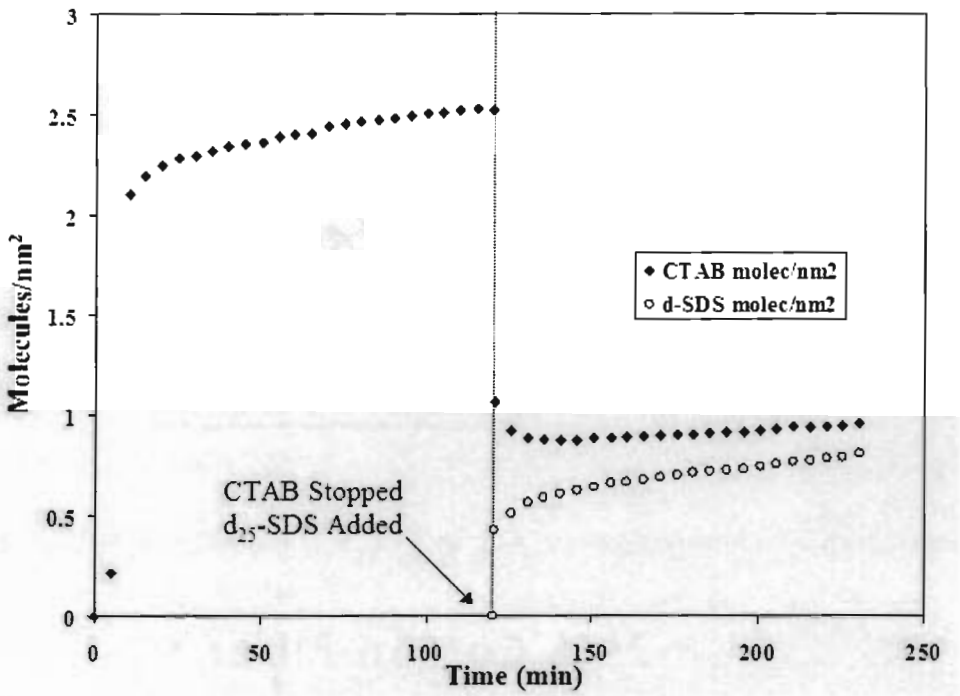

Figure 4.4 Time dependent change in the amount of CTAB and d_{25}-SDS adsorbed on TiO_2 at pH 10.3 using a 1.0 mM CTAB solution followed by addition of 5.0 mM d_{25}-SDS solution.

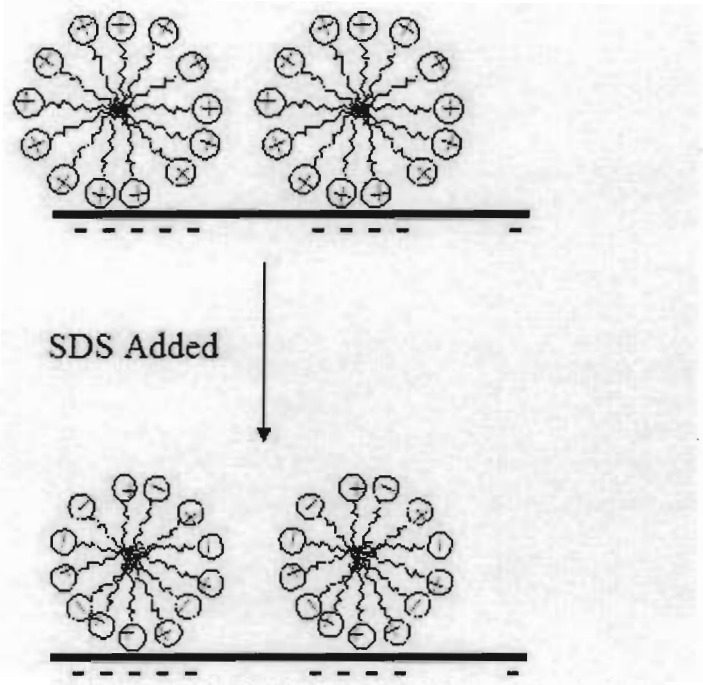

Scheme 4.3 Uptake of SDS by CTAB micelles

4.3.4 Headgroup Region of d_{25}-SDS

Figure 4.5 shows the changes occurring in the headgroup band region of d_{25}-SDS during the uptake of d_{25}-SDS for the 0.01 mM CTAB experiment (i.e., during uptake by the hemimicelle CTAB layer as depicted in Figure 4.2). Three bands are observed in the headgroup region and two are assigned as S-O antisymmetric stretching bands (ν_{as} S-O) at 1248 and 1221 cm^{-1} and the third band is the S-O symmetric stretching band (ν_s S-O) at 1038 cm^{-1}. All three bands increase in intensity with incubation time and this is primarily due to an increase in amount of d_{25}-SDS on the surface (see Figure 4.2). However, on closer inspection, the spectra clearly show that the ν_{as} S-O band at 1248 cm^{-1} increases at a different rate relative to the lower antisymmetric mode at 1221 cm^{-1}.

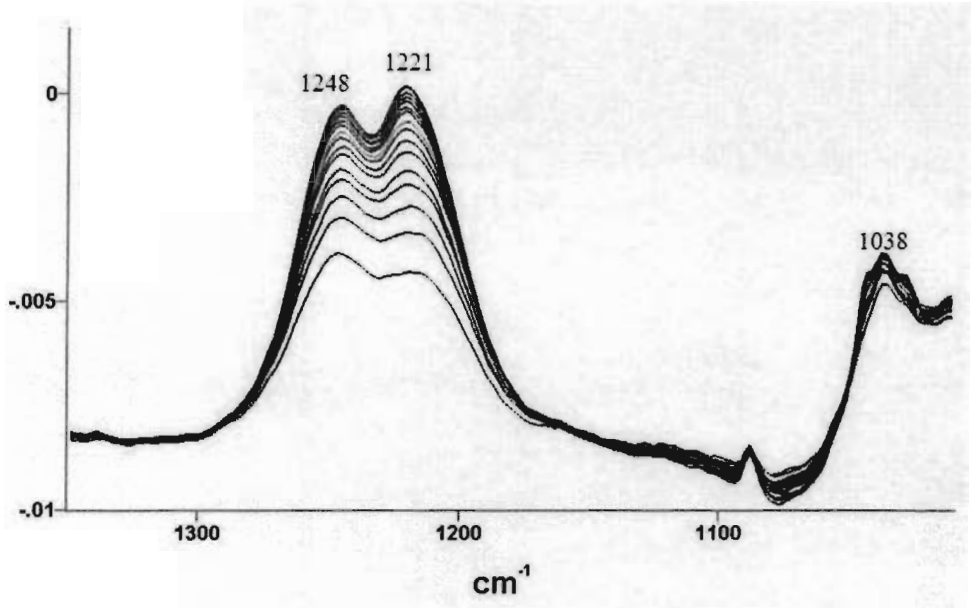

Figure 4.5 Change in the intensity of the S-O headgroup bands as a function of reaction time during the uptake of d_{25}-SDS into the preadsorbed CTAB layer as described in Figure 4.2.

Interpretation of the spectral changes of the d_{25}-SDS headgroup in terms of surfactant structures requires an understanding of how these bands respond to changes in their local environment. As with the previous work with CTAB, I rely on the detailed solution studies of mixed CTAB/SDS micelles reported by others.[80, 81] In their work, Scheuing and Weers[76] found that the ν_s S-O mode shifted to lower frequency with the loss of interaction of the SDS headgroup with counterions present in the diffuse double layer. The transition dipole moment of the ν_s S-O is located in the direction normal to the micelle surface (see scheme 4.4) and thus changes in the counterion density located in the diffuse double layer affects the ν_s S-O band to the greatest extent Using similar arguments, a direct interaction of the d_{25}-SDS headgroup with charged surface sites or head-to-head adsorption with CTAB should affect the frequency of this band. In the

spectra shown in Figure 4.5, the frequency position of the ν_s S-O band remains constant during the uptake of the d_{25}-SDS. This shows that the adsorption of the d_{25}-SDS does not occur through vertical head-to-head interaction with the CTAB molecules. On the other hand, a constant ν_s S-O frequency suggests that the uptake of the d_{25}-SDS in the CTAB hemimicelle occurring primarily through lateral surfactant-surfactant interactions as these interactions would occur in a direction that is orthogonal to the transition moment vector of the ν_s S-O band.

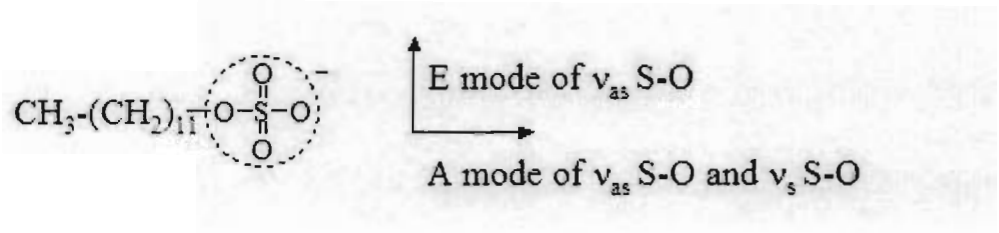

Scheme 4.4 Transition dipole moment vectors for S-O Stretching modes of SDS

In their solution studies, Scheuing and Weers noted that the changes in intensity and frequency position occurring in the ν_{as} S-O bands were more difficult to interpret because this region had two overlapping bands. Nevertheless, in their solution studies with mixed SDS/CTAB micelles, they attributed the splitting and shifting in the ν_{as} S-O bands to a lowering of the symmetry of the SO_4 headgroup resulting from changes in the lateral electrostatic interactions between the SDS and CTAB molecules. In Figure 4.5, the most significant spectral changes occur in the relative intensity of the two ν_{as} S-O modes. During the initial stage the 1248 cm^{-1} peak is higher in intensity than the 1221 cm^{-1} peak, whereas at the latter stage the 1221 cm^{-1} peak is more intense than the 1248 cm^{-1} peak accordingly, these changes indicate a strong lateral interaction between d_{25}-SDS and CTAB molecules.

The structural interpretation of the changes in the two ν_{as} S-O modes put forward by Schuring and Weers was based on the assumption that the transition moment vector for two ν_{as} S-O modes lies parallel to the micelle direction and thus would be sensitive to lateral interactions and changes in the number of adjacent CTAB molecules. However, on closer inspection, the transition moment vectors of the two ν_{as} S-O modes are not in the same direction but rather, normal to each other which lead me to offer an alterative explanation for interpretation of the spectral changes shown in Figure 4.5.

Starting with a free sulfate ion belonging to T_d point group, the ν_{as} S-O mode is a triply degenerate T vibration and ν_s S-O band is a non-degenerate A vibration.[84] In SDS, the symmetry of the sulfate headgroup is lowered to the C_{3v} point group which splits the triply degenerate ν_{as} S-O stretching mode into two bands; one band is a doubly degenerate E vibration and a second non-degenerate A vibration. From spectroscopic considerations, the directions of the dipole moment for the A and E vibrational mode are orthogonal to each other as shown in scheme 4.4. Both the ν_{as} S-O band at 1221 cm^{-1} and ν_s S-O band at 1038 cm^{-1} are A vibrations and are sensitive to changes (either couterions or surface charges) in the direction normal to the micelle surface. Thus, it is anticipated that these two bands will be more sensitive by intimate contact with a charge surface site much like that found for the δ_s ^{+}N-CH_3 band for CTAB adsorbed on TiO_2.

Supporting evidence for assignment of the three SDS headgroup bands was provided by a separate experiment in which d_{25}- SDS was introduced to a positively charged TiO_2 surface at pH 3.5. In this case, the E vibration of the ν_{as} S-O (E ν_{as} S-O) appeared at the same frequency of 1248 cm^{-1} as shown in Figure 4.5 whereas, the two A vibrations (A ν_{as} S-O at 1221 cm^{-1} and A ν_s S-O at 1038 cm^{-1} in Figure 4.5) shifted to

1205 and 1034 cm^{-1}, respectively. Since the transition dipole moment for both A vibrations are normal to the micelle surface, a shift in frequency for both these bands with adsorption of the d_{25}-SDS headgroups on positively charged surface sites was anticipated. In contrast, the transition dipole moment for the E ν_{as} S-O vibrational band is in the lateral direction (see scheme 4.4) and thus would not be affected by adsorption onto charged sites on the surface.

Returning to Figure 4.5, it was observed that the two ν_{as} S-O modes show different changes in intensity with time as more d_{25}-SDS is incorporated into the CTAB layer. An initial examination of the spectra in Figure 4.5 show that the A ν_{as} S-O at 1221 cm^{-1} increases at a faster rate than the E ν_{as} S-O at 1248 cm^{-1}. This would be counter to the expected trend as it was anticipated that the intensity of the E ν_{as} S-O would be sensitive and the A ν_{as} S-O insensitive to lateral CTAB-SDS interactions. However, the trend is difficult to discern from Figure 4.5 because both ν_{as} S-O bands are also increasing due to an increase in the amount of d_{25}-SDS adsorbed on the TiO_2. A more relevant measure from a structure standpoint is the change in intensity of the A and E ν_{as} S-O vibrations normalized to the intensity of the CD_2 band at 2090 cm^{-1}. This normalized value would account for the fluctuation in number of d_{25}-SDS molecules on the surface and thus provide a measure of the average change in the intensity of each headgroup band per d_{25}-SDS molecule.

Figure 4.6 is a plot of the normalized intensity with time for both ν_{as} S-O modes. This plot shows that the normalized A ν_{as} S-O vibration remains constant whereas, in fact, it is the normalized E ν_{as} S-O vibration that decreases as more d_{25}-SDS is incorporated into the CTAB structure. The ν_s S-O mode at 1038 cm^{-1} (not shown) also

has a constant intensity per d_{25}-SDS molecule and shows no shift in frequency with the uptake of d_{25}-SDS. Given the vector orientation of the transition dipole moment for the two ν_{as} S-O bands, the data in Figure 4.6 shows that the incorporation of d_{25}-SDS into the hemimicelle CTAB structure is through lateral surfactant-surfactant interactions.

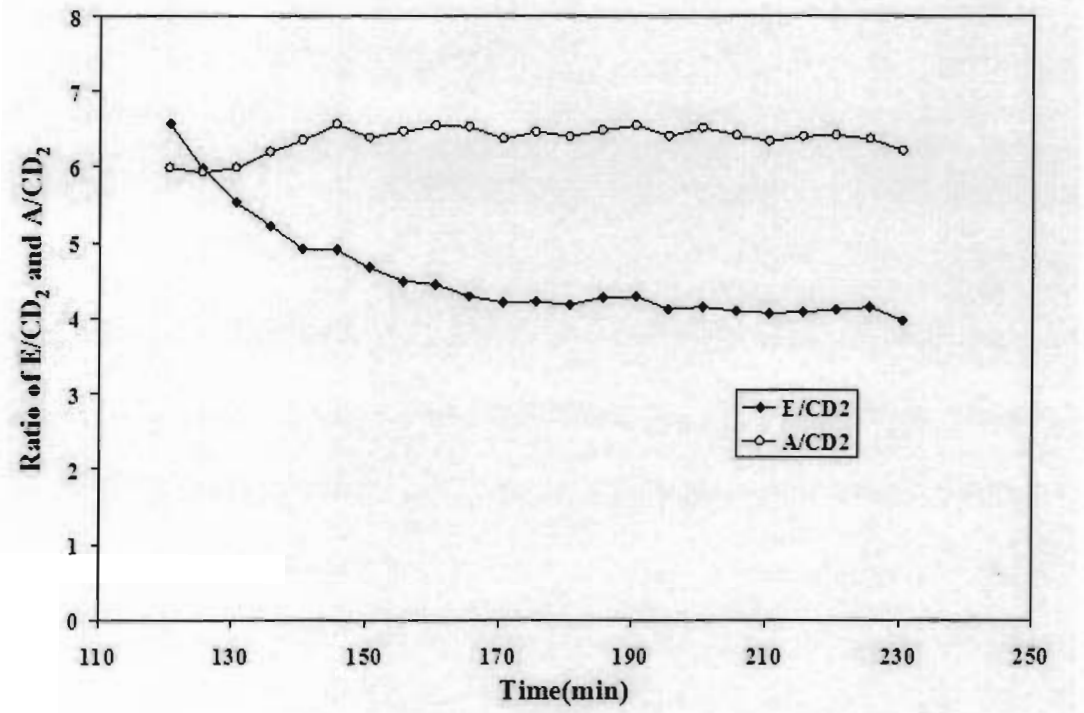

Figure 4.6 Normalized values of the A (o) and E(♦) ν_{as} S-O modes for the spectra shown in Figure 4.5.

It is interesting to note that the normalized E ν_{as} S-O band decreases with d_{25}-SDS uptake. One would expect an increase in the normalized E ν_{as} S-O band with a decrease in the average distance between the two oppositely charged headgroups. I recall that there is a shift to lower frequency in the CH_2 stretching modes with increasing uptake of d_{25}-SDS which, in turn, translates to an average decrease in the distance between CTAB and d_{25}-SDS headgroups. From this factor alone, an increase and not a decrease in the normalized E ν_{as} S-O band would be expected.

A decrease in the intensity of the normalized E ν_{as} S-O band is also expected for a decrease in the average countercharge density surrounding the d_{25}-SDS headgroup. This is indeed the situation with the uptake of d_{25}-SDS by the CTAB hemimicelle. As more d_{25}-SDS is added into the gaps of the patchy CTAB bilayer, the average number of CTAB molecules surrounding each d_{25}-SDS molecule decreases. Given the trend shown in Figure 4.6, it would appear that the decrease in the average countercharge density surrounding the d_{25}-SDS headgroup, dominates over the average decrease in CTAB/SDS distance in determining intensity of the normalized E ν_{as} S-O band.

It is anticipated that the above analysis of the changes in the d_{25}-SDS headgroup bands will provide information on the mixed surfactant structures formed when d_{25}-SDS is added to admicelle and micelle CTAB structures. When d_{25}-SDS is added to all three CTAB structures, it is found that the time dependent value for the intensity of the normalized E ν_{as} S-O band decreases and the intensity of the normalized A ν_{as} S-O mode remains constant. This shows that the incorporation of d_{25}-SDS into all three structures on the surface is primarily through lateral surfactant interactions.

There is, however, a difference in absolute intensity of the E ν_{as} S-O mode relative to the A ν_{as} S-O band for the three SDS/CTAB equilibrium structures. This is shown in Figure 4.7. For comparative purposes, the spectra in Figure 4.7 are scaled to a constant intensity of the A ν_{as} S-O band at 1221 cm^{-1}. In actuality, the spectra have different absolute intensities because there are different amounts of adsorbed d_{25}-SDS. In Figure 4.7, the value calculated for the intensity ratio of the normalized E ν_{as} S-O/CD_2 bands was 4, 2.75 and 1.28 for uptake of d_{25}-SDS by the hemimicelle, admicelle and micelle CTAB structures, respectively. I recall that the intensity of the E ν_{as} S-O

vibration depends on two factors; the average number of surrounding CTAB molecules and the CTAB/SDS headgroup-headgroup distance. From the frequency shift of the CH_2 symmetric mode, the packing density for adsorption of d_{25}-SDS by CTAB micelles is higher than CTAB admicelles or hemimicelles. Thus, the proximity of d_{25}-SDS and CTAB headgroups would be the closest in the mixed micelle structure and from this standpoint alone; this would lead to the highest value for the intensity of the normalized E ν_{as} S-O band. However, the lowest value is obtained for the normalized E ν_{as} S-O vibration with addition of d_{25}-SDS to preadsorbed CTAB micelles. Thus, as found for the uptake of d_{25}-SDS by the CTAB hemimicelle, the dominant factor contributing to the overall intensity of the E ν_{as} S-O band is the relative number of CTAB molecules surrounding the d_{25}-SDS molecule. The number ratio of CTAB/SDS decreases from 1.8, 1.3 to 1.2 for addition of d_{25}-SDS to CTAB hemimicelles, admicelles and micelles, respectively and this is consistent with the trend in the normalized E ν_{as} S-O values. In effect, the addition of d_{25}-SDS to the CTAB micelles has a lower average number of CTAB surrounding the d_{25}-SDS molecule leading to the lowest value for the normalized E ν_{as} S-O intensity.

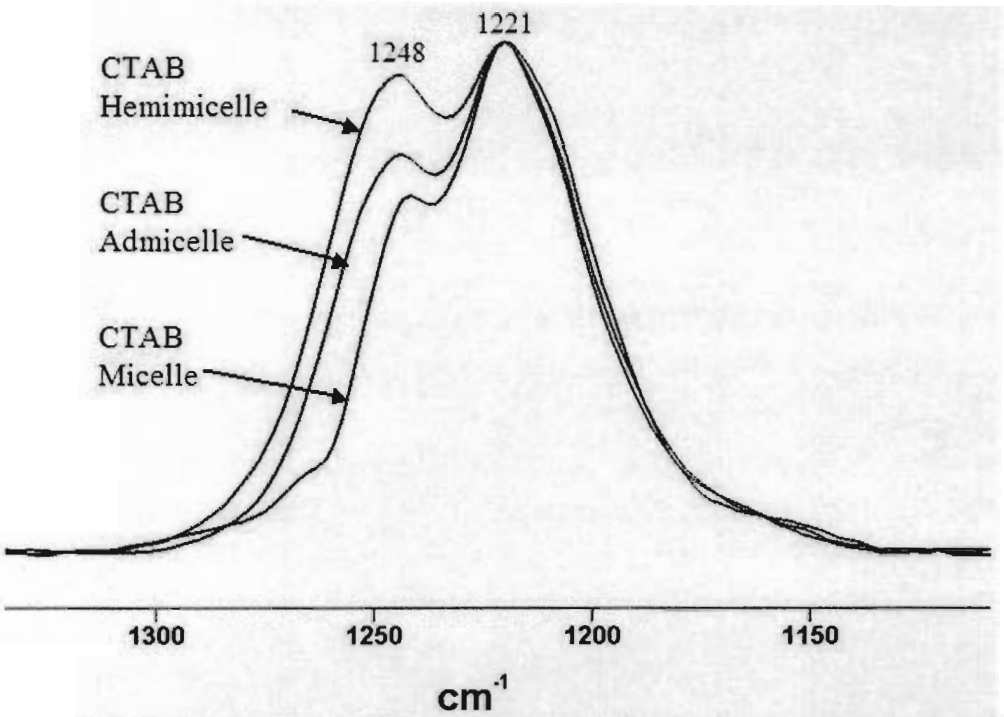

Figure 4.7 Relative intensity of the ν_{as} S-O modes obtained at equilibrium for addition of d_{25}-SDS to the indicated CTAB structures. The spectra are scaled to the intensity of the band at 1221cm^{-1}.

4.3.5 CTAB Headgroup

It is also anticipated that formation of the mixed SDS/CTAB structures would also lead to a perturbation of the CTAB headgroup bands. Figure 4.8 shows the headgroup CTAB spectral region just before addition of d_{25}-SDS and recorded at the equilibrium point after d_{25}-SDS addition for all three CTAB concentrations. The key headgroup bands are assigned as δ_{as} $^{+}$N-CH$_3$ at 1490 cm^{-1} and 1479 cm^{-1} and the δ_s $^{+}$N-CH$_3$ at 1396 cm^{-1}.[14] All other bands are various CH_2 and CD_2 modes.

For all three cases, the δ_{as} $^{+}$N-CH$_3$ bands at 1479 cm^{-1} and 1490 cm^{-1} change in position and shape with the uptake of d_{25}-SDS. The change in these bands is most pronounced with the uptake of d_{25}-SDS by the CTAB micelles and admicelles that result

in the appearance of a broad ill-defined feature at 1482 cm^{-1}. The transition dipole moment for the δ_{as} $^{+}N-CH_3$ modes lie in the same direction[23, 80] as the E ν_{as} S-O vibration of the d_{25}-SDS headgroup and thus are affected by lateral surfactant-surfactant interactions. The change in the δ_{as} $^{+}N-CH_3$ is less with d_{25}-SDS addition to adsorbed CTAB hemimicelles than either adsorbed CTAB admicelles or micelles and this is consistent with the trend in the E ν_{as} S-O band.

Of particular note are the changes that occur in the 1396/2850 ratios. The transition dipole moment for the 1396 cm^{-1} band (δ_s $^{+}N-CH_3$) is in the same direction as the A vibrations of the ν_{as} S-O and ν_s S-O bands. Changes to the 1396/2850 ratio has been shown to be sensitive to the number of CTAB directly interacting with the surface.[23] Addition of d_{25}-SDS to adsorbed CTAB micelles leads to an increase in the 1396/2850 ratio and this means that a higher proportion of the remaining CTAB are bound to oppositely charged surface sites. This is not surprising as 63% of the CTAB are ejected from the surface with addition of the d_{25}-SDS and it would be more easy to eject those CTAB molecules in the sections of the micelle that are not in intimate contact with charged surface sites. I recall that the picture obtained from the shift in the CH_2 symmetric mode along with the spectral data form the d_{25}-SDS headgroup suggests a tightly aggregated mixed micelle adsorbed on the surface. A higher 1396/2850 ratio shows that this mixed micelle is not uniformly distributed, but rather, is enriched in CTAB near the surface. In effect, the incoming d_{25}-SDS occupies regions of the outer micelle in a higher concentration than the area near the surface containing the CTAB that are bound to the negative surface sites. This gives rise to CTAB enriched micelle (the CTAB/SDS number ratio was 1.2).

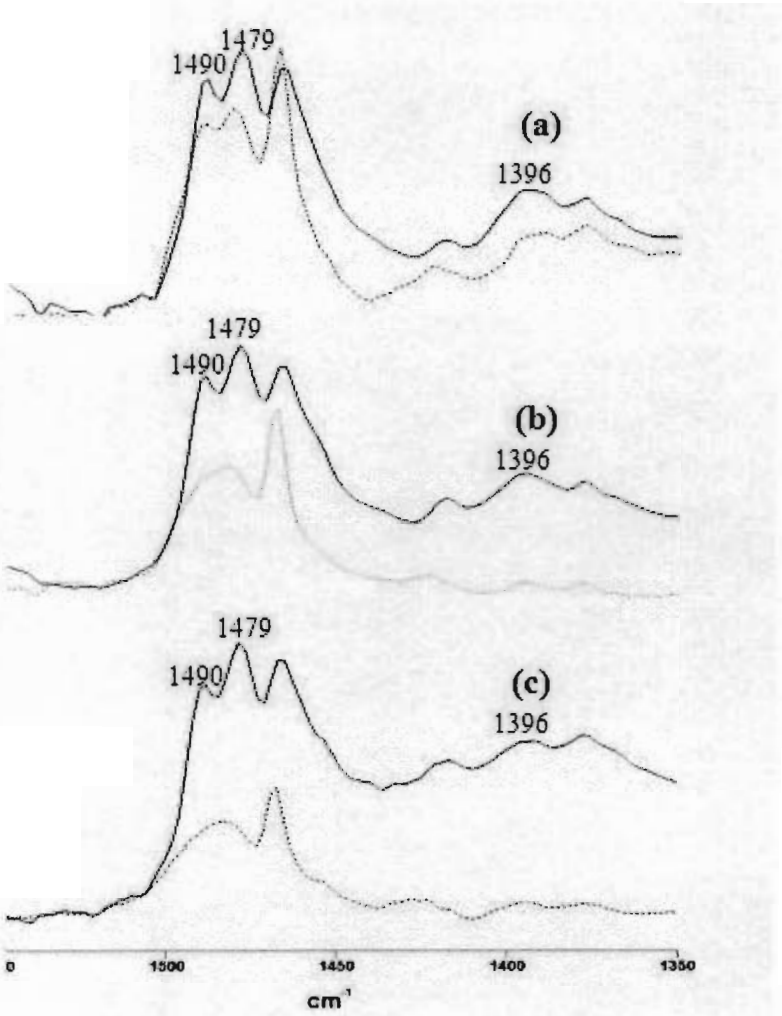

Figure 4.8 IR bands of CTAB headgroup before (solid curve) and after d_{25}-SDS addition (dashed curve) for adsorbed CTAB using CTAB solution concentrations of (a) 0.01 mM, (b) 0.1 mM and (c) 1mM.

In contrast to the addition of d_{25}-SDS to CTAB micelles, the 1396/2850 ratio decreases slightly for both addition of d_{25}-SDS to CTAB hemimicelles and admicelles. The reduction of this ratio shows that a fewer percentage of the remaining CTAB on the surface are in direct contact with charged surface sites. This implies that some of the adsorbed CTAB in the first layer of both the adsorbed hemimicelle and admicelle rearranges to the upper layer to interact with the d_{25}-SDS.

4.4 Conclusions

The subtle changes in the infrared bands due to surfactant headgroups provide a unique insight to the aggregated structures of mixed surfactants on charged metal oxide surfaces. Both the CTAB and SDS headgroup contain bands with transition dipole vectors that are orthogonal to each other. It is found that bands whose transition dipole vectors that lie parallel to the micelle surface (δ_{as} $^{+}N\text{-}CH_3$ CTAB bands at 1479 cm^{-1}, 1490 cm^{-1} and ν_{as} S-O band of SDS at 1248 cm^{-1}) change in intensity/position due to lateral-lateral interactions. In contrast, bands whose transition dipole vectors are perpendicular to the surface (δ_s $^{+}N\text{-}CH_3$ CTAB bands at 1396 cm^{-1}, ν_{as} S-O band at 1221 cm^{-1}, and ν_s S-O band at 1038 cm^{-1}) are sensitive to head-head interactions between surfactants and with adsorption onto charged surface sites. Combining the spectroscopic information from the headgroup region with the measurement of the adsorbed amount obtained from bands due to the alkyl tails has resulted in a clearer understanding of the interaction of mixed surfactants on surfaces.

CHAPTER 5. INTERACTION OF SODIUM POLYACRYLATE ADSORBED ON TIO_2 WITH CATIONIC AND ANIONIC SURFACTANTS

5.1 Introduction

In chapters 3 and 4, It was found that the changes in the headgroup bands of adsorbed cationic and anionic surfactants provide a more sensitive probe than the bands due to alkyl chains for identifying the nature of the aggregated structure on the surface. In this chapter, this concept of using low frequency IR bands to simultaneously measure dynamically the adsorbed amount and structures was extended for a mixed polymer/surfactant system. Specifically, time dependent spectra are recorded during the adsorption of sodium polyacrylate (NaPA) on a positively charged TiO_2 and when the adsorbed NaPA structure is probed with anionic SDS and cationic CTAB surfactants. The choice of the polymer and surfactants are based on their common use as model polymers and surfactants in many adsorption studies and because of the widespread usage in paper coating formulations.

5.2 Experimental Section

The materials and flow through experimental setup using the TiO_2 coated ATR crystals is described in chapter 2. Once mounted in the flow-through cell, the TiO_2 coated ZnSe crystal was continually flushed with water adjusted to the desired pH until reproducible spectra were obtained at 15 minute intervals. A reference spectrum was then recorded with water flowing across the TiO_2 coated ZnSe crystal. All experiments were conducted at ambient temperature and a peristaltic pump operation at a rate of 5.8 ml/min

was used to flow water and the polymer/surfactant solutions in the flow-through cell. A solution containing 20 ppm NaPA was then introduced into the cell and spectra were recorded at specified intervals. The polymer bands that appear in the spectrum are due solely to adsorbed species as, at the concentration of 20 ppm, the NaPA in solution is not detected. This was verified by recording the spectrum of 20 ppm flowing across a bare ZnSe ATR crystal. In this case, bands due to NaPA were not detected. The total contact time with the NaPA solution was typically 4 hrs. Prior to addition of the SDS or CTAB solution, the cell was flushed with pure water for 5 seconds to remove the excess NaPA in the solution phase. The removal of NaPA in solution and the flushing with pure water did not lead to a change in the amount of adsorbed polymer. In separate experiments, it was found that the adsorbed NaPA on the surface did not desorb when pure water was flowed for 2 hrs.

The adsorbed amount of CTAB and SDS were calculated using the integrated intensity of CH_2 symmetric mode located at 2850 cm^{-1} and the amount of NaPA was determined from the integrated intensity of the CH_2 mode at 1455 cm^{-1}. The procedure for calculating the adsorbed amount is described in chapter 2.

The bands at 1713 and 1545 cm^{-1} were used to monitor the change in the number of COOH and COO^- groups, respectively. A valley-valley baseline from 1770 to 1660 cm^{-1} was used for the integrated band intensity of the 1713 cm^{-1} band and from 1610 to 1483 cm^{-1} for the band at 1545 cm^{-1}. Sandwiched between the 1713 and 1545 cm^{-1} peaks is the strong water deformation mode centered at 1635 cm^{-1}. This band typically appeared as either a weak positive or negative band in the spectrum arising from small changes in the amount of water probed by the IR beam relative to the reference spectrum. The water

deformation mode overlapped with the integration limits of the 1713 and 1545 cm^{-1} bands and thus had to be removed because it contributed to the calculated integrated intensity of these two peaks. The water peak was removed by subtraction using a prerecorded spectrum of water. The subtraction the water contribution was done such that the absorbance value obtained at 1660 and 1610 cm^{-1} were equal to that of the baseline value at 1770 cm^{-1}. Figures 5.1 and 5.2 show examples of spectra with the water peak removed. In spectra where the water subtraction first appeared to be overcompensated and undercompensated, the integrated areas for either the 1713 or 1545 cm^{-1} peaks differed by ±1%.

5.3 Result and Discussion

5.3.1 IR Spectrum of NaPA

Figure 5.1 is a typical IR spectrum obtained for the adsorption of a 20 ppm sodium polyacrylate (NaPA) solution in contact with the TiO_2/water interface at pH 3.5. This spectrum highlights the key bands of adsorbed NaPA used in this study. Assignment of these bands as well as those obtained for NaPA in solution are given in Table 5.1.[85] In this work, the integrated intensity of the CH_2 bending mode (1455 cm^{-1}) is used to monitor the adsorbed amount of polymer. The C=O stretching mode of the COOH group appears near 1713 cm^{-1} and the bands at 1545 cm^{-1} and 1414 cm^{-1} are due to the antisymmetric and symmetric vibration mode of the COO^- group. These bands are of particular importance as their relative intensity provides a measurement of the percentage COOH and COO^- sites on the polymer backbone.

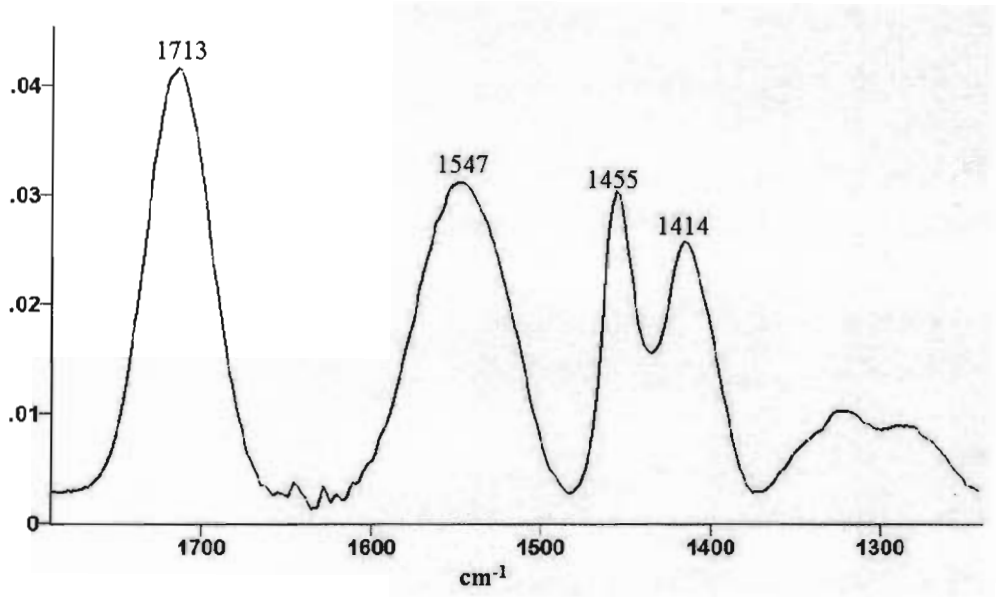

Figure 5.1 Infrared spectrum of NaPA adsorbed from a 20 ppm solution onto TiO_2 at pH 3.5

Table 5.1: Assignment for IR bands of NaPA in solution (10,000 ppm) and after adsorption from 20 ppm NaPA solution onto the TiO_2 particles at pH 3.5

Peak Positions(cm^{-1}) in solution(at pH 3)	Peak Positions(cm^{-1}) on surface(at pH 3.5)	*Peak Assignment*
1715 s, b	1713 s, b	ν C=O(free COOH)
1554 s, b	1545 s, b	ν_{as}(R-COO-)
1453 m	1455 m	δ $(CH_2)_n$
1404 m	1414 m	ν_s(R-COO^-)

s=strong m=medium b=broad

The adsorption of NaPA on TiO_2 occurs primarily through an interaction between the negatively charged COO^- groups on the polymer and positively charged surface sites.

It is possible to determine the mode of attachment between the COO^- groups and the surface sites from the frequency difference ($\Delta\nu$) between the antisymmetric and symmetric modes of the COO^- groups.[86] When the $\Delta\nu$ is of the same magnitude as the polymer in solution then the attachment is bidentate bridging and when the $\Delta\nu$ is less in magnitude of the polymer in solution then the attachment is bidentate chelating (see scheme 5.1). From table I, the $\Delta\nu$ of these two bands for NaPA in solution is about 150 cm^{-1}, while the corresponding frequency difference in Figure 5.1 for NaPA adsorbed on TiO_2 surface at pH 3.5 is 133 cm^{-1} indicating bidentate chelating with TiO_2 surface site.[87]

(I) (II)

Scheme 5.1 (I) bidentate chelating and (II) bidentate bridging structures on metal oxide surfaces

The change in intensities of the COOH band (centered near 1713 cm^{-1}) and the COO^- bands (centered near 1545 cm^{-1} and 1414 cm^{-1}) are related; an increase in the band at 1713 cm^{-1} is mirrored by a decrease in intensity of the bands at 1545 cm^{-1} and 1414 cm^{-1} and vice versa. This is not surprising given that the formation of a COO^- functionality occurs at the expense of a COOH group. It was found that a more meaningful molecular description emerges when the intensity of these bands is converted to the relative number of COOH and COO^- groups on the polymer backbone.

The conversion of the intensity of both the COOH and COO^- bands to a measurement of %COOH and %COO^- groups on the polymer is done by using spectra of

NaPA in solution recorded as a function of pH. At pH < 2 the NaPA is fully in its protonated form and this spectrum showed a band solely due to the COOH (1713 cm^{-1}). There were no bands due to COO^- groups. Therefore at pH < 2, the intensity of the band at 1713 cm^{-1} represents the point of 100% COOH groups on the NaPA. Conversely, at pH values > 9, the spectrum shows only bands due to the COO^- and the band at 1713 cm^{-1} vanishes. At intermediate pH values between 2 and 9, the spectra of NaPA have bands for both COOH and COO^- groups (see Figure 5.2).

To take into account that the amount of NaPA adsorbed on TiO_2 will vary with contact time, (and thus the intensity of the COOH or COO^- bands will also vary with adsorbed amount) the intensity of the band at 1713 cm^{-1} was ratioed to the integrated intensity of the CH_2 mode at 1455 cm^{-1}. This normalization to the CH_2 mode provides a measure of the average %COOH groups per polymer molecule. Figure 5.3 is a plot of the % COOH computed for NaPA in solution using the normalized COOH band at 1713 cm^{-1} and the $\%COO^-$ using the normalized COO^- band at 1545 cm^{-1}. There is the anticipated relationship between the two curves in Figure 5.3 as they intersect near the 50 %COOH value. The total values of COOH and COO- for each pH in Figure 5.3 is 100% ± 2% demonstrating the validity of the integration procedure described in the experimental section. As further validation of the calibration curves, it is noted that the 50% COOH point occurs at a pH value of 4.8 and this is the same value reported for the pKa of NaPA polymers.[88]

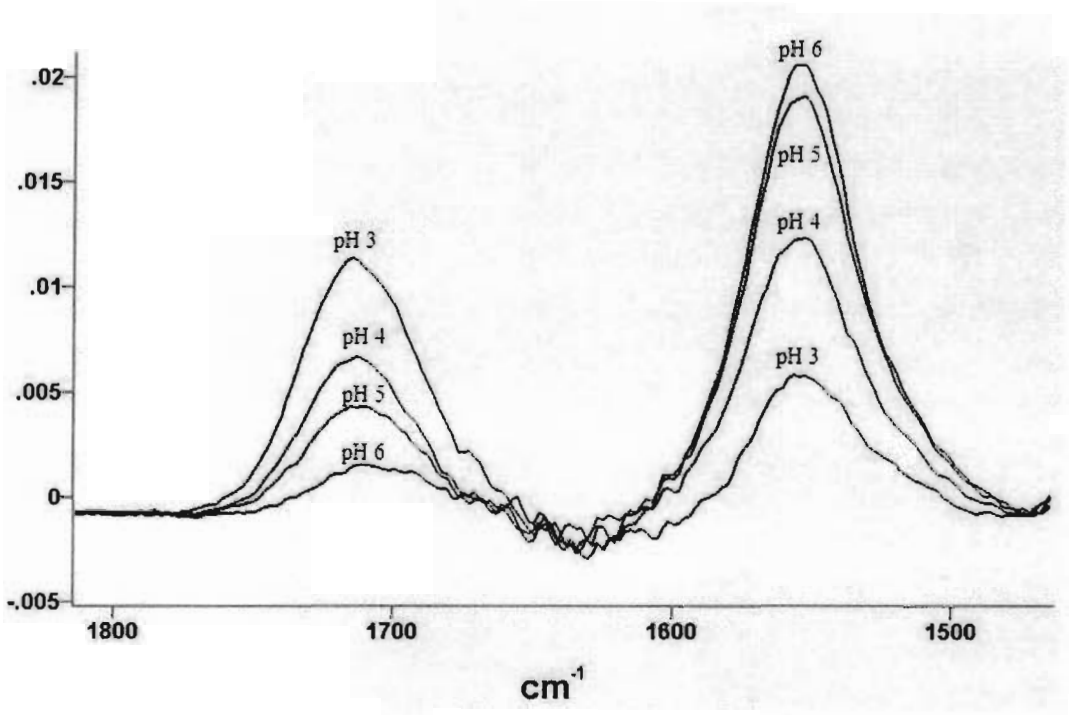

Figure 5.2 Infrared spectrum of 10,000 ppm NaPA in solution recorded at different pH.

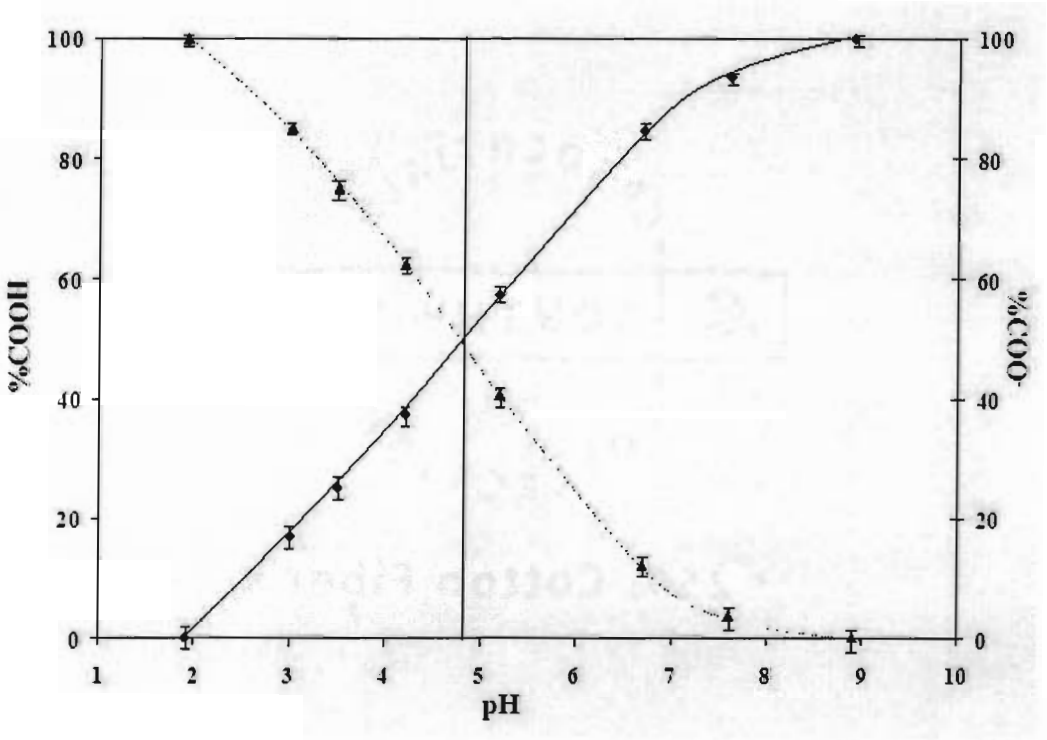

Figure 5.3 pH dependence of %COOH (▲) and % COO^- (♦) for NaPA in solution.

5.3.2 Adsorption of NaPA

The relative amount of NaPA adsorbed as a function of time at different solution pH is shown in Figure 5.4. The isoelectric point (IEP) of the titania is 6.5 and at pH values below the IEP the surface is positively charged. The amount of NaPA adsorbed on the titania will vary with solution pH as both the number of negatively charged COO^- sites on the polymer and the number of positively charged sites on the surface are pH dependant. From an electrostatic perspective, there are two counteractive trends occurring as the solution pH is lowered below 6. While the number of positively charged sites on the TiO_2 surface increases with lowering pH, the number of negative charged sites (COO^-) on the polymer chain decreases.

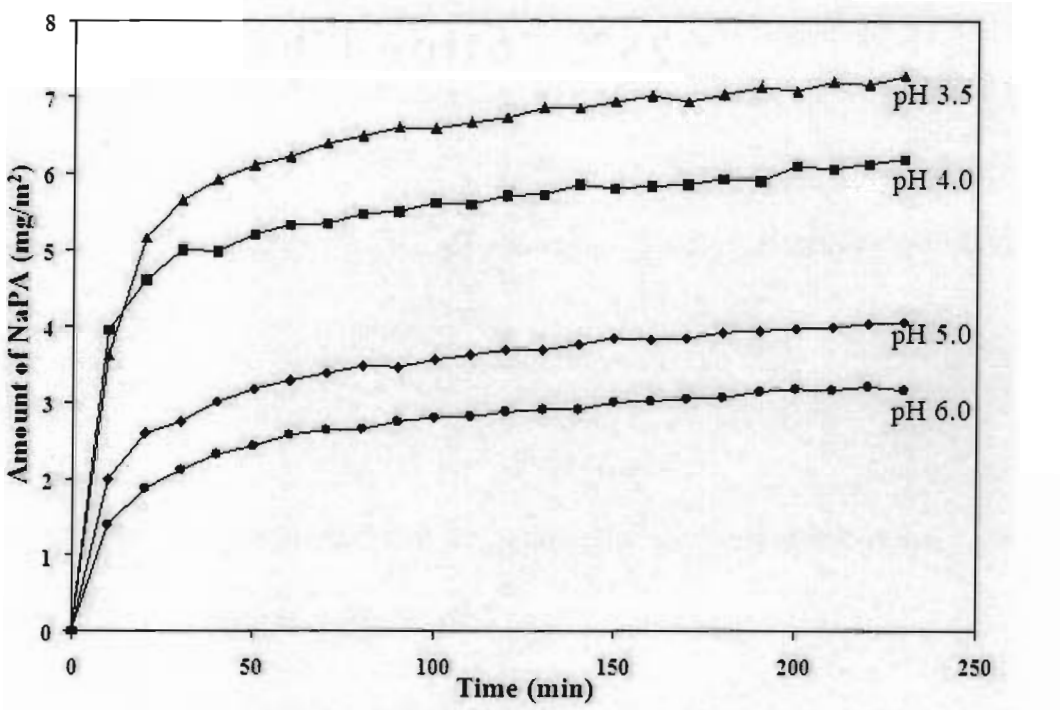

Figure 5.4 Amount of NaPA adsorbed from a 20 ppm solution onto TiO_2 at different pH.

The data in Figure 5.4 shows that the amount of NaPA adsorbed at pH 3.5 is a factor of 2.3 times higher than the amount adsorbed at pH 6. At the same time, the number of negative sites on the NaPA in solution approaching the surface decreases from 84% COO^- at pH 6.0 to 25 % COO^- at pH 3.5 in solution (see Figure 5.3). It is also interesting to note that the NaPA adsorbed onto the TiO_2 has a different %COOH than the corresponding polymer in solution. Figure 5.5 shows the %COOH groups calculated for the polymer both in solution and when adsorbed on TiO_2. The two lines in Figure 5.5 show that the %COOH in the bulk solution is always higher in value than that obtained for the adsorbed polymer on the TiO_2. This can be explained by competing equilibria processes as depicted in scheme 5.2. In essence, the binding of COO^- groups with the positive TiO_2 sites results in a re-adjustment of the equilibrium between the remaining COO^-/COOH groups of the polymer.

$$NaPA + H^+ \rightleftharpoons HPA + Na^+ \text{ (in solution)}$$

$$+$$

$$TiOH_2^+$$

$$\downarrow\uparrow$$

$$TiOH_2PA + Na^+$$

(On surface)

Scheme 5.2. Competing Equilibrium Processes for NaPA Adsorption on TiO_2 surfaces

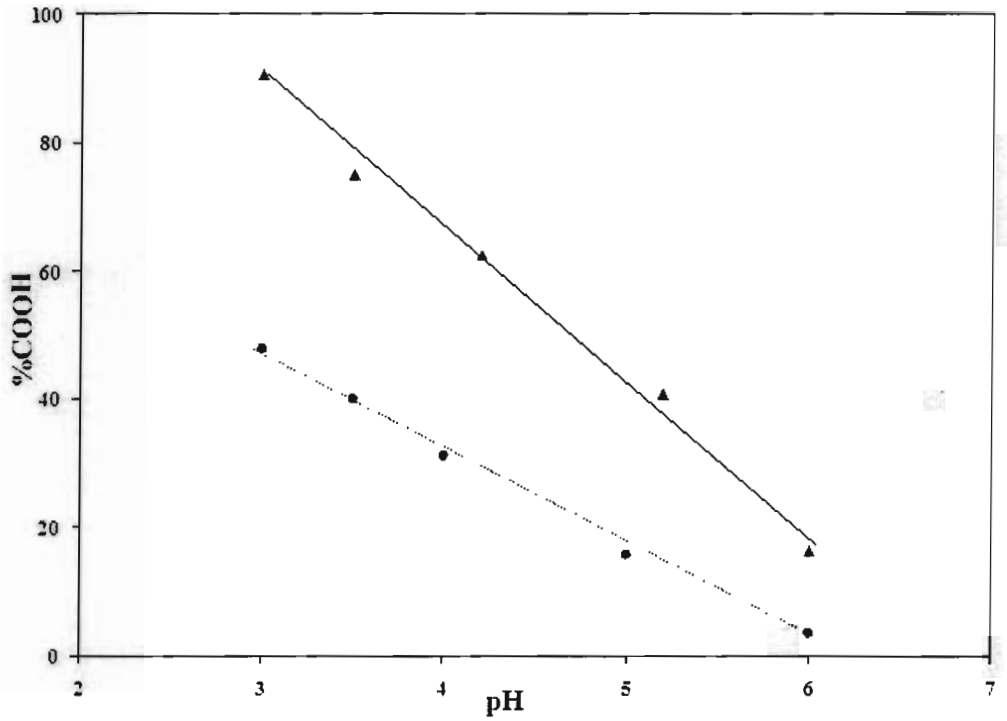

Figure 5.5 % COOH of NaPA in solution (▲) and adsorbed on TiO_2 (•).

This difference in %COOH for NaPA in solution compared to the adsorbed state provides a relative measurement of the number of COO^- groups bound to surface sites. At pH 6, the NaPA in solution shows the largest net change in %COOH (16% → 4%) between the solution and adsorbed state and this difference narrows as the pH is lowered. This suggest that the polymer adsorbs at a higher bound fraction at pH 6 than at pH 3.5.

Since the COO^-/COOH ratio for segments not bound to the surface are expected to follow the same COO^-/COOH ratio for NaPA in solution, it is possible to estimate the %COO^- groups bound to surface sites. For example, at pH 6 the COO^-/COOH ratio for NaPA in solution is 5.25. Thus a value of 4% COOH measured for NaPA adsorbed at pH 6 implies that there is 5.25 times this amount of free COO^- groups (i.e, 21% free COO^-). Therefore, the remaining 75% COO^- groups are bound to the surface.

The calculated bound COO^- for NaPA adsorption at the various solution pH is given in table II. At pH 3.5, the NaPA adsorbed on TiO_2 has about 47% bound COO^- showing that there is a loosely adsorbed polymer layer. This observation is consistent with the trend in adsorbed amount. At the lower pH, there is a higher adsorbed amount of polymer and thus the polymer would adopt a structure that has a lower bound fraction to accommodate the higher density of polymer on the surface.

Table 5.2 Computed bound $\%COO^-$ for NaPA in solution and adsorbed on TiO_2 from a 20 ppm solution at different pH conditions.

pH	Free %COOH	Free $\%COO^-$	Bound $\%COO^-$	$\nu_s COO^-$ (cm^{-1})	$\nu_{as} COO^-$ (cm^{-1})	$\Delta\nu$ (cm^{-1})
6	4%	21%	75%	1407.4	1551.8	144.4
5	16%	20%	64%	1409.5	1551.4	140.9
4	31%	15%	54%	1412.4	1546.4	134.0
3.5	40%	13%	47%	1413.5	1545.4	131.9
3	48%	13%	39%	1414.5	1539	124.5

The frequency position for both the antisymmetric and symmetric stretching mode of COO^- of NaPA in solution over the pH range of 3-6 is essentially constant with values of 1553.5 ± 0.5 and 1403.5 ± 0.6 cm^{-1}, respectively. However, both bands shift in frequency for NaPA adsorbed on TiO_2. The difference in bound COO^- is accompanied by a change in the $\Delta\nu$ between the antisymmetric and symmetric stretching mode of COO^- (see Table 5.2). A plot of the $\Delta\nu$ vs bound $\%COO^-$ gives a linear relationship (R^2 = 0.985) showing that an increase in bound $\%COO^-$ is associated with a change in bonding character from a bidentate chelating to bidentate bridging structure. Comparing the two

pH extremes (i.e., adsorption from solution pH of 3 and 6), the NaPA adsorbed at pH 6 has the lower adsorbed amount, a higher bound fraction, and a higher fraction of bidentate bridging of the COO^- with surface sites. A bidentate bridging structure occupies two surface sites per bound COO^- molecule whereas a bidentate chelating occupies one surface site per bound COO^- molecule. Thus a transition from bidentate bridging structure to bidentate chelating would facilitate a higher amount of polymer adsorbed on TiO_2.

5.3.3 Dynamics of NaPA Adsorption

The data in Figure 5.5 clearly shows that there is a difference in the %COOH in free polymer in solution and the adsorbed state and I have ascribed this to the bound fraction of the polymer. If this is the case, then the bound $\%COO^-$ should provide information on the conformational changes that occurs with time as the polymer solution contacts the bare TiO_2 surface. The results obtained for the adsorption from a 20 ppm NaPA solution as a function of contact time at pH 3.5 is shown in Figure 5.6. There is an initial, rapid increase in the amount of polymer adsorbed followed by a slow gradual increase after 50 min (shown in curve 5.6a). A plot of the change in the bound $\%COO^-$ with contact time is shown in curve 5.6b. Curve 5.6b shows an initial rapid increase for the first measurement (10 minute contact time) from a total of 25% COO^- in solution to total of 76% COO^- of which 69% are bound COO^-. This is followed by a decrease to the plateau equilibrium value of 47% bound COO^-. The initial 69% bound COO^- shows that the polymer approaching the bare surface adsorbs by a high bound fraction (see Figure 5.7). After the surface is covered by the polymer layer, the adsorbed layer adopts a

conformation with a lower bound fraction in order to accommodate the adsorption of more incoming polymer to the surface. As a result of this lower bound fraction, the bound %COO^- decreases from 69% to 47%. After about 50 min, there is small increase in adsorbed amount and a small decrease in bound %COO^- showing that some rearrangement does occur from this time onward.

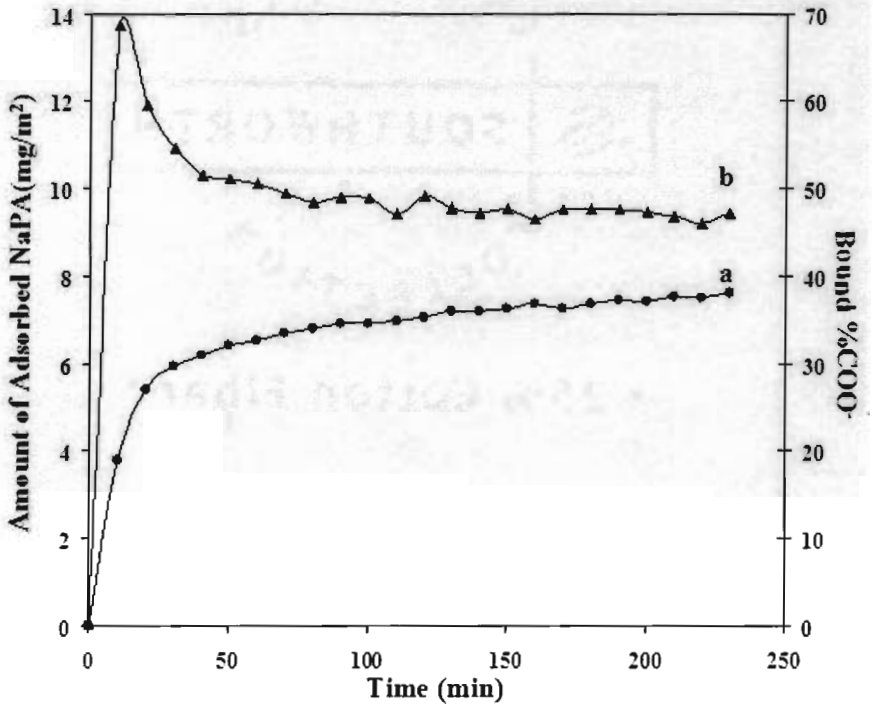

Figure 5.6 Time evolution of (a) the adsorbed amount and (b) the bound %COO^- when NaPA is adsorbed from a 20 ppm solution onto TiO_2 at pH 3.5.

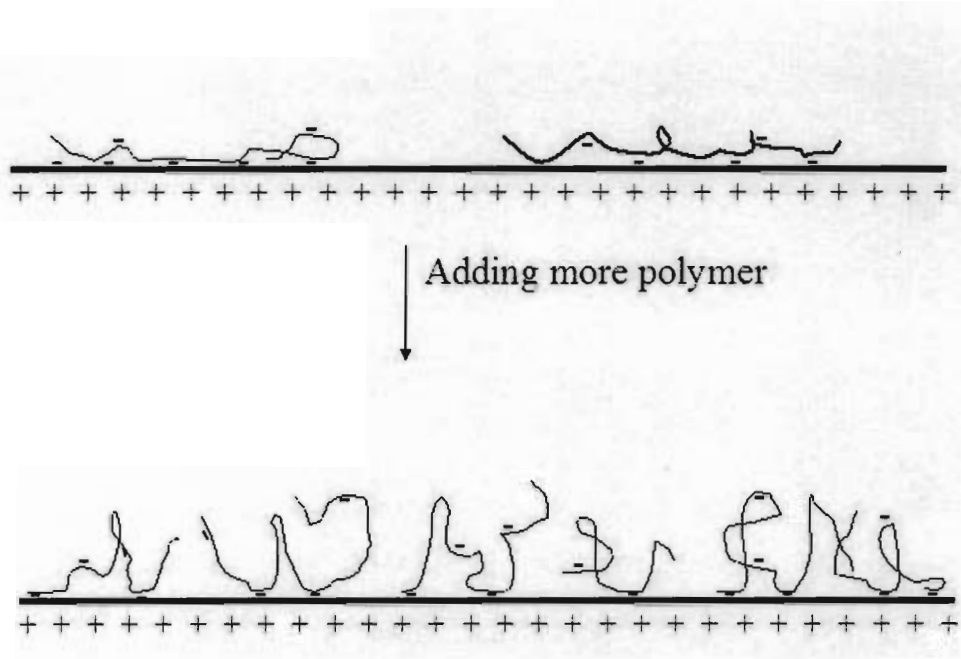

Figure 5.7 Representative structures consistent with bound %COO^- values during the adsorption of NaPA on TiO_2.

5.3.4 Sequential Adsorption of NaPA then SDS

Monitoring the change in bound %COO^- could also provide information on the nature of the interaction of NaPA with surfactants. In this section I examine the spectral changes occurring during the interaction of the adsorbed NaPA with a negatively charged SDS and in the next section, the interaction with the positively charged CTAB. Since both SDS and NaPA are negatively charged, it is anticipated that there is little or no interaction between SDS and NaPA but rather, a competitive adsorption for the positive surface sites.

Figure 5.8 shows the dynamic change in the NaPA and SDS obtained after flowing a 0.1 mM solution of SDS across the adsorbed polymer layer. The 20 ppm NaPA solution was first allowed to adsorb at the TiO_2/water interface for 4h, followed by addition of a 0.1 mM SDS solution. The point of SDS introduction is indicated by the

arrow in the curves shown in Figure 5.8. The integrated area of symmetric mode of CH_2 (2850 cm^{-1}) was used to measure the amount of adsorbed SDS and the amount of adsorbed NaPA and bound %COO- was determined as before, using the integrated intensity of the band at 1455 cm^{-1} and the band ratio of 1713/1455 cm^{-1}, respectively. When SDS was added, there was an initial rapid rise in the amount of SDS adsorbed followed by a slow continuous rise. After 4 hrs contact with the SDS solution, the amount of SDS adsorbed is about 50% of the value obtained in a separate experiment for the adsorption of SDS on a bare TiO_2 surface under the same pH and surfactant concentration. The contact of the SDS with the adsorbed NaPA resulted in only a small, yet rapid drop of 8% of the adsorbed amount of the NaPA followed by a slower and smaller decrease with time. At the same time, there was an abrupt decrease in the bound $\%COO^-$ from 47% to about 39% with initial contact with the SDS solution followed by a slow increase to a value of 43% bound COO^- after 4 hrs.

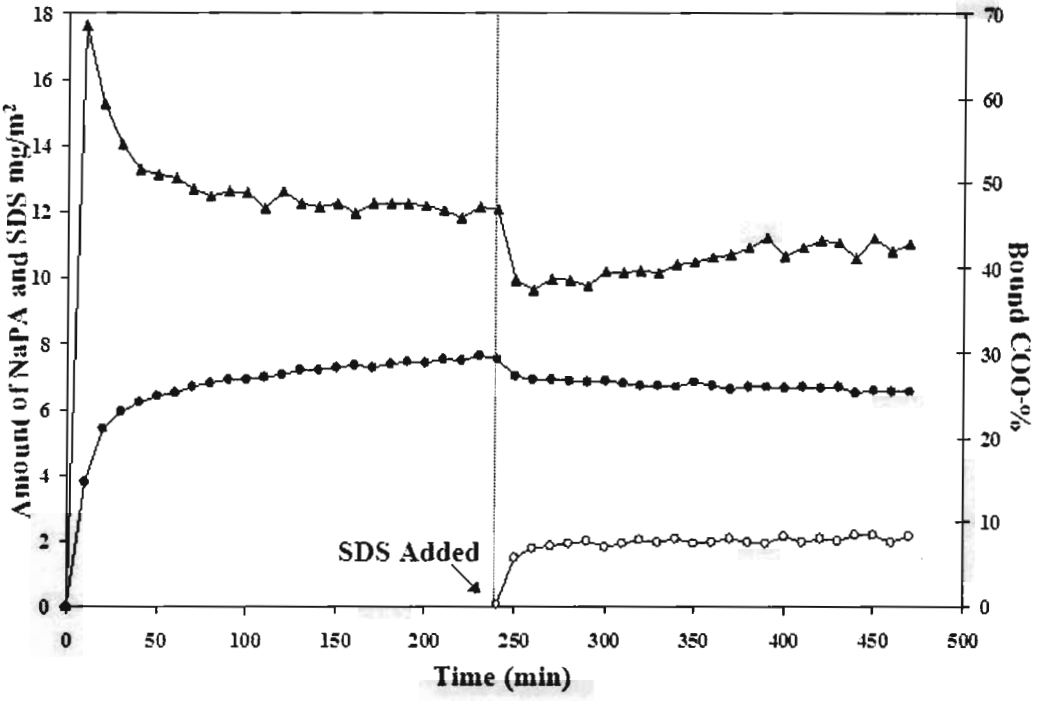

Figure 5.8 Adsorption dynamics for the sequential addition of NaPA followed by SDS onto TiO_2 at pH 3.5. [NaPA]=20 ppm, [SDS]= 0.1mM, (o) SDS adsorbed amount, (•) NaPA adsorbed amount, (▲) bound $\%COO^-$.

When the SDS is introduced, there is a large uptake on the surface (50% of the value obtained for a bare TiO_2 surface) suggesting that there are both a large number of sites not covered by the polymer and that the SDS dislodges bound NaPA segments from the surface (see Figure 5.9). It is noted that the rapid increase in %COOH of the remaining adsorbed NaPA with SDS introduction supports the contention that the SDS also displaces polymer segments without removing the polymer. This leads to an adsorbed NaPA with a lower bound fraction on the surface. There is only a small decrease in the adsorbed amount of NaPA because the NaPA is adsorbed through multi-

segments. A complete release of the polymer molecule from the surface requires simultaneous displacement of all adsorbed segments by the SDS.

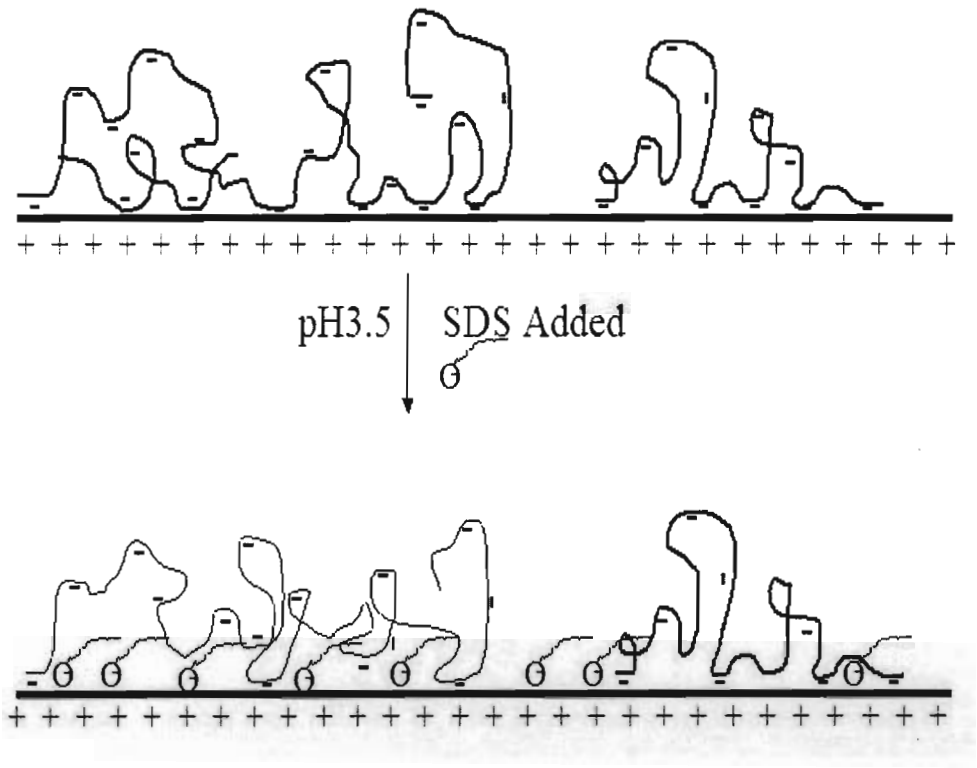

Figure 5.9 Representative structures consistent with bound %COO^- values and adsorbed amount of NaPA and SDS during the sequential addition of NaPA followed by SDS.

The slow increase in the bound %COO^- from 39% to 42% occurring with prolonged incubation in a flowing SDS solution is accompanied by a small decrease in the amount of adsorbed NaPA. A possible explanation for this trend is that the ejected polymer are from those molecules with a low bound fraction leaving polymer molecules with a higher bound fraction on the surface. This would produce an apparent increase in the bound %COO^-.

5.3.5 Sequential Adsorption of NaPA then CTAB

In contrast to the negatively charged SDS and NaPA system in which there is a competitive process for surface sites, the CTAB is positively charged and thus it is anticipated that a corporative adsorption process would occur between the NaPA and the CTAB. There is no competition for surface sites as both CTAB and TiO_2 are positively charged at pH 4.0. The data obtained for the sequential adsorption of the NaPA /CTAB system is shown in Figure 5.10. At pH 4.0, a 20 ppm NaPA solution was allowed to adsorb to the TiO_2/water interface for 4h. Then a 0.1 mM CTAB solution was introduced and allowed to interact with the pre-adsorbed NaPA layer for 2h. As with the SDS, the amount of CTAB is monitored using the integrated area of the symmetric CH_2 stretching mode at 2850 cm^{-1}. When the CTAB was introduced, there was an initial rapid adsorption of the CTAB, no desorption of NaPA, and a rapid increase in the bound $\%COO^-$. This contrasts to the addition of SDS where there was a small decrease in adsorbed amount of NaPA and a decrease in the bound $\%COO^-$. In a separate experiment, it was found that CTAB does not adsorb on a bare TiO_2 surface at pH 4.0 and thus the rapid increase of CTAB must be due to adsorption to the polymer layer. The increase in the bound $\%COO^-$ is consistent with the CTAB binding to the negatively charged COO^- sites of the adsorbed polymer layer (see Figure 5.11). The equilibrium mass ratio of 6.0 mg/m^2 and 1.5 mg/m^2 for adsorbed NaPA and CTAB respectively, converts to an approximate ratio of 1 CTAB per every 15.5 $COOH/COO^-$ group on the polymer backbone. Assuming that the 15% increase in bound COO^- is only due to free COO^- binding to CTAB, (i.e., does not change the $\%COO^-$ bound to the surface) then a NaPA/CTAB ratio of about 6.7 would be expected. However, this value is lower than

15.5 obtained for the NaPA/CTAB ratio obtained from the amount adsorbed on the TiO_2. This implies that the complexation of CTAB to the NaPA leads to a change in the conformation of the NaPA resulting in an increase in the number of COO^- groups bound to surface sites. It is noted that the binding of CTAB to the free COO^- groups would lead to a lower solubility of the loops and tails of the NaPA due to the presence of the hydrophobic tails of the CTAB. The lower solubility would force the NaPA closer to the surface leading to an increase the number of bound COO^- groups.

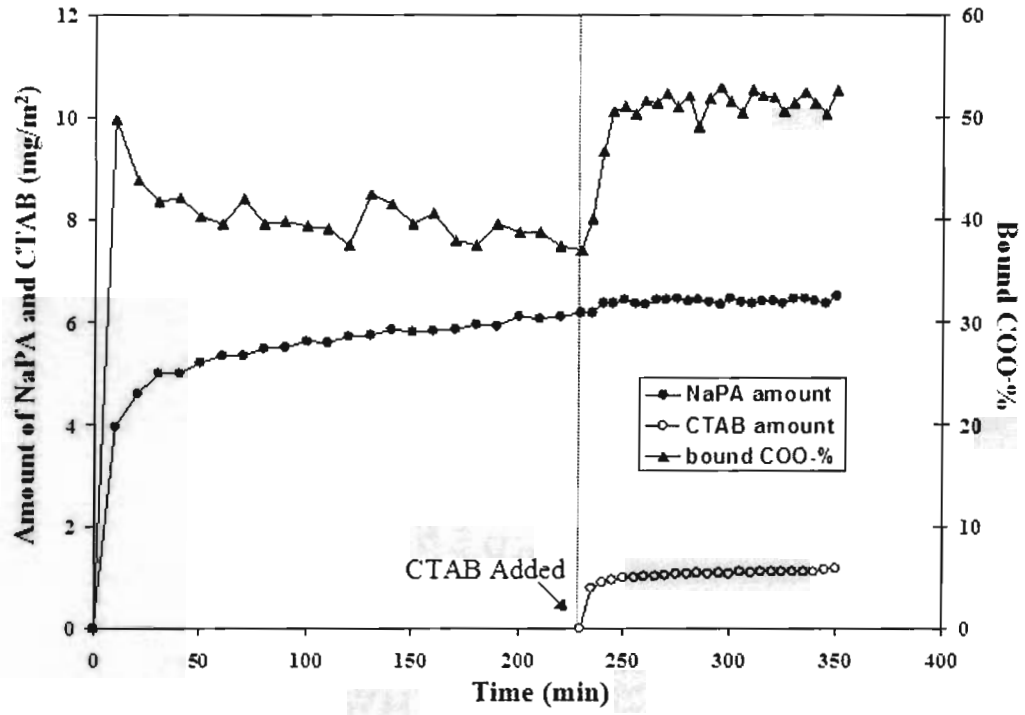

Figure 5.10 Adsorption dynamics for the sequential addition of NaPA followed by CTAB onto TiO_2 at pH 4.0. [NaPA]=20 ppm, [CTAB]= 0.1 mM, (o) CTAB adsorbed amount, (•) NaPA adsorbed amount, (▲) $\%COO^-$.

It has been demonstrated that the changes in bands due to COOH and COO^- of the NaPA are useful in providing conformational information of the adsorbed structure and surfactant/polymer interactions. However, additional conformational information can be obtained by examining the bands due to the headgroup of the surfactant. For example, confirmation of the adsorption of the CTAB onto the free COO^- sites of NaPA is provided by bands in the region between 1500 cm^{-1} and 1300 cm^{-1} assigned to various modes of the CTAB headgroup.[23] As shown in Chapter 3, an increase in the band intensity of symmetric bending mode of $+N(CH_3)_3$ at 1396 cm^{-1} relative to the CH_2 modes represents an increase in the percentage of CTAB molecules interacting with negatively charged sites on the TiO_2 surface. This arises because the transition dipole moment for the symmetric bending mode of $+N(CH_3)_3$ is perpendicular to the surface and increases in magnitude when interacting directly with an oppositely charged site on the surface. Figure 5.12 is a difference spectrum of adsorbed CTAB on the NaPA coated TiO_2. This spectrum was obtained by subtracting the spectrum recorded just prior to addition of CTAB from the spectrum recorded after 4hr incubation with the CTAB solution. Thus, negative bands represent bonds that have been removed from the NaPA coated TiO_2 and positive bands represent bonds that been added to this surface. In Figure 5.12, all positive bands except for the band at 1545 cm^{-1} are due to CTAB. The 1545 cm^{-1} is due to an increase in the COO^- on the NaPA arising from a decrease in the COOH group (negative band at 1713 cm^{-1}).

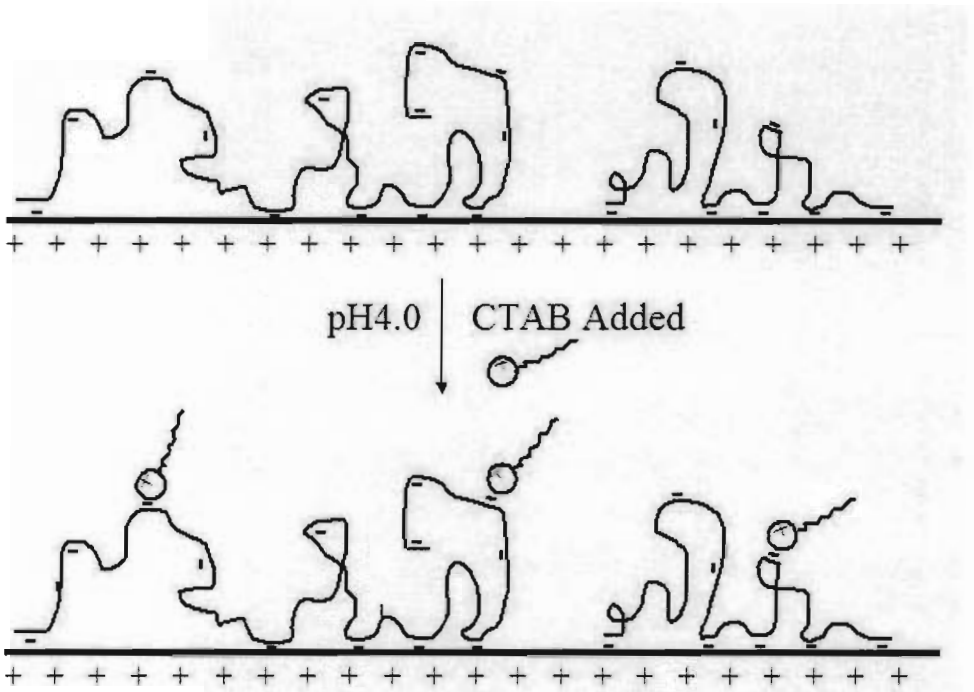

Figure 5.11 Representative structures consistent with bound %COO^- values and adsorbed amount of NaPA and CTAB during the sequential addition of NaPA followed by CTAB.

The bands at 2920 and 2850 cm^{-1} are the CH_2 antisymmetric and symmetric modes of the surfactant tail and show that CTAB has adsorbed on the surface. The key features are the bands in the region between 1500 and 1300 cm^{-1} and these are shown in the inset. The bands are assigned as 1490 cm^{-1} (δ_{as} ^+N-CH_3), 1479 cm^{-1} (δ_{as} ^+N-CH_3), 1467 cm^{-1} (CH_2 scissor mode) and 1396 cm^{-1} (δ_s ^+N-CH_3). Of particular note is the intensity of the 1396 cm^{-1} band relative to the CH_2 modes of the surfactant tail. Comparing the 1396/2850 cm^{-1} ratio in Figure 5.12 with those for different aggregated structures of CTAB on TiO_2,[23] it is in the range expected where each CTAB molecule is involved in a 1:1 interaction with COO^- sites. Our previous work showed that adsorption from a 0.1 mM CTAB solution onto TiO_2 at a solution pH of 10.3 resulted in a much

lower 1396/2850 cm^{-1} band intensity ratio than shown in Figure 5.12. This was attributed to the formation of admicelles on the surface. It was only at CTAB solution concentration of <0.01 mM where adsorption onto TiO_2 at pH 10.3 gave rise to a similar 1396/2850 cm^{-1} ratio as shown in Figure 5.12.

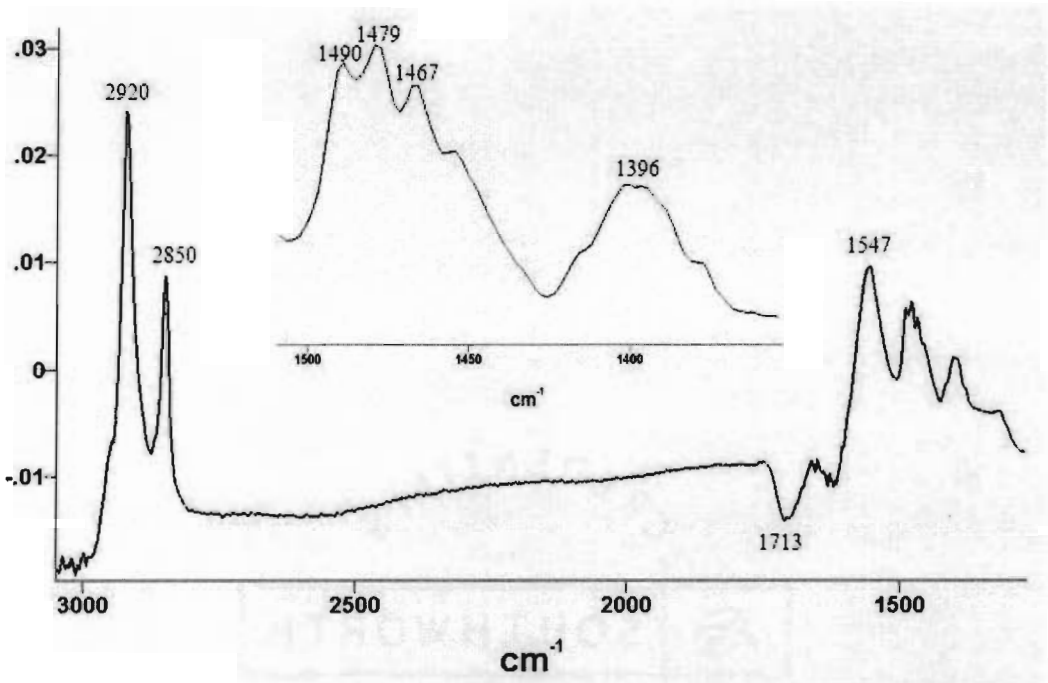

Figure 5.12 Infrared spectrum of CTAB adsorbed onto NaPA coated TiO_2. The NaPA coated TiO_2 was used as the reference spectrum.

5.4 Conclusion

We have demonstrated a general approach in which changes in infrared bands of functional groups on a polyelectrolyte can be used to determine the nature of the adsorbed polymer structure on surfaces. Specifically, by measuring the changes in the COO^-/COOH IR bands in tandem with the adsorbed amount of NaPA on a charged TiO_2 surface, it was possible to identify the adsorbed polymer structures and to determine the

nature of the interaction of the adsorbed polymer to cationic or anionic surfactants. In particular, the relative intensity of the antisymmetric COO^- and the COOH stretching modes of the NaPA changes as the polymer is adsorbed on the positively changed TiO_2 surface and this is related to the bound fraction. The dynamic changes in the COO^-/COOH IR bands show that the polymer approaching the bare TiO_2 surface adopts a flat configuration and adsorbs with a high bound fraction. The polymer layer then rearranges to a lower bound fraction to accommodate more polymer on the surface.

The change in the adsorbed NaPA structure when exposed to cationic and anionic surfactant can also be determined by the change in the bound $\%COO^-$ on the polymer backbone. Addition of an anionic surfactant, SDS, results in the desorption of a small amount (8%) NaPA and the remaining polymers have a higher %COOH showing that the SDS also displaces polymer segments without removing the polymer. This leads to a lower bound fraction of the polymer on the surface. When a positively charged surfactant, CTAB is added to pre-adsorbed NaPA, the CTAB binds to free COO^- groups on the polymer. This is determined from the change of the bound $\%COO^-$ as well as the change in intensity of the symmetric bending mode (δ_s ^+N-CH_3) of CTAB.

CHAPTER 6. AN INFRARED STUDY OF THE INTERACTION OF CHARGED SILICA PARTICLES WITH TiO_2 PARTICLES CONTAINING ADSORBED CATIONIC AND ANIONIC POLYELECTROLYTES

6.1 Introduction

Polymers/surfactants are used to control and modify the surface properties of particulate suspensions.[1] The interaction of the polymers and surfactants on surfaces are complex leading to a variety of aggregated structures that depends on factors such as the nature of the surfactant and polymers, the properties of the surface, pH, ionic strength, solution concentration of the adsorbates as well as kinetic factors such as the order and time of addition of surfactant/polymer.[2-7] It is the nature of the aggregated structure on the surface that often dictates the interfacial properties of the colloidal suspension. As a result, there is voluminous literature dedicated to the study of surfactant/polymer adsorption on single well-defined surfaces.[13, 14, 16-23]

On the other hand, there are relatively few studies of surfactant/polymer adsorption in mixed particulate systems. This is not because of a lack of interest as most industrial processes involving particulate suspensions are not single component systems. For example, in the paper coating industry, it is common to prepare a final coating formulation by mixing different pre-stabilized pigment and binder suspensions. The behavior of the resulting formulation is often unpredictable. Clearly, the interfacial interactions are more complex in a mixed particulate system as additional processes such as migration of polyelectrolytes/surfactants between the different pigments are possible.

While there are several experimental methods able to extract information on adsorbed polymer/surfactants in a single component system, the number dwindles when extrapolated to studies of mixed particulate system. AFM[89, 90] and surface force measurements[91, 92] methods have been the main experimental approach as it is possible to measure the interfacial forces of adsorbed polyelectrolytes on dissimilar surfaces. Meagher, *et. al.* studied the interaction between silica and α-alumina surfaces in the presence and absence of polyelectrolyte and the mixture of anionic polyelectrolyte sodium poly(styrene sulfonate) (PSS) and the cationic surfactant cetyltrimetlylammonium bromide (CTAB).[89] A silica particulate was attached to the AFM tip and force-distance curves were measured between the coated tip and a flat alumina plate. They found that the interaction between the bare silica and an uncharged bare alumina surface in water was weakly repulsive at long distances and van der Waals attraction occurred at smaller separation distances. Co-addition of PSS and CTAB to the solution resulted in a strong repulsive force between the two surfaces and this was attributed to the co-adsorption of negatively charged PSS/CTAB complex on the alumina. Structural information was deduced from measuring the thickness of the adsorbed layer. The authors found that the adsorbed PSS/CTAB did not extend out into the solution but rather adopted a flat conformation with few loops and tails extending from the surface. In another AFM study, Hartley, *et. al.* measured the interaction between negatively charged mica and silica surfaces bearing an adsorbed cationic polyelectrolyte.[90] When the highly negatively charged silica was introduced to the weakly negatively charged polymer coated mica, a long-range attraction was found between the two different surfaces. This long rang attractive force agreed with predictions by the dissimilar double layer theory. While the

force-distance measurements by AFM or the surface force apparatus provide valuable information on the interfacial forces between dissimilar surfaces, they do not measure the surface excess of each surfactant/polymer and provide little information on the nature of the aggregated structure. Furthermore, dynamics of the interactions are not obtained by AFM as the measurements are performed at equilibrium.

Recently an ATR-IR technique was developed to measure dynamically the adsorbed structures formed when surfactants,[14] polymers,[23] mixed surfactant/polyelectrolytes[93] and mixed surfactant/surfactant[94] adsorb on TiO_2. The advantage of this IR-based approach is that it can be used to measure the adsorbed amount of each compound as well as the nature of the aggregated structure. In particular, structure insensitive bands such as CH_2 modes of the alkyl tail of the surfactants and the polymer backbone are used to measure the adsorbed amount whereas bands due to the surfactant headgroup and functional moieties of the polymer provide evidence of the mixed polymer/surfactant architecture.

In a typical experiment, TiO_2 particles are anchored to a bare ATR crystal and infrared spectra are recorded as a function of time while solutions containing polymers and surfactants are flowed across the anchored TiO_2 particles. Given this simple experimental setup, it is a natural extension to apply this approach to the interaction of polymers/surfactants on dissimilar surfaces. In this case, a solution containing a different particulate is passed across a bare or polymer/surfactant coated TiO_2. It should be possible to identify and follow changes to infrared bands of the particulates while simultaneously measuring the change in the adsorbed amount and structure of polyelectrolyte/surfactant on these dissimilar surfaces.

In this chapter, the potential of this IR method was demonstrated for studying adsorption of polymers on mixed particulate systems. In particular, infrared spectra are recorded while solutions containing bare and aminosilane modified silica powders are flowed across bare and polymer coated TiO_2 particles anchored to an ATR crystal. The silica has an isoelectric point (I.E.P.) of pH 2-3 whereas the aminosilanated silica has an I.E.P. at pH 7.0. By using the two types of silica it is possible to flow positively charged or negatively charged particles through the cell at a given solution pH. For example at pH 3.5, the silica is negatively charged whereas the aminosilanated silica is positively charged.

The TiO_2 is either coated with the anionic sodium polyacrylate (NaPA) or cationic poly(diallyldimethylammonium) chloride (PDADMAC). The amount of silica deposited on the TiO_2 and changes in the structure and adsorbed amount of the polymer layer are measured from the IR spectra. To the best of our knowledge, this is the first study in which IR spectroscopy has been used to study the interaction of an adsorbed polymer layer between dissimilar surfaces. More important, this work demonstrates the usefulness of this experimental approach for obtaining a better molecular understanding of the interactions that occur when different particulates containing adsorbed polymers are mixed together.

6.2 Experimental Section

Sodium polyacrylate (NaPA) and poly(diallyldimethylammonium) chloride (PDADMAC) were purchased from Aldrich and used as received. The average molecular weight for the NaPA is 30,000 and average molecular weight for the PDADMAC is 150,000. The structures of the two polymers are shown in scheme 6.1. Fumed TiO_2 (P25)

and silica powder (Aerosil 380) were obtained from Dugussa. The TiO_2 has a BET N_2 surface area of 50 m^2/g and the corresponding value for silica is 380 m^2/g. The details for preparing the TiO_2 coated ATR crystal and in performing the flow-through ATR experiments are described in chapter 2.

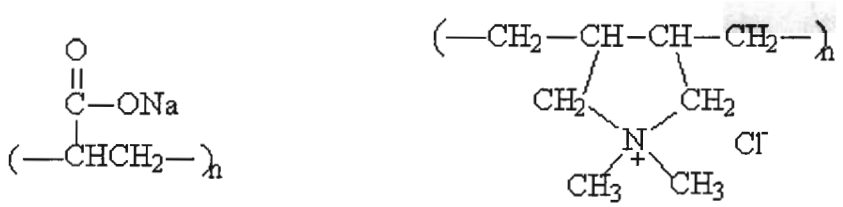

Scheme 6.1 Structures of polyacrylate sodium (NaPA) and Poly(diallyldimethylammonium) chloride (PDADMAC)

To prepare the aminosilanated silica powder, 500 mg of the silica powder was mixed with 125 mg of 3- aminopropyldimethylethoxysilane (APDMES) in 20 ml toluene, and stirred at room temperature for 6 hrs. The mixture was centrifuged and washed 4 times with toluene and dried. The measured isoelectric point of the aminosilanated silica was pH 7.0.

The TiO_2 coated ZnSe crystal was prepared as described in chapter 2. The reference spectrum was recorded with the water flowing through the cell. A suspension containing 12.5 mg silica or aminosilanated silica powder was prepared by dispersing the powder in 500 ml water adjusted to the desired pH and sonicated for 30 min. The suspension containing bare or aminosilanated silica particles was flowed through a bare or polymer-coated TiO_2 surface and spectra were recorded as a function of time. Preparation of the polymer coated TiO_2 was done in advance of the addition of the silica

suspension by flowing a polyelectrolyte solution (either 5 ppm NaPA at pH 3.5 or 30 ppm PDADMAC at pH 10.3) through the cell. Spectra were recorded as a function of contact time and the polymer solution was passed through the cell until no further changes were observed in the spectra. This typically required about 4 hrs. The cell was then rinsed for 5 minutes with flowing water at the specified pH to remove excess polymer from solution. This short rinse did not remove any polymer from the surface. In separate control experiments, it was found that rinsing either the NaPA or PDADMAC coated TiO_2 with water for a period of 24 hrs did not lead to a change in the IR spectra. After the short rinse with water, the silica suspensions were then flowed through the cell.

6.3 Results and Discussion

6.3.1 Adsorption of Bare and Aminosilanated Silica on Bare TiO_2

The first series of experiments were baseline measurements using a suspension of bare and aminosilanated silica particles flowing across the bare TiO_2 surface. Since the isoelectric point (IEP) of silica, aminosilanated silica and TiO_2 occur at pH 2.0-3.0, 7.0 and 6.5 respectively, there will be a pH dependence in the interaction of the silica and the TiO_2. Figure 6.1a is the spectrum obtained for contact of the TiO_2 with a 25 ppm suspension of bare silica particles at solution pH of 10.3. A flat spectrum is obtained with no bands. In this case, both the silica and TiO_2 are negatively charged. The absence of bands shows that the silica does not adsorb on the TiO_2 particles and that no TiO_2 particles are removed from the ATR crystal. Adsorption of silica would be identified by a band near 1100 cm^{-1} and removal of TiO_2 would produce a negative feature in the 900-600 cm^{-1} region. The 1100 and 900-600 cm^{-1} bands are the strongest bulk modes for each

oxide. This spectrum also shows that at the concentration of 25 ppm, bands due to silica in the solution phase are not detected.

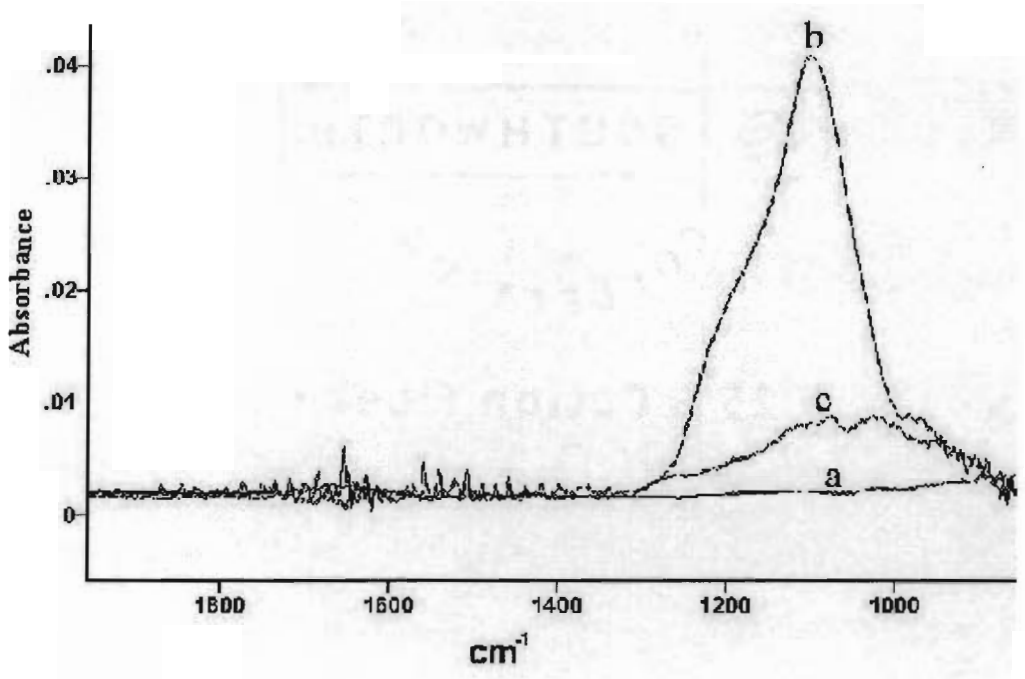

Figure 6.1 Infrared spectra recorded after contact of a 25 ppm suspension of (a) untreated silica with TiO_2 at pH 10.3 (b) untreated silica with TiO_2 at pH 3.5 (c)aminosilanated silica with TiO_2 at pH 3.5. The reference spectrum was recorded with water flowing through the cell at specified pH.

In contrast, at pH 3.5, the TiO_2 is positively charged and the spectrum obtained after flowing the 25 ppm suspension of silica particles has a broad silica peak centered near 1100 cm^{-1} (see Figure 6.1b). This shows that the negatively charged silica is deposited on the TiO_2. The spectrum was obtained after 120 minutes contact time and no further increase in the band at 1100 cm^{-1} was found with longer incubation. It is also

%COO^- = 1. The details for calculating the above values from the integrated intensities of the various bands are described in my earlier study.[93]

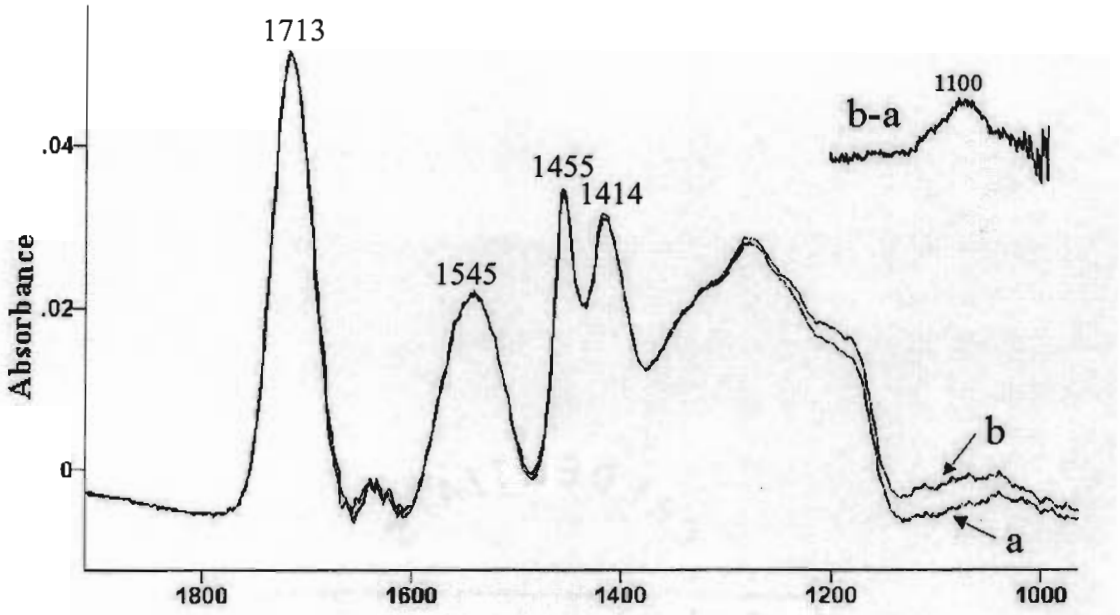

Figure 6.2 IR spectra of (a) NaPA adsorbed on TiO_2 from a 5 ppm NaPA solution at pH 3.5 followed by a 5 minute rinse with water at pH 3.5 and then (b) addition of a 25 ppm suspension of untreated silica at pH 3.5 for 120 minutes.

In chapter 5, it was found that the %COOH groups on the polymer backbone decreased when a polymer chain in solution adsorbed on the positively charged TiO_2. For example, at pH 3.5 the %COOH for NaPA in solution was 75% and this was lowered to a value of 40 %COOH for the polymer on the surface. This was explained by competing equilibria processes as depicted in scheme 5.2 in which the interaction of COO^- groups with the positive TiO_2 sites results in a re-adjustment of the equilibrium between the remaining COO^-/COOH groups of the polymer.

From the knowledge of the $COOH/COO^-$ ratio of the polymer in solution it was possible to calculate the values of free %COOH and free $\%COO^-$ located in the loops and tails of an adsorbed polymer as well as the bound $\%COO^-$ to charged surface sites. To differentiate between bound and free $\%COO^-$ it was assumed that the $COOH/COO^-$ ratio of the loops and tail regions of an adsorbed polymer was the same as the ratio for the polymer in solution. For example, a value of 40 %COOH was obtained for NaPA adsorbed on TiO_2 at pH 3.5 and thus the total $\%COO^-$ for the polymer on the surface is 60%. Since the $\%COOH/\%COO^-$ ratio of NaPA in solution at pH 3.5 is 3, the free $\%COO^-$ in the loops and tails of the adsorbed polymer would have this same ratio giving a value of free 13% COO^-. The bound $\%COO^-$ is then the remaining groups that are not either free %COOH or free $\%COO^-$. In the above example this value for bound $\%COO^-$ to surface sites is 47%. In chapter 5, the bound $\%COO^-$ was measured dynamically during contact of the NaPA solution with the TiO_2 and provided insight into the structure of the adsorbed polymer.[93]

It was also shown that changes in the bound $\%COO^-$ occurred when the adsorbed NaPA interacted with other charged molecules. For example, the addition of the cationic surfactant CTAB resulted in a 15% increase in the bound $\%COO^-$ and this was attributed to interaction of the positively charged CTAB with the free COO^- groups located in the loops and tails of the adsorbed polymer. In contrast, addition of the negatively charged surfactant, sodium dodecyl sulfate (SDS), leads to a competition of the surfactant and adsorbed polymer for the positive charged sites. In this case, the bound $\%COO^-$ decreased when the polymer layer was exposed to a SDS solution showing that the surfactant displaced some COO^- groups of the NaPA bound to positive surface sites. By

analogy, the interaction of positively charged silica particles with the free COO^- groups of an NaPA molecule bound to a TiO_2 particle should produce changes to both the COOH and COO^- infrared bands at 1713, 1545 and 1414 cm^{-1}. These changes in band intensities are, in turn, are interpreted as changes to the free %COOH, free %COO^- and bound %COO^-.

Figure 6.2b is the spectrum obtained after a 25 ppm suspension of silica particles at pH 3.5 is flowed across the NaPA coated TiO_2 surface. At this pH, the underlying TiO_2 is positively charged and both the adsorbed NaPA layer and the silica particles in suspension are negatively charged. It is anticipated that the addition of the silica suspension this may lead to a competition of the silica and the NaPA for charged TiO_2 sites as this is analogous from a charge perspective to chapter 5 with addition of an SDS solution to the NaPA coated TiO_2. Figure 6.2b shows that there is some silica adsorbing on the surface as evidenced by the weak band near 1100 cm^{-1} (more clearly illustrated in the subtracted spectrum shown in the inset in Figure 6.2). Compared to Figure 6.1b, the amount of silica adsorbed on the NaPA treated TiO_2 is about 10% of the total amount of silica adsorbed on a bare TiO_2. A lower amount of silica depositing on the TiO_2 is not surprising as the NaPA would cover most of the positively charged surface sites leading to charge reversal of the TiO_2 and electrostatic repulsion of the negatively charged silica.

As with the adsorption of SDS on a NaPA coated TiO_2,[93] it is tempting to conclude that the negatively charged silica displaces the adsorbed NaPA in order to access the positive surface sites. However, this does not occur as there is no change in the band at 1455 cm^{-1} and therefore no loss of polymer from the TiO_2 surface. A second possibility is that the polymer is not desorbed but that some segments are displaced by

the silica leading to a polymer adsorbed by a lower bound fraction. In this case, the dislodging of bound segments would lead to a readjustment of the COOH/COO^- ratio resulting in lower value of bound % COO^-. This also does not occur as the COOH and COO^- bands in Figures 6.2a and 6.2b are identical. The absence of any change in the COOH and COO^- bands shows that the silica does not interact with the polymer layer. Thus the most likely explanation for the small amount of adsorbed silica is that there are uncovered positive surface sites on the TiO_2 that can be accessed by the silica particles. It is noted that the adsorbed amount of NaPA obtained from a solution concentration of 5 ppm is 2.1 mg/m^2 and this is lower than the value of 7.5 mg/m^2 obtained for adsorption from a 20 ppm solution.[93] Thus, in this experiment there are open areas on the surface as the amount of NaPA is below saturation coverage of the surface.

6.3.3 Adsorption of Aminosilanated Silica with NaPA Coated TiO_2

The aminosilanated silica has a positive charge at pH 3.5 and thus a cooperative interaction with the NaPA coated TiO_2 was anticipated. As shown in Figure 6.3, this is indeed the case. In fact, there is more aminosilanated silica adsorbed on the NaPA coated surface than obtained with the bare silica particles on the bare TiO_2 (see Figure 6.1b). Given the absence of aminosilanated silica depositing on the bare TiO_2 at pH 3.5 (see Figure 6.1c), the large amount of aminosilanated silica in Figure 6.3b shows that the silica is participating in a electrostatic interaction with the NaPA.

Evidence supporting an interaction with the NaPA is provided by the decrease in the COOH bands at 1713 cm^{-1} and the increase in the COO^- bands at 1545, and 1414 cm^{-1}. The corresponding values of %COOH, free %COO^- and bound %COO^- are given in Table 6.1. With adsorption of the aminosilanated silica, the bound %COO^- increases

from 37% to 43%. This suggests that only 6% of the free %COO^- located in the loops and tails of the NaPA adsorbed on the surface participate in the adsorption of the aminosilanated silica particles.

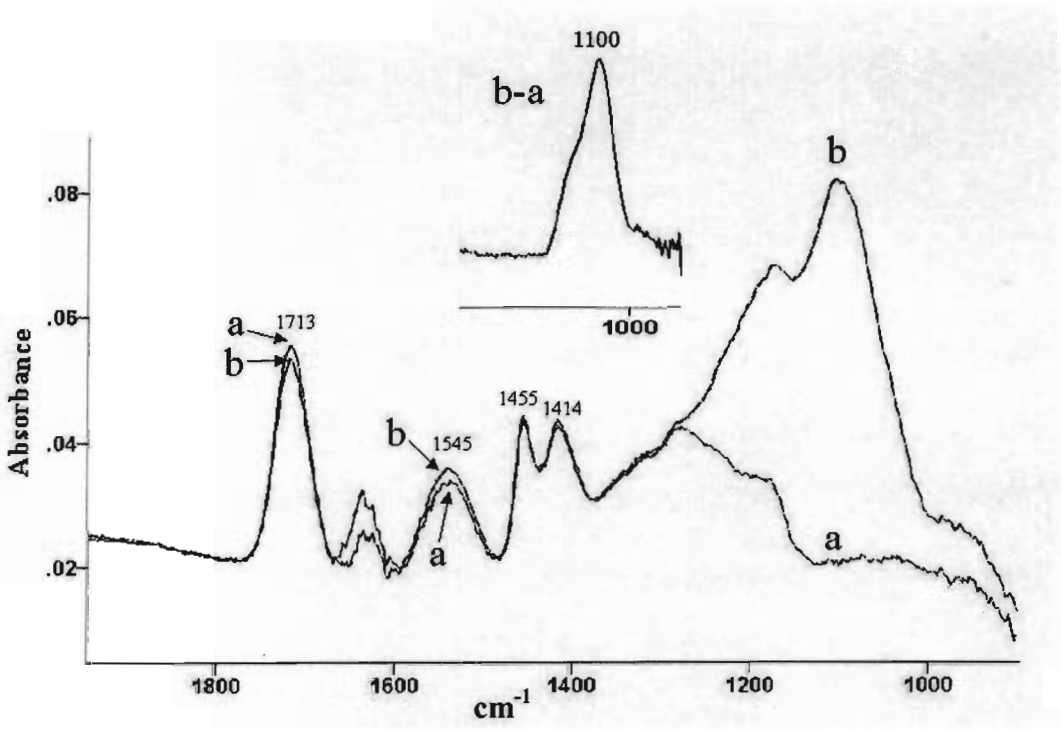

Figure 6.3 IR spectra of (a) NaPA adsorbed on TiO2 from a 5 ppm NaPA solution at pH 3.5 followed by a 5 minute rinse with water at pH 3.5 and then (b) addition of a 25 ppm suspension of aminosilanated silica at pH 3.5 for 240 minutes.

Table 6.1 Computed values for NaPA adsorbed on TiO_2 before and after addition of 25 ppm suspension of aminosilanated silica.

	Free %COOH	Free $\%COO^-$	Bound $\%COO^-$
Before aminosilanated silica added	47%	16%	37%
After aminosilanated silica added	43%	14%	43%

The primary particle size of the silica is about 7 nm but these are clustered in larger aggregates of about 200 nm in diameter. Thus for steric reasons, it is most likely that the functional groups of the adsorbed NaPA that lie in the regions extended out into the solution participate in binding to the silica forming a bridge between the two particles (see scheme 6.2). It is noted that under similar reaction conditions, the addition of a CTAB solution to the NaPA adsorbed on TiO_2 led to a 15% increase in the bound $\%COO^-$.[93] This value is higher than the 6% increase in bound $\%COO^-$ obtained after addition of the aminosilanated silica suspension and is consistent with the anticipated higher penetration of the CTAB into the NaPA layer.

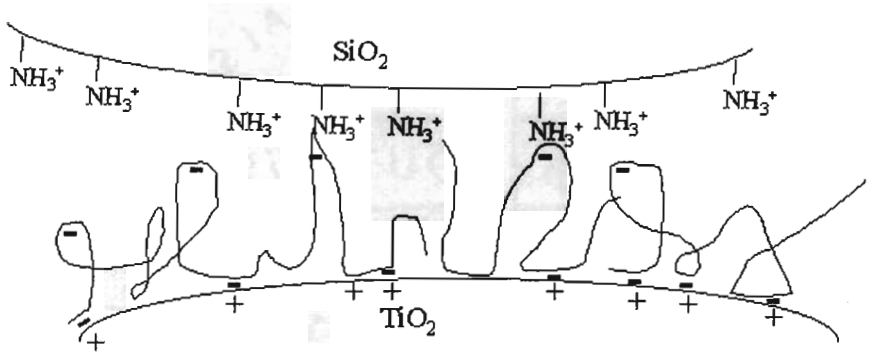

Scheme 6.2 Interaction of Silica with NaPA coated TiO_2

6.3.4 Adsorption of SiO_2 on PDADMAC Coated TiO_2

It is expected that the extension of this ATR approach to other adsorbed polymeric material will require an understanding of how changes in the infrared bands due to functional groups of the polymer can provide information of the polymer structure on the surface. Polydiallyldimethylammonium chloride (PDADMAC) and in general, almost all cationic polymers, derive the positive charge from a pendent $^{+}N\text{-}CH_3$ functional group (see scheme 6.1). In this case, the spectral interpretation of the adsorbed polymer structure will benefit from an understanding of the changes occurring to bands assigned to the $^{+}N\text{-}CH_3$ functionality.

Figure 6.4a shows the spectrum of PDADMAC adsorbed on TiO_2 from a 30 ppm solution of the polymer at pH 10. At this pH the surface of TiO_2 is negatively charged. The band at 1453 cm^{-1} is due to a CH_2 bending mode[95] and is used to measure the adsorbed amount of the PDADMAC. Of particular interest is the band at 1396 cm^{-1} because this band is assigned to the symmetric bending modes of the $^{+}N\text{-}CH_3$ ($\delta_s{}^{+}N\text{-}CH_3$) functional group.[23, 93] Compared to the spectrum of the pure PDADMAC compound

shown in Figure 6.4c, the 1396 cm^{-1} band is clearly much higher in intensity relative to the CH band at 1453 cm^{-1}.

To explain this difference in intensity I draw analogy to chapter 3 describing on the adsorption of CTAB on TiO_2.[23] Both the CTAB and the PDADMAC have similar $^{+}N\text{-}CH_3$ functionality and both have a band at 1396 cm^{-1}. For CTAB, the transition dipole moment vector associated with the $\delta_s{}^{+}N\text{-}CH_3$ is perpendicular to the micelle surface and intensifies when the CTAB molecule directly interacts with a countercharged surface site.[23] The value of the 1396/2850 cm^{-1} band intensity (the 2850 cm^{-1} is due to a CH_2 mode) was shown to be related to the percentage of CTAB molecules adsorbed through direct interaction with the surface. In the same respect, the band at 1396 cm^{-1} in Figure 6.4a for PDADMAC adsorbed on TiO_2 is larger than its counterpart in the spectrum of the pure polymer (see Figure 6.4c) because some of the $^{+}N(CH_3)_3$ moieties are interacting with negative surface sites. Thus a change in intensity of the 1396 cm^{-1} band correlates to a change in the number of $^{+}N(CH_3)_3$ groups directly interacting with oppositely charged sites.

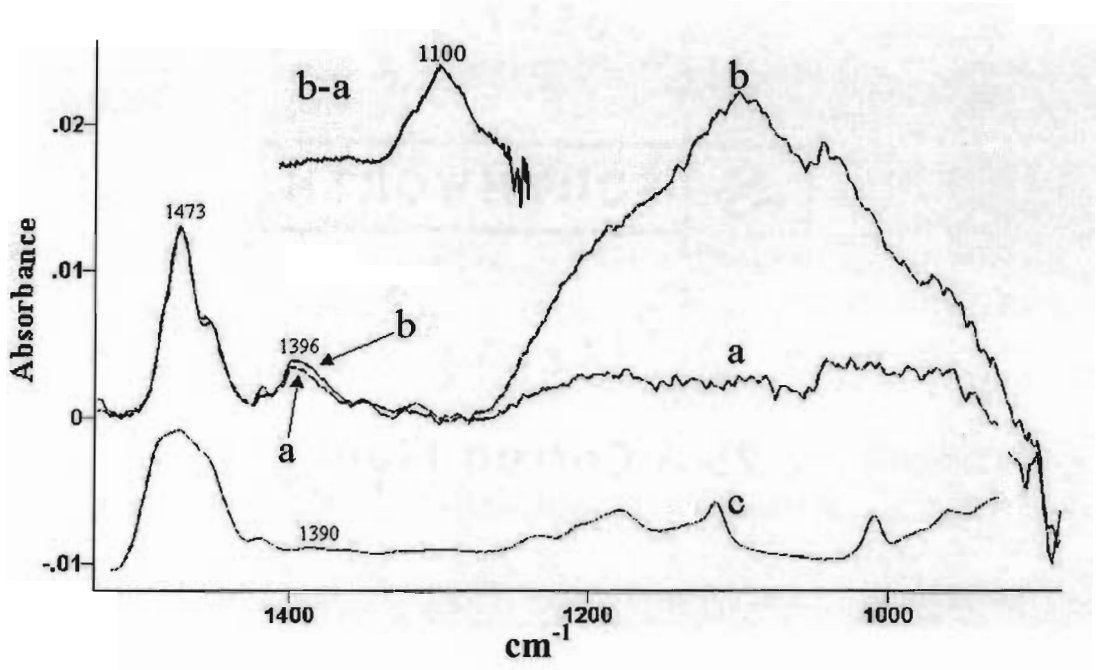

Figure 6.4 IR spectrum of (a) PDADMAC adsorbed on TiO2 from a 30 ppm PDADMAC solution at pH 10 followed by a 5 minute rinse with water at pH 10 and then (b) addition of 25 ppm suspension of untreated silica at pH 10 for 240 minutes (c)absorbance spectrum of pure PDADMAC cast onto a ZnSe infrared window.

Figures 6.4a and 6.4b shows the IR spectra measured before and after a suspension of untreated silica particles is passed through the cell containing the PDADMAC coated TiO_2. After the silica is introduced, the intensity of the CH_2 mode at 1453 cm^{-1} remains constant while the intensity of the $\delta_s{}^{+}N\text{-}CH_3$ peak increases. There is also a strong and broad peak appeared at 1100 cm^{-1} due to silica depositing on the surface. We recall that no silica was deposited on the surface when a silica suspension at pH 10 was flowed through the cell containing bare TiO_2 particles. Thus adsorption of the silica occurs with the positively charged polymer layer. The spectra in Figure 6.4 clearly

show that no PDADMAC is displaced from the surface as evidenced by the constant intensity of the CH band at 1453 cm^{-1}. Furthermore, the increase in intensity of the $\delta_s{}^{+}N\text{-}CH_3$ peak shows that the negatively charged silica adsorbs onto the PDADMAC through an electrostatic interaction with the $^{+}N(CH_3)_3$ groups.

6.4 Conclusion

An ATR-IR method for studying the interaction of dissimilar surfaces bearing adsorbed polymers has been developed. Using this method it is possible to track the amount of silica particles deposited on the surface and, at the same time, determine the change that occurs in the amount and structure of the adsorbed polymer layer. In the case of adsorbed NaPA on TiO_2, the polymer does not transfer from the TiO_2 to the positively charged silica particles but rather, forms a few bridged bonds with the COO^{-} groups located in the outer regions of the loops and tails extending furthest away from the TiO_2 surface. A similar picture emerges when the PDADMAC coated TiO_2 particles come in contact with negatively charged silica particles. In this case the silica forms a bridge bond with the $^{+}N(CH_3)_3$ moieties of the PDADMAC. The results show that once adsorbed on the TiO_2 particle, the PDADMAC or the NaPA does not migrate to the silica particles.

REFERENCES

[1] Myers, D. Surfactant Science and Technology; VCH: New York, **1992.**

[2] Esumi, K.; Iitaka, M.; Koide, Y. Simultaneous adsorption of poly(ethylene Oxide) and cationic surfactant at the Silica/Water interface. *J. Colloid Interface Sci.* **1998**, *208*, 178.

[3] Esumi, K. Interactions between surfactants and particles:dispersion, surface modification and adsolubilization. *J. Colloid Interface Sci.* **2001**, *241,* 1.

[4] Langevin, D. Polyelectrolyte and surfactant mixed solutions. Behavior at surfaces and in thin films. *Adv. Colloid Interface Sci.* **2001**, *89-90,*467.

[5] Dedinaite, A.; Claesson, P. M.; Bergstrom, M. Polyelectrolyte-surfactant layers: adsorption of performed aggregates versus adsorption of surfactant of preadsorbed polyelectrolyte. *Langmuir* **2000**, *16*, 5257.

[6] Taylor, D. J. F.; Thomas, R. K.; Li, P. X. Adsorption of oppositely charged polyelectrolyte/surfactant mixtures. neutron reflection from alkyl trimethylammonium bromides and sodium poly(styrenesulfonate) at the air/water interface: the effect of surfactant chain length. *Langmuir* **2003**, *19*, 3712.

[7] Liu, J. F.; Min, G.; Ducker, W. A. AFM study of adsorption of cationic surfactants and cationic polyelectrolytes at the silica-water interface. *Langmuir* **2001**, *17*, 4895.

[8] Okubo, T.; Suda, M. Multilayered adsorption of macrocations and macroanions on colloidal spheres as studied by dynamic light scattering measurements. *Colloid & Polymer Sci.* **2003**, *281*, 782.

[9] Chen, J.; He, T.; Wu, W.; Cao, D.; Yun, J.; Tan, C. K. Adsorption of sodium salt of polyacrylic acid (PAANa) on nano-sized $CaCO_3$ and dispersion of nano-sized $CaCO_3$ in water. *Colloids Surf. A: Physicochem. Eng. Aspects* **2004**, *232*, 163.

[10] Nystrom, R.; Backfolk, K.; Rosenholm, J. B.; Nurmi, K. The effect of pretreatment of calcite dispersions with anionic sodium polyacrylate on their flocculation behavior induced by cationic starch. *J. Colloid and Interface Sci.* **2003**, *262*, 48.

[11] Kolesnikova, T. P.; Polunina, I. A.; Roldughin, V. I. Adsorption modification of dispersed aluminum: the effect of surfactant and polymer adsorption on the colloidal and mechanical properties of aluminum organo suspensions. *Colloid Journal* **2002**, *64*, 319.

[12] Strauss, H.; Heegn, H.; Strienitz, I. Effect of PAA adsorption on stability and rheology of TiO_2 dispersions. *Chemical Engineering Science* **1993**, *48*, 323.

[13] Sjoberg, M.; Bergstrom, L.; Larsson, A.; Sjostrom, E. V. A. The effect of polymer and surfactant adsorption on the colloidal stability and rheology of kaolin dispersions. *Colloids and Surfaces A: Physicochem. Eng. Aspects* **1999**, *159*, 197.

[14] Ninness, B.J.; Bousfield, D.W.; Tripp, C. P. The importance of adsorbed cationic surfactant structure in dictating the subsequent interaction of anionic surfactant and polyelectrolytes with pigment surfaces. *Colloids and Surfaces A: Physicochem. Eng. Aspects* **2002**, *203*, 21.

[15] Fan, A.; Somasundaran, P.; Turro, N. J. Role of sequential adsorption of polymer/surfactant mixture and their conformation in dispersion/flocculation of alumina. *Colloids and Surfaces A: Physicochem. Eng. Aspects* **1999**, *146*, 397.

[16] Biswas, S.C.; Chattoraj, D.K. Polysaccharide-surfactant Interaction. 1. Adsorption of cationic surfactants at the cellulose/water interface. *Langmuir **1997**, 13,* 4505.

[17] Ghosh, L.; Das, K. P.; Chattoraj, D. K. Kinetics of adsorption of ionic surfactants at Alumina-water Interface. *J. Indian Chem. Soc.* **1986**, LXIII, 144.

[18] Sharma, B. G.; Basu, S.; Sharma, M. M. Characterization of adsorbed ionic surfactants on a Mica substrate. *Langmuir* **1996**, *12*, 6506.

[19] Scamehorn, J. F.; Schechter, R. S.; Wade, W. H. Adsorption of surfactants on mineral oxide surfaces from aqueous solutions. *J. Colloid Interface Sci.* **1982**, *85*, 463.

[20] Somasundaran, P.; Fuerstenau, D. W. Mechanisms of alkyl sulfonate adsorption at the alumina-water interface. *J. Phys. Chem.* **1966**, *70*, 90.

[21] Huang, L.; Somasundaran, P. The change in structure of surfactant aggregates during adsorption/desorption processes and its effect on the stability of alumina suspension. *Colloids and Surfaces A: Physicochem. Eng. Aspects* **1996**, *117*, 235.

[22] Hulden, M.; Sjoblom, E. Adsorption of some common surfactants and polymers on TiO_2-pigments. *Progr. Colloid & Polym Sci.* **1990**, *82*, 28.

[23] Li, H.; Tripp, C. P. Spectroscopic identification and dynamics of adsorbed cetyltrimethylammonium bromide structures on TiO_2 surfaces. *Langmuir* **2002**, *18*, 9441.

[24] Berglund, K. D.; Przybycien, T. M.; Tilton, R. D. Coadsorption of sodium dodecyl sulfate with hydrophobically modified nonionic cellulose polymers. 2. Role of surface selectivity in adsorption hysteresis. *Langmuir* **2003**, *19*, 2714.

[25] Pagac, E. S.; Prieve, D. C.; Tilton, R. D. Kinetics and mechanism of cationic surfactant adsorption and coadsorption with cationic polyelectrolyte at the silica-water interface. *Langmuir* **1998**, *14*, 2333.

[26] Windsor, R.; Neivandt, D. J.; Davies, P. B. Temperature and pH effects on the Coadsorption of Sodiun Dodecyl sulfate and Poly(ethylenimine). *Langmuir* **2002**, *18*, 2199.

[27] Artyukhin, A. B.; Burnham, K. J.; Levchenko, A. A.; Talroze, R. V.; Stroeve, P. Polyelectrolyte adsorption onto a surface-confined surfactant. *Langmuir* **2003**, *19*, 2243.

[28] Thibaut, A.; Misselyn-Bauduin, A. M.; Broze, G.; Jerome, R. Adsorption of poly(vinylpyrrolidone)/surfactant(s) mixtures at the silica/water interface: A calorimetric investigation. *Langmuir* **2000**, *16*, 9841.

[29] Braem, A. D.; Prieve, D. C.; Tilton, R. D. Elecrostatically tunable coadsorption of sodium dodecyl sulfate and poly(ethylene oxide)-poly(propylene oxide)-poly(ethylene oxide) triblock copolymer to silica. *Langmuir* **2001**, *17*, 883.

[30] Berglund, K. D.; Przybycien, T. M.; Tilton, R. D. Coadsorption of sodium dodecyl sulfate with hydrophobically modified nonionic cellulose polymers. 1. Role of polymer hydrophobic modification. *Langmuir* **2003**, *19*, 2705.

[31] Barhoumi, M.; Beurroies, I.; Denoyel, R.; Said, H.; Hanna, K. Coadsorption of alkylphenols and nonionic surfactants onto kaolinite. *Colloids and Surfaces A: Physicochem. Eng. Aspects* **2003**, *219*, 25.

[32] Torn, L. H.; Keizer, A. D.; Koopal, L. K.; Lyklema, J. Mixed adsorption of poly(vinylpyrrolidone) and sodium dodecylbenzenesulfonate on kaolinite. *J. Colloid and Interface Sci.* **2003**, *260*, 1.

[33] Kramer, G.; Somasundaran, P. Conformational behavior of polyelectrolyte complexes at the solid/liquid interface. *Langmuir* **2002**, *18*, 9357.

[34] Fleming, B. D.; Wanless, E. J.; Biggs, S. Nonequilibrium mesoscale surface structures: The adsorption of polymer: Surfactant mixtures at the solid/liquid interface. *Langmuir* **1999**, *15*, 8719.

[35] Maurdev, G.; Gee, M. L.; Meagher, L. Controlling the adsorbed conformation and desorption of polyelectrolyte with added surfactant via the adsorption mechanism: A direct force measurement study. *Langmuir* **2002**, *18*, 9401.

[36] Ninness, B.J. A molecular investigation of adsorption onto mineral pigments. *Ph. D. Thesis,* University of Maine, December **2001.**

[37] Jiang, C.; Li, H.; Tripp, C. P. Infrared Method for In Situ Studies of Polymer /Surfactant Adsorption on Silica Powders from Aqueous Solution. *Applied Spectroscopy,* **2003**, *57,* 1419.

[38] Ninness, B. J.; Bousfield, D. W.; Tripp, C. P. An *in situ* Infrared technique for studying adsorption onto particulate Silica surfaces from aqueous solutions. *Appl. Spectrosc.* **2001**, *55*, 655.

[39] Neivandt, D. J.; Gee, M. L.; Hair, M. L.; Tripp, C. P. Polarized infrared attenuated total reflection for the *in situ* determination of the orientation of surfactant adsorbed at the solid/solution interface. *J. Phys. Chem. B* **1998**, *102*, 5107.

[40] Neivandt, D.; Gee, M. L.; Tripp, C. P.; Hair, M. L. The coadsorption of polystyrenesulfonate and ceyltrimethylammonium bromide on silica as studied by attenuated total reflection techniques. *Langmuir* **1997**, *13*, 2519.

[41] Harrick, N. J. *Internal Reflection Spectroscopy*; 3rd ed; John Wiley & Sons: New York, **1987.**

[42] Rosen, M. J. *Surfactants In Emerging Technologies*; Marcel Dekker: New York, **1987**.

[43] Gao, Y.; Du, J.; Gu, T. Hemimicelle formation of cationic surfactants at the silica gel-water interface. *J. Chem. Soc., Faraday Trans. 1* **1987**, *83*, 2671.

[44] Gaudin, A. M.; Fuerstenau, D. W. "Streaming Potential Studies--Quartz Flotation with Cationic Collectors," *Trans. AIME* **1955**, *202*, 958.

[45] Somasundaran, P.; Healy, T. W.; Fuerstenau, D. W. Surfactant adsorption at the solid-liquid interface 1. Dependence of mechanism on chain length. *J. Phys. Chem.* **1964**, *68*, 3562.

[46] Schulz, J. C.; Warr, G. C. Adsorbed layer structure of cationic and anionic surfactants on mineral surfaces. *Langmuir* **2002**, *18*, 3191.

[47] Johnson, R. A.; Nagarajan, R. Modeling self-assembly of surfactants at solid-liquid interfaces. II. Hydrophilic surfaces. *Colloids and Surfaces A: Physicochem. Eng. Aspects* **2000**, *167*, 21.

[48] Johnson, R. A.; Nagarajan, R. Modeling self-assembly of surfactants at solid/liquid interfaces. I. Hydrophobic surfaces. *Colloids and Surfaces A: Physicochem. Eng. Aspects* **2000**, *167*, 31.

[49] Yeskie, M. A.; Harwell, J. H. On the structure of aggregates of adsorbed surfactants: The surface charge density at the hemimicelle/admicelle transition. *J. Phys. Chem.* **1988**, *92*, 2346.

[50] Biswas, S. C.; Chattoraj, D. K. Kinetics of adsorption of cationic surfactants at silica-water Interface. *J. Colloid Interface Sci.* **1998**, *205*, 12.

[51] Stratton-Crawley, R.; Shergold, H. L. Extraction of titanium dioxide into oil from cationic surfactant solutions. *Colloids and Surfaces.* **1981**, *2*, 145.

[52] Ducker, W. A.; Wanless, E. J. Adsorption of hexadecyltrimethylammonium bromide to mica: Nanometer-scale study of binding-site competition effects. *Langmuir* **1999**, *15*, 160.

[53] Nishimura, S.; Scales, P. J.; Biggs, S. R.; Healy, T. W. AFM studies of amine surfactant hemimicelle structures at the mica-water interface. *Colloids and Surfaces A: Physicochem. Eng. Aspects* **1995**, *103*, 289.

[54] Ceotto, G.; de Souza, E. F.; Teschke, O. Ionic surfactant films imaged by atomic force microscopy. *J. Mol. Cat. A* **2001**, *167*, 225.

[55] Li, B.; Fujii, M.; Fukada, K.; Kato, T.; Seimiya, T. *In situ* AFM observation of heterogeneous growth of adsorbed film on cleaved mica surface. *Thin Solid Films* **1998**, *312*, 20.

[56] Singh, P. K.; Adler, J. J.; Rabinovich, Y. I.; Moudgil, B. M. Investigation of self-assembled surfactant structures at the solid-liquid interface using FTIR/ATR. *Langmuir* **2001**, *17*, 468.

[57] Atkin, R.; Craig, V. S. J.; Biggs, S. Adsorption kinetics and structural arrangements of cationic surfactants on silica surfaces. *Langmuir* **2000**, *16*, 9374.

[58] Fleming, B. D.; Biggs, S.; Wanless, E.J. Slow organization of cationic surfactant adsorbed to silica from solutions far below the CMC. *J. Phys. Chem. B* **2001**, *105*, 9537.

[59] Portet-Koltalo, F.; Desbene, P. L.; Treiner, C. Self-desorption of mixtures of anionic and nonionic surfactants from a silica/water interface. *Langmuir* **2001**, *17*, 3858.

[60] Thibaut, A.; Misselyn-Bauduin, A. M.; Grandjean, j.; Broze, G.; Jerome, R. Adsorption of an aqueous mixture of surfactants on silica. *Langmuir* **2000**, *16*, 9192.

[61] Kitahara, A.; Hasumuma, M. Floculation-defloculation effect of polymer additive in nonaqueous dispersions. *J. Colloid Interface Sci.* **1972**, *41*, 383.

[62] Uchida, H.; Hirao, S.; Torimoto, T.; Kuwabata, S.; Sakata, T.; Mori, H.; Yoneyama, H. Preparation and Properties of size-quantized TiO_2 particles immobilized in polyvinylpyrrolidinone gel films. *Langmuir* **1995**, *11*, 3725.

[63] Hoogeveen, N. G.; Cohen Stuart, M. A.; Fleer, G. J. Polyelectrolyte adsorption on oxides 1. Kinetics and adsorbed amounts. *J. Colloid Interface Sci.* **1996**, *182*, 133.

[64] Hoogeveen, N.G.; Cohen Stuart, M.A.; Fleer, G. J. Polyelectrolyte adsorption on oxides 2. Reversibility and Exchange. *J. Colloid Interface Sci.* **1996**, *182*,146.

[65] Lambert, O.; Jada, A.; Dumas, P. Adsorption of triarm starblock copolymers based on polystyrene, poly(ethylene oxide) and poly (e-caprolactone) at the solid-solution interface. *Colloids and Surf.* **1998**, *136,* 263.

[66] Losoi, T. Surface treatment of TiO_2 pigments and aqueous stability. In: *Surface phenomena and additives in water-based coatings and printing technology.* Sharma, M. K. ed.; Plenum Press, New York, **1991.**

[67] Huang, N-P.; Csucs, G.; Emoto, K.; Nagasaki, Y.; Kataoka, K.; Textor, M.; Spencer, N.D. Covalent attachment of novel poly(ethylene glycol)-poly(DL-lactic acid) copolymeric micelles to TiO_2 surfaces. *Langmuir* **2002**, *18,* 252.

[68] Vermohlen, K.; Lewandowski, H.; Narres, H.D.; Koglin, E. Adsorption of polyacrylic acid on aluminium oxide: DRIFT spectroscopy and *ab initio* calculations. *Colloids and Surfaces A: Physicochem. Eng. Aspects* **2000,** *170,* 181.

[69] Pan, Z.; Campbell, A.; Somasundaran, P. Polyacrylic acid adsorption and conformation in concentrated alumina suspensions. *Colloids and Surfaces A: Physicochem. Eng. Aspects* **2001**, *191,* 71.

[70] Jarnstrom, L. The polyacrylate demand in suspensions containing ground calcuim carbonate. *Nord. Pulp & Pap. Res. J.* **1993**, *8,* 27.

[71] Esumi, K.; Nakaie, Y.; Sakai, K.; Torigoe, K. Adsorption of poly(ethyleneglycol) and poly(amidoamine)dendrimer from their mixtures on alumina.water and silica/water interfaces. *Colloids and Surfaces A: Physicochem. Eng. Aspects* **2001,** *194,*7.

[72] Ishiduki, K.; Esumi, K. Adsorption characteristics of poly(acrylic acid) and poly(vinyl pyrrolidone) on alumina from their mixtures in aqueous solution. *J. Colloid Interface Sci.* **1997**, *185,* 274.

[73] Liu, J. F.; Min, G.; Ducker, W. A. AFM study of adsorption of cationic surfactants and cationic polyelectrolyteds at the silica water interface. *Langmuir* **2001**, *17,* 4895.

[74] Fan, A.; Somasundaran, P.; Turro, N. J. Role of sequential adsorption of polymer/surfactant mixtures and their conformation in dispersion/flocculation of alumina. *Colloids and Surfaces A: Physicochem. Eng. Aspects* **1999,** *146,* 397.

[75] Simister, E. A.; Thomas, R. K.; Penfold, J.; Aveyard, R.; Binks, B. P.; Cooper, P.; Fletcher, P. D. I.; Lu, J. R.; Sokolowski, A. Comparison of neutron reflection and surface tension measurements of the surface excess of tetradecyltrimethylammonium bromide layers at the air/water interface. *J. Phys. Chem.* **1992**, *96*, 1383.

[76] Scheuing, D. R.; Weers, J. G. A Fourier Transform Infrared spectrocopic study of dodechytrimethylammonium chloride/ sodium dodecyl sulfate surfactant mixtures. *Langmuir* **1990**, *6*, 665.

[77] Weers, J. G.; Scheuing, D. R. Micellar sphere to rod transitions. In *Fourier Transform Infrared Spectroscopy in Colloid and Interface Science*; Scheuing, D. R., ed.; American Chemical Society: Washington, **1991**.

[78] Sidorova, M.; Golub, T.; Musabekov, K. Electrokinetic and adsorption properties of SiO2 in polymer and surfactant solutions. *Adv. Colloid Interface Sci.* **1993**, *43*, 1.

[79] Thorstenson, T. A.; Tebelius, L. K.; Urban, M. W. Surface and Interfacieal FTIR spectroscopic studies of latexes. VII. EA/MAA Latex suspensions stability and surfactant migration. *J. Appl. Polym. Sci.* **1993**, *50*, 1207.

[80] Weers, J. G.; Scheuing, D.R. Micellar sphere to rod transitions. In *Fourier Transform Infrared Spectroscopy in Colloid and Interface Science*; Scheuing, D.R., ed.; American Chemical Society: Boston, MA, **1990**.

[81] Yang, P. W.; Mantsch, H. H.; Baudais, F. A critical evaluation of three types of diffuse reflectance infrared accessories. *Appl. Spectrosc.* **1986**, *40*, 974.

[82] Velegol, S. B.; Fleming, B. D.; Biggs, S.; Wanless, E. J.; Tilton, R. D. Couterion effects on hexadecyltrimethylammonium surfactant adsorption and self-assembly on silica. *Langmuir* **2000**, *16*, 2548.

[83] Wang, W.; Li, L.; Xi, S. A fourier transform infrared study of the coagel to micelle transition of cetyltrimethylammonium bromide. *J. Colloid Interface Sci.* **1993**, *155*, 369.

[84] Nakamoto, K. *Infrared and Raman Spectra of Inorganic and Coordination Compounds.* **1986,** 4th ed. John Wiley and Sons, New York.

[85] Kirwan, L. J.; Fawell, P. D.; van Bronswijk, W. *In situ* FTIR-ATR examination of poly(acrylic acid) adsorbed onto hematite at low pH. *Langmuir* **2003**, *19*, 5802.

[86] Jones, F.; Farrow, J. B.; van Bronswijk, W. An infrared study of a polyacrylate flocculant adsorbed on hematite. *Langmuir* **1998**, *14*, 6512.

[87] Allara, D. L.; Nuzzo, R. G. Spontaneously organized molecular assemblies. 1. Formation, dynamics, and physical properties of n-Alkanoic acids adsorbed from solution on an oxidized aluminum surface. *Langmuir* **1985**, *1*, 45.

[88] Hilborn, J.; Gupta, B.; Garamszegi, L.; Laurent, A.; Plummer, C. J. G.; Bisson, I.; Frey, P.; Hedrick, J. L. Grafted poly(acrylic acid) brushes for cell-surface interactions.. *Mater. Res. Soc. Symp. Proc.* **2000**, *629*, FF4.1.1.

[89] Meagher, L.; Maurdev, G.; Gee, M.L. Interaction forces between a bare silica surface and an alumina surface bearing adsorbed polyelectrolyte and surfactant. *Langmuir* **2002**, *18*, 2649.

[90] Hartley, P. G.; Scales, P. J. Electrostatic properties of polyelectrolyte modified surfaces studied by direct force measurement. *Langmuir* **1998**, *14*, 6948.

[91] Hartley, P. G.; Bailey, A. I.; Luckham, P. F.; Batts, G. Non-specific interactions between heparin and poly-L-lysine surfaces. *Colloids and Surfaces A: Physicochem. Eng. Aspects : Physicochemical and Engineering Aspects,* **1993**, *77*, 191.

[92] Claesson, P. M.; Paulson, O. E. H.; Blomberg, E.; Burns, N. L. Surface Properties of Poly(ethylene imine)-coated mica surfaces—salt and pH effects. *Colloid and Surfaces A: Physicochemical and Engineering Aspects,* **1997**, *123-124*, 341.

[93] Li, H.; Tripp, C. P. Interaction of sodium polyacrylate adsorbed on TiO_2 with cationic and anionic surfactants. *Langmuir,* **2004**, *In Press.*

[94] Li, H.; Tripp, C. P. Use of infrared bands of the surfactant headgroup to identify mixed surfactant structures adsorbed on titania. *Journal of Physical Chemistry,* **2004**, *In Press.*

[95] Kim, S. J.; Yoon, S. G.; Kim, S. I. Synthesis and characteristics of interpenetrating polymer network hydrogels composed of alginate and poly(diallyldimethylammoniu chloride). *J. Appl. Polym. Sci.* **2004**, *91*,3705.

BIOGRAPHY OF THE AUTHOR

Haiyan Li was born in Tianjin, the People's Republic of China, on September 24th, 1974. She was raised in Tianjin and graduated from the No. 1 High School of Yangcun, Tianjin in 1993. In 1993, she attend the Nankai University, Tianjin, China, and graduated in 1997 with a Bachelor's degree in Chemistry with a focus on polymer Chemistry. In the same year she entered the polymer chemistry graduate program in Nankai University, Tianjin, China. In the fall of 2000, she finished the graduate study in China and began her graduate study at University of Maine. She is a candidate for the Doctor of Philosophy degree in Chemistry from the University of Maine in December, 2004.